Impact of Bolt-Nut Interface Modeling Assumptions on the Calculated Low Cycle Fatigue Life of Aircraft Engine Turbine Rotor Bolted Joints

A thesis

submitted by

Luke Jensen

in partial fulfillment of the requirements
for the degree of

Master of Science
In
Mechanical Engineering

Tufts University

November 2012

Advisor: Professor Anil Saigal

Abstract

Finite element analysis is used extensively in the aircraft turbine engine industry to predict stresses to calculate low cycle fatigue (LCF) life. An accurate prediction of stresses is especially important to a specific subset of engine hardware that is defined by the FAA as life-limited parts (LLP's). LLP's include rotor and major structural parts such as disks, spacers, hubs, shafts, high pressure casings, and non-redundant mount components. A failure of an LLP can lead to a potentially catastrophic event due to non-containment of high energy debris, uncontrolled fire, or a complete inability to shut the engine down. Under-predicted stress can cause the life limits to be set too high, which is a safety hazard. Over-predicted stress can cause the life limits to be set too low, which adds cost due to the need to replace expensive engine hardware more frequently. High fidelity stress analysis is necessary to appropriately set LCF life limits.

One common engine feature analyzed with 3D stress analysis is a rotor bolted joint. Geometrical features associated with bolted joints such as holes, fillets, and scallops cause stress concentrations. Often the life limiting feature in a rotor LLP is a geometrical feature in close proximity to the joint. Unfortunately, the detailed stress analysis associated with accurately predicting stress in the joint is costly and time consuming. Analysis assumptions that can simplify the effort, yet still produce accurate results, would be valuable to the industry.

ii

The focus of this study is on the bolt-nut interface modeling assumptions associated with a rotor bolted joint stress analysis for LCF predictions. A 3D finite element model of an actual aircraft engine rotor bolted joint is created. A series of eleven cases are analyzed and compared to investigate how the thread modeling assumptions affect the calculated life in the mated rotor LLP hardware. Walker-adjusted alternating stress, $\sigma_{0,alt}$, is used to measure the life impact.

The impact is limited to the edges of the two critical features closest to the bolt-nut interface. The results demonstrate that factors such as the thread mesh density, elastic versus elastic-plastic bolt/nut material properties, and the inclusion of the helical thread shape have only minor impact. The inclusion of contact elements at the interface instead of couples has a moderate impact of 1.1 to 1.2 ksi. When couples are used, the placement of the first couple is critical, impacting the results by 1.1 to 2.6 ksi. Also, when couples are used to join the interface, the explicit inclusion of the thread shape has only 0.5 to 0.6 ksi impact.

Acknowledgements

I would like to thank my wife Mary Kay for all her support, encouragement, and patience through this process. I would also like to thank my baby boy Anders for the extra motivation he gave me to take this work to completion. I would like to thank David Kelpe for providing the idea for this research, for providing guidance along the way, and for serving on my thesis committee. I would like to thank Peter Perivolarakis who, despite not being formally involved in the research, shared his time generously in many helpful, insightful discussions. I would also like to thank Professor James for serving on my thesis committee. And finally, I would like to thank Professor Saigal for serving as my advisor and the chairperson of my thesis committee. Without his support and guidance this thesis would not have been completed.

Table of Contents

List of Figures

Chapter 1: Overview

1.1 Introduction

Section 33.70 of the Federal Aviation Regulations (FAR) identifies certain critical aircraft engine hardware as Life-Limited Parts (LLP's). LLP's are parts "whose primary failure is likely to result in a hazardous engine effect," [1]. Hazardous engine effects defined in FAR Section 33.75 consist of events such as non-containment of high-energy debris, uncontrolled fire, and complete inability to shut the engine down [2], each of which can cause a catastrophic event. LLP's include rotor and major structural parts such as disks, spacers, hubs, shafts, high pressure-casings, and non-redundant mount components.

Failures of LLP's led to tragedy for the 1980 LOT Flight 7 in Poland and the 1989 United Airlines Flight 232 in Sioux City, Iowa. In the LOT Flight 7 failure, fatigue caused the LPT (Low Pressure Turbine) shaft to fail and separate from the fan. The separation caused the LPT rotor to overspeed which led to LPT disk burst. The exploding disk fragments damaged two of the remaining three engines and the rudder and elevator controls on the aircraft. All 87 crew and passengers were killed in the subsequent crash [3]. Per the NTSB Aircraft Accident Report for United Flight 232, a hard-alpha inclusion in the ingot used to create the forging for the titanium fan disk caused a fatigue crack. After years of cycling, the fatigue crack caused a structural failure of the fan disk. Shrapnel from the

1

failed disk punctured all three hydraulic lines in the aircraft, rendering the aircraft controls useless. Using only the throttle angles for the remaining engines to control the aircraft, the pilots crash-landed the aircraft at the Sioux City Gateway Airport. 111 of the 296 occupants of the plane perished [4]. Due to the criticality of these parts, aircraft engine manufacturers are required to set low cycle fatigue (LCF) operating limits on LLP's to ensure safety of the aircraft.

FE stress analysis is used extensively in the aircraft engine industry as an integral part of the process to set the LCF life of LLP's. The ability to accurately predict stress is critical. Under-predicted stress can cause life limits to be set too high which can compromise the safety of the aircraft. Over-predicted stresses can cause the life limits to be set too low which add operational costs to the engine. More replacement parts would need to be purchased and engines would need to be overhauled more frequently.

Rotor LLP's tend to be highly stressed due to the rotating speed and thermal loading which they are subjected to during engine operation. Due to the complexity of the hardware and the need to produce accurate stress results, complex 3D stress analysis is often necessary to support LCF life calculations. One particularly common feature to analyze in a 3D finite element model is a rotor bolted joint. LCF life in a rotor is often limited to a feature in the bolted region due to the stress concentrations associated with bolt holes, scallops, fillets, or other geometric features that are often in close proximity to the joint. Accurate stress predictions in the joint are essential. Unfortunately, however, a multi-part

interaction FE transient 3D stress analysis that includes friction can take an analyst months of effort to complete. This effort can be a burden to an engine program in terms of cost and schedule. Any analysis assumptions that can simplify the effort, yet still produce accurate results, is valuable to the industry.

1.2 Objective

This thesis focuses on the 3D finite element stress analysis of bolted joints for LCF calculations in rotating aircraft engine LLP hardware. Specifically, the assumptions that go into the modeling of the bolt-nut interface are examined. Factors studied include the explicit versus implicit inclusion of the threads, analytical methods of joining the mating threads, thread mesh density, elastic versus elastic-plastic material properties, inclusion of the helical shape of the thread versus a simplified circular shape, and the sensitivity of stress to the chosen thread friction coefficient. Since the bolt and nut themselves are not LLP's, they act as boundary conditions in the analysis. The objective of this research is to understand the magnitude of the impact of each of the potential assumptions on the calculated LCF life in the mated LLP hardware. This information can help guide an analyst in determining the appropriate level of bolt-nut interface complexity to use in a 3D bolted joint stress analysis.

A significant amount of past research has been performed related to the fatigue of bolted joints. Early work by Goodier [5] and Sopwith [6] addressed the distribution of load in bolt threads. In a standard threaded connection the vast

3

majority of the load is transferred in the first few threads, while later threads carry little load. Pedersen [7] used axisymmetric FE analysis to optimize threads for stress by using an elliptical shape root fillet as opposed to the standard circular shape. Honarmandi [8] studied four geometrical parameters – thread flange type, thread root radius, thread run-out, and head fillet radius. He proposed an optimized bolt configuration he called the "Fatigue-Bolt-Improvement" (FBI) method. Venkatesan [9] looked at numerous design options to reduce stress concentrations in bolt-nut connections. The consistent theme to these articles and much of the other available literature is that the motivation for the work is to address the fatigue life of the fasteners, not the mating hardware. Fatigue failures in bolted joints that are primarily loaded in axial tension tend to occur in the fasteners. Generally the failure occurs in the bolt at the first engaged thread, the thread run-out, or in the fillet between the bolt head and shank where stress levels tend to be the highest.

In the normal operation of an aircraft rotor, the bolted joints are subjected to axial loading, however the primary loading generally occurs in the circumferential direction. The primary loads are generally speed and temperature gradients which cause thermal stress. Axial loads tend to be relatively small. Under this type of loading, fatigue failure generally occurs in the mated hardware. Typically the location of failure is the bolt hole or some other local geometrical feature that is a source of a stress concentration.

Chakherlou's work is more relevant to this type of loading. His research analytically and experimentally evaluated a single plate in uniaxial tension with a bolted hole [10]. His work demonstrated that increased clamp loads lead to higher fatigue life of the bolt hole. The compression of the bolted joint creates pre-stress in the tangential direction due to the Poisson effect which reduces the cycling. Also the bolt head and nut provide frictional resistance to the local material to resist tangential expansion under the tangential loading. In effect, the bolt and nut shield the bolt hole from load. This shielding effect is also discussed in other work by Chakherlou investigating the effect of bolt shank interference and bolt clamping load on double shear lap joints [11].

The literature, however, is silent on the topic of how the analytical modeling assumptions in the bolt-nut interface affects the calculated fatigue life of the mated hardware. To fill this void, a 3D finite element stress model of an aircraft engine rotor bolted joint has been created. In this model, eleven cases covering a range of bolt-nut interface assumptions have been analyzed. For each of the cases, the model is run through two cycles of a simple, path-dependent speed-only friction transient. In this transient, the model is cycled between a no-speed condition and a take-off speed condition. The stress results from the eleven cases are compared. The effect of each modeling assumption is quantified.

1.3 Thesis Structure

This thesis is divided into seven sections. The first section introduces the topic and provides the objective of the research. The second section discusses the hardware configuration modeled, the critical features of interest, the FE model mesh, the analysis assumptions, and a description of the eleven cases analyzed. The third section discusses governing equations behind the fatigue failure theory used in this study. The fourth section provides a sample set of results from one of the eleven analysis cases. In the fifth section, the results of the eleven analysis cases are compared and discussed. The sixth section validates the assumption to exclude thermal stress in this study. The final section features conclusions from this work and provides suggestions for future study.

Chapter 2: Experimental Methodology

2.1 Hardware Description

A bolted joint from an actual aircraft gas turbine engine is used in this study. The

joint attaches the compressor spool, the compressor discharge piston (CDP) seal,

and the high pressure turbine (HPT) front shaft. These parts are part of the

rotating core of the engine. The joint is in the aft end of the compressor, just

before the combustor. Figure 1 shows a view of the bolted hardware.
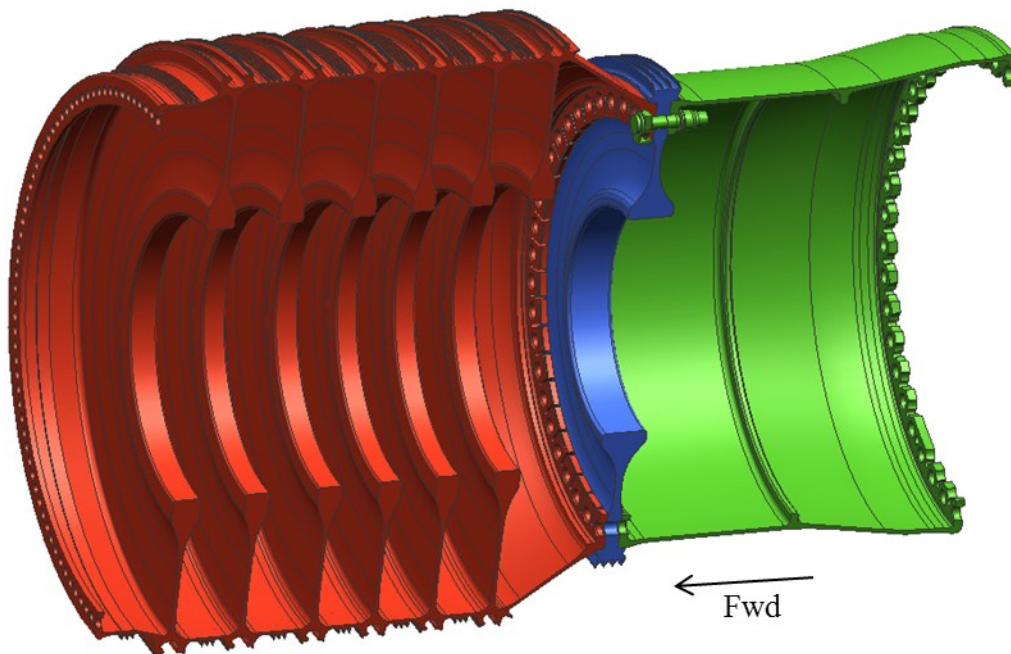
**Figure 1: Cut-away view of compressor spool (red), compressor
discharge piston (CDP) seal (blue), high pressure turbine (HPT)
front shaft (green). Only a single bolt/nut is shown.**

The compressor spool consists of a series of disks joined together by inertia welds

to form a single part. Each disk carries a set of blades which are used to compress

7

the air as it travels aft through the engine flowpath. The dovetail geometry at the OD of each disk serves to hold the blades in place. In between each disk a set of seal teeth helps to prevent air flow from leaking around the stator vanes which are attached to the compressor case (not pictured). At the aft end of the spool a conical arm extends down to the bolted joint. The aft flange of the spool has forty-eight bolt holes and forty-eight scallops. A scallop sits between each hole which helps to shield the bolt hole to lower the stress. Figure 2 provides a cross-sectional and a 3D view of the compressor spool.
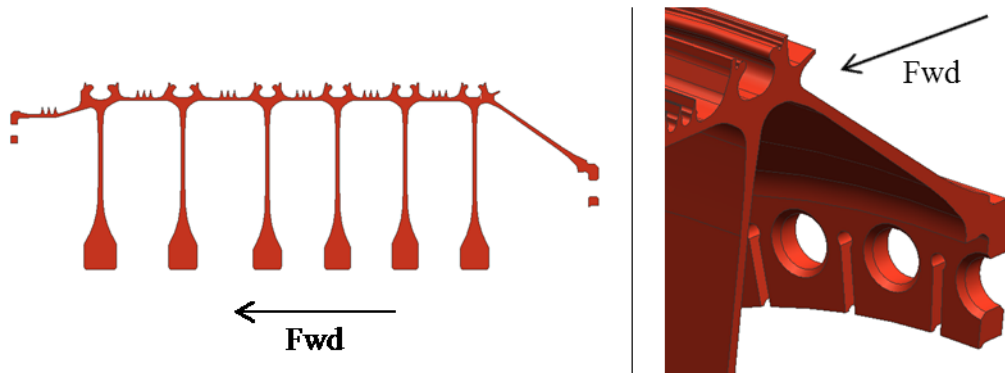
Figure 2: Compressor Spool

The CDP seal sits between the compressor spool and the HPT front shaft. Its outer diameter has four seal teeth. The seal's purpose is to restrict air flow between rotating CDP seal and the mating stator hardware. A web and bore help to carry the rotational load of the part. Through the web forty-eight bolt holes are drilled. Figure 3 shows a cross-sectional and 3D view of the CDP seal.
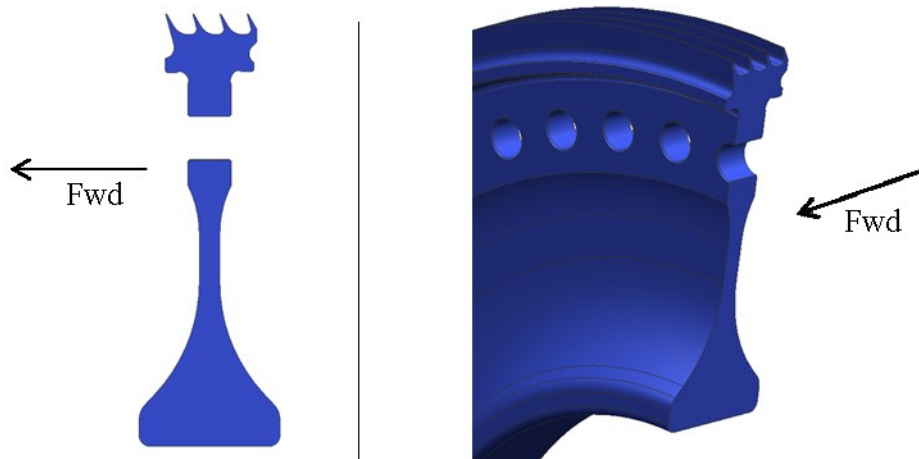
Figure 3: CDP Seal

The HPT front shaft connects the compressor rotor to the high pressure turbine rotor. The combustor resides radially outwards of the HPT front shaft. Air flows through the compressor, into the combustor where it's combined with fuel and ignited, and then flows through the turbine. Similar to the compressor spool aft flange, the HPT front shaft has forty-eight bolt holes and forty-eight stress-shielding scallops. The compressor spool, CDP seal, and HPT front shaft are all made of the nickel-based alloy Inconel 718[®1]. A cross-sectional and a 3D view of the HPT front shaft is shown in figure 4.

---

[1] Inconel 718 is a registered trademark of Special Metals Corporation
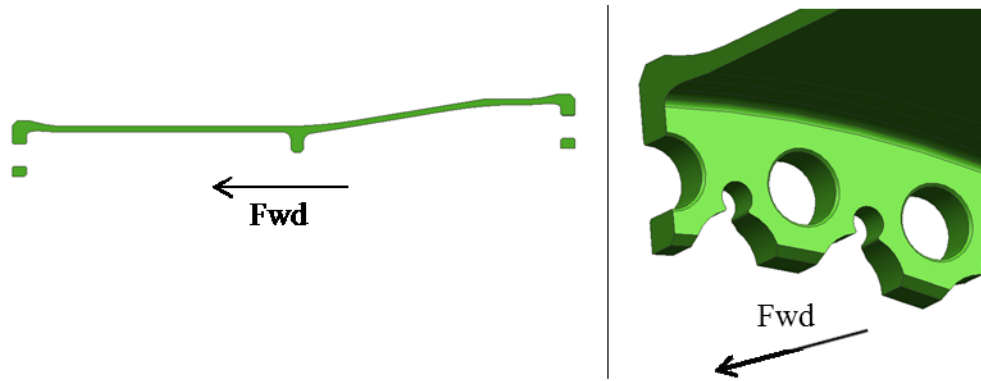
Figure 4: HPT Front Shaft

Both the compressor spool aft flange and the HPT forward flange are rabbeted to the CDP seal with interference fits. These rabbets help to strengthen the joint by preventing any joint slippage.

Forty-eight bolts and forty-eight nuts clamp the three parts together. The outer diameter of the bolt head is D-shaped. The flat portion sits against a surface on the compressor spool, preventing rotation when the nut is tightened on the aft end of the joint. The bolt has a backward "J" shaped hook at the bottom of the head to aid in the assembly process. The hook is a non-structural feature and is ignored in this study. The bolts are made of Inconel 718$^{®}$. The nuts are made of Waspaloy$^{®}$[2], which is another nickel-based alloy. The bolt and nut are shown in figure 5.

---

[2] Waspaloy is a registered trademark of United Technologies Corporation
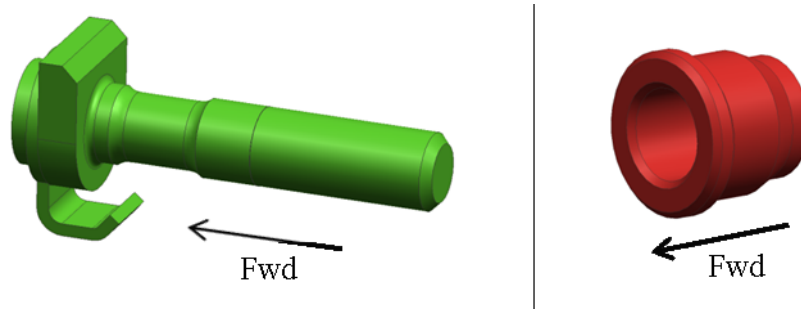
Figure 5: Bolt and Nut

Since the focus of this study is on the bolted joint, portions of the compressor spool and HPT front shaft are not included in the finite element model. Figure 6 identifies the FE modeled regions.
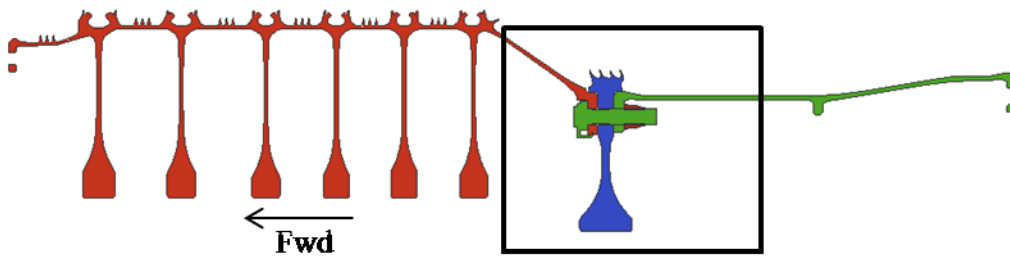
Figure 6: Cross-section of assembled spool, seal, and shaft. FE modeled region identified.

The finite element model is built to include ½ of a bolt hole, which is a 1/96th sector. This sector size is appropriate, as it is the minimum sector size that achieves geometric symmetry. However, for the helically threaded analysis cases the model sector size is doubled. For these cases, a full bolt is necessary to achieve geometric symmetry. Figure 7 shows the half bolt model.
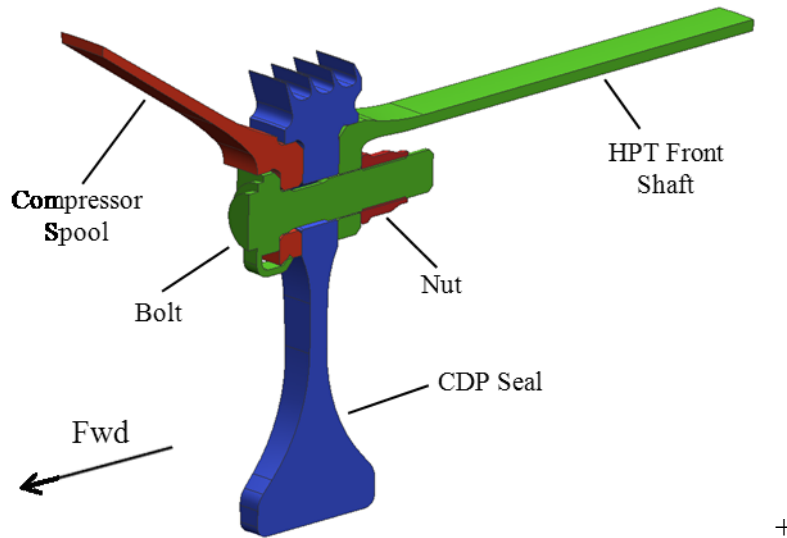
Figure 7: Half Bolt Model

2.2 Critical Features

A number of critical features have been identified for this study. The geometry of each of these features causes a stress concentration, which makes them candidates to be LCF limiting locations. The critical features include bolt holes, fillets, and scallops. The critical features are identified in Figure 8.
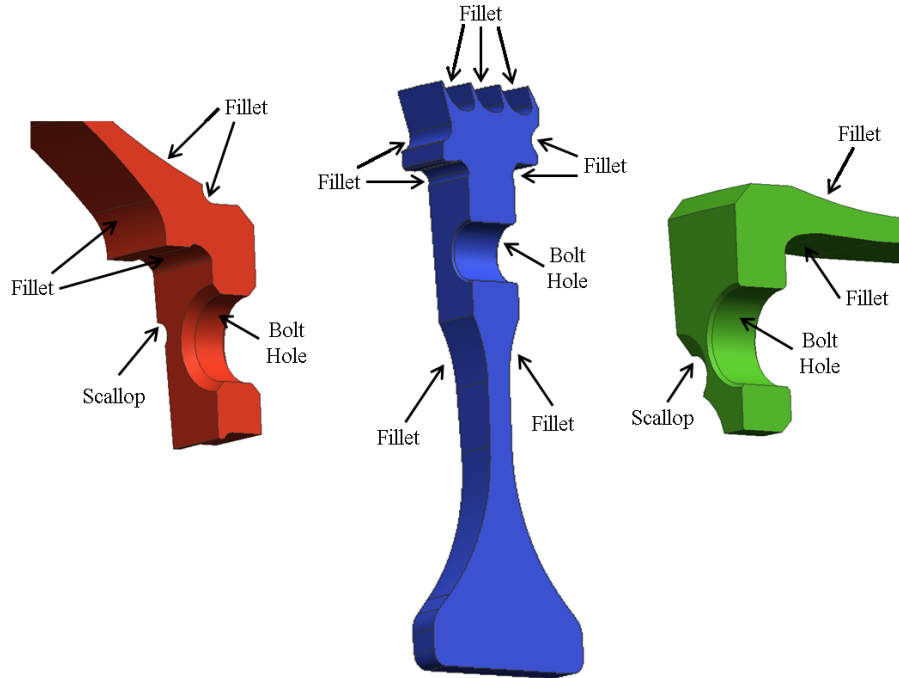
Figure 8: Bolted Joint Critical Features

2.3 Model Mesh

A CAD software called Unigraphics [12] was used to create solid models of the

five parts used in this study. The CAD models were converted to .iges files for

importation into the meshing software.

The finite element model mesh was created using CD-adapco's Star-CD software

[13]. This software is primarily designed for CFD applications. The meshing

portion of this software allows significant flexibility to the user. Nodes and

elements are created and manipulated using the imported CAD geometry as the

guide, but they are not rigidly bound or controlled by the geometry as is the case

in the meshing portion of ANSYS or of many other finite element programs. This

and other flexibilities allow the user to create a well-shaped, high-quality mesh in the critical regions and transition efficiently to a more coarse mesh in other areas. A low element count can be maintained. Modeling in this way can allow a user to accurately predict stress with reduced file size and computational time. The completed mesh was then brought into ANSYS version 11 SP1 [14] where load application, solving, and post-processing was performed.

Mesh pictures of the compressor spool, CDP seal, and the HPT front shaft can be seen in the figures below. All fillets of interest are built with a minimum of 12 elements per 90 degrees. The aspect ratio in the fillets is limited to a maximum of 3-to-1. All bolt holes have 18 elements per 90 degrees. The upper portion of the compressor spool scallop where the peak stress occurs has 14 elements per 90 degrees. The upper portion of the HPT front shaft scallop has 18 elements per 90 degrees. In the bolt holes and scallops, the aspect ratio is close to 1. For each feature, two or three rows of similarly-sized well-shaped elements are included before the transition to more coarse elements. 33,500 elements and 41,515 nodes make up the compressor spool, CDP seal, and HPT front shaft mesh. Figures 9-11 show the mesh of these three parts.
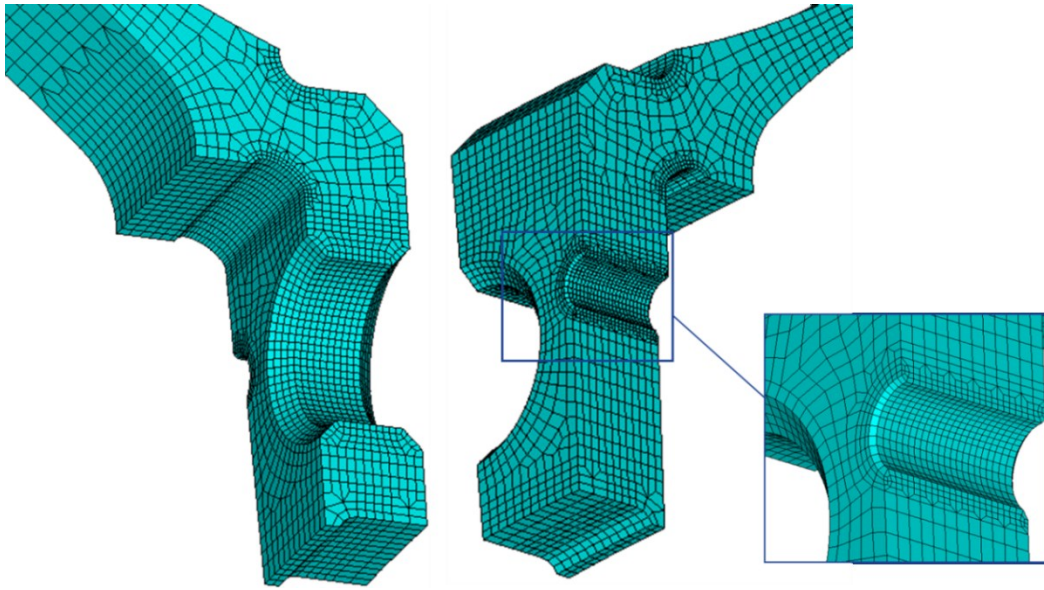
Figure 9: Compressor Spool Mesh
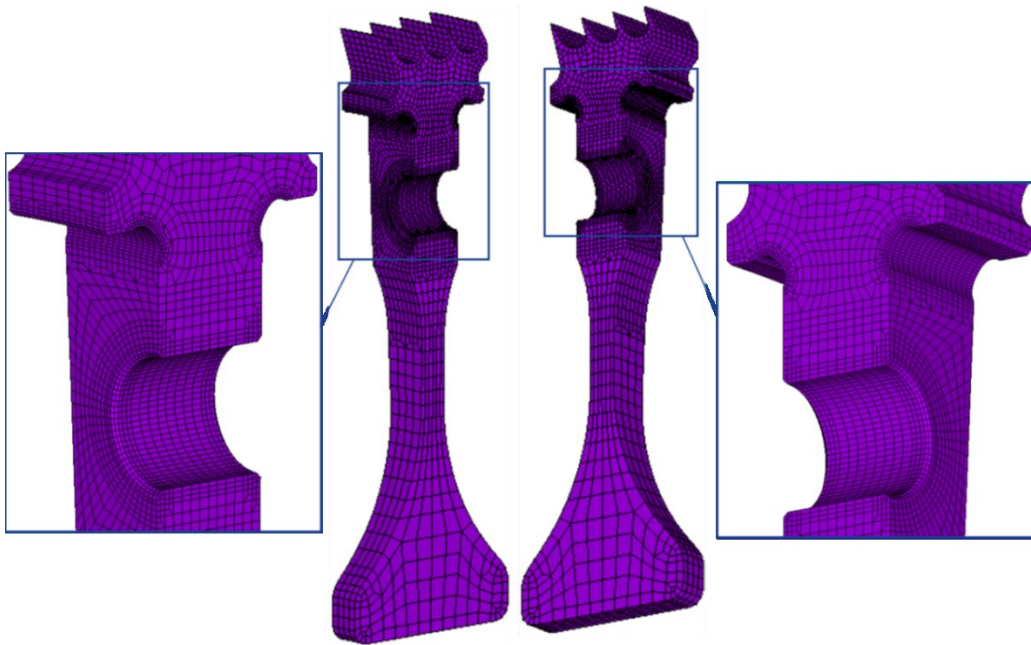
Figure 10: CDP Seal Mesh
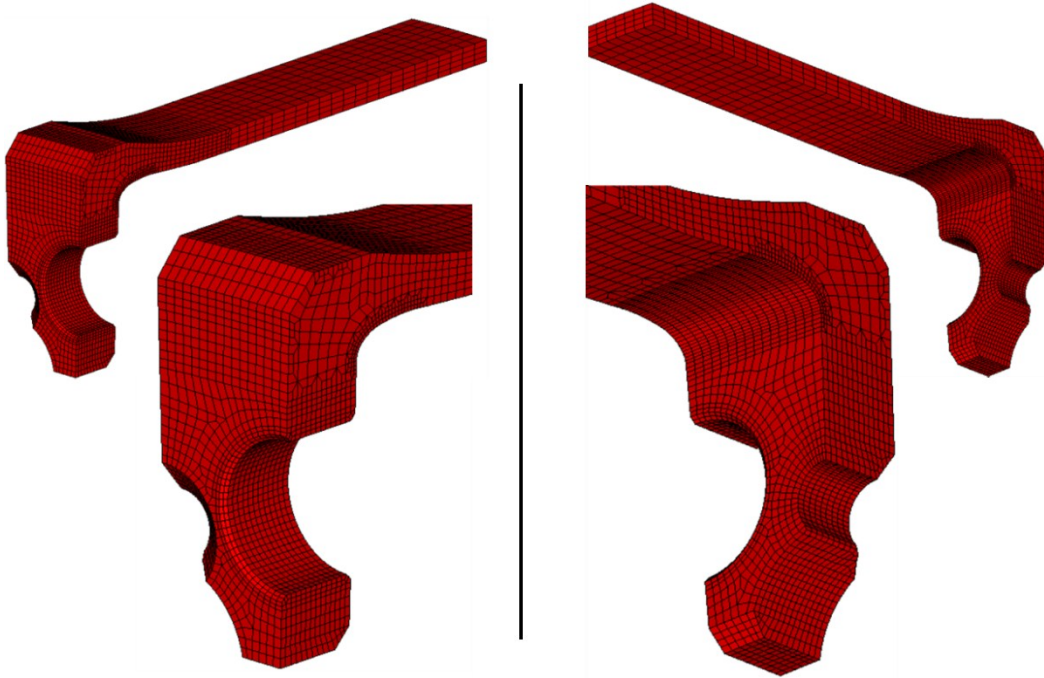
Figure 11: HPT Front Shaft Mesh

An identical mesh with the same elements and nodes for these three LLP's are used for each analysis case. By maintaining an identical mesh, differences in the mesh can be excluded as a factor that can affect the results. Also, because the same element and node numbers are used, delta plots comparing the difference in results can be made. The one exception to this rule is the analysis case that uses helical threads. As mentioned earlier, the helically threaded analysis case sector size is twice that of the other cases. The compressor spool, CDP seal, and HPT front shaft mesh is doubled by reflecting the mesh across the sector plane with the bolt hole.

As per the intent of the thesis, the modeling of the bolt and the nut interface vary from case to case. Four significantly unique mesh configurations are used. Each of the eleven analysis cases uses one of the four mesh configurations, or some

minor variation of it. The four mesh configurations have element counts ranging from 24,930 to 136,422 elements.

Figures 12-14 show the mesh configuration where the threads are explicitly modeled with a fine mesh. The thread geometry is accurately captured, modeled per SAE Aerospace Standard AS8879 Revision D [15].
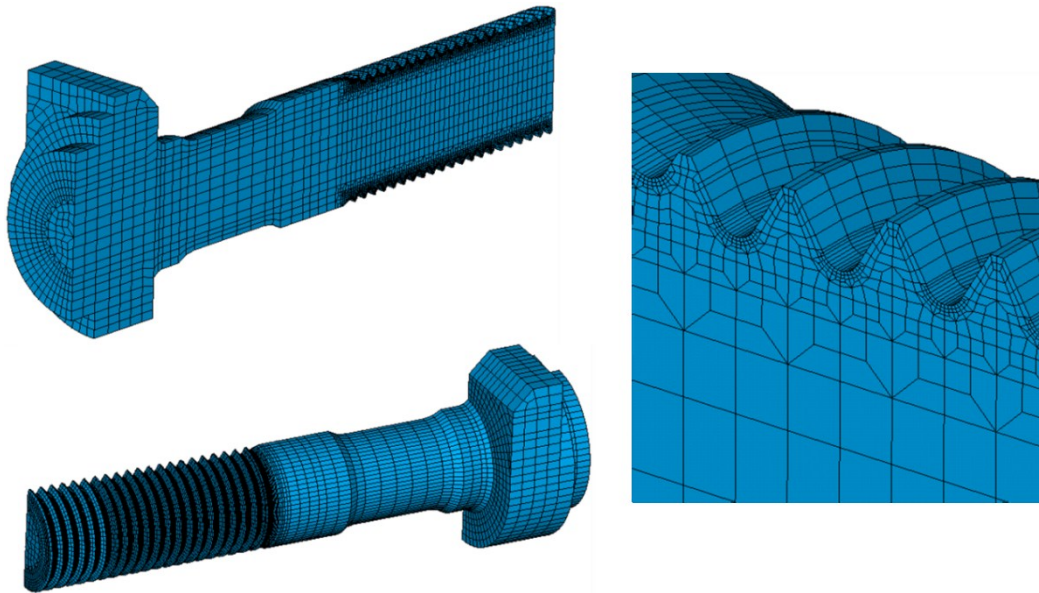
Figure 12: Fine Bolt Thread Mesh
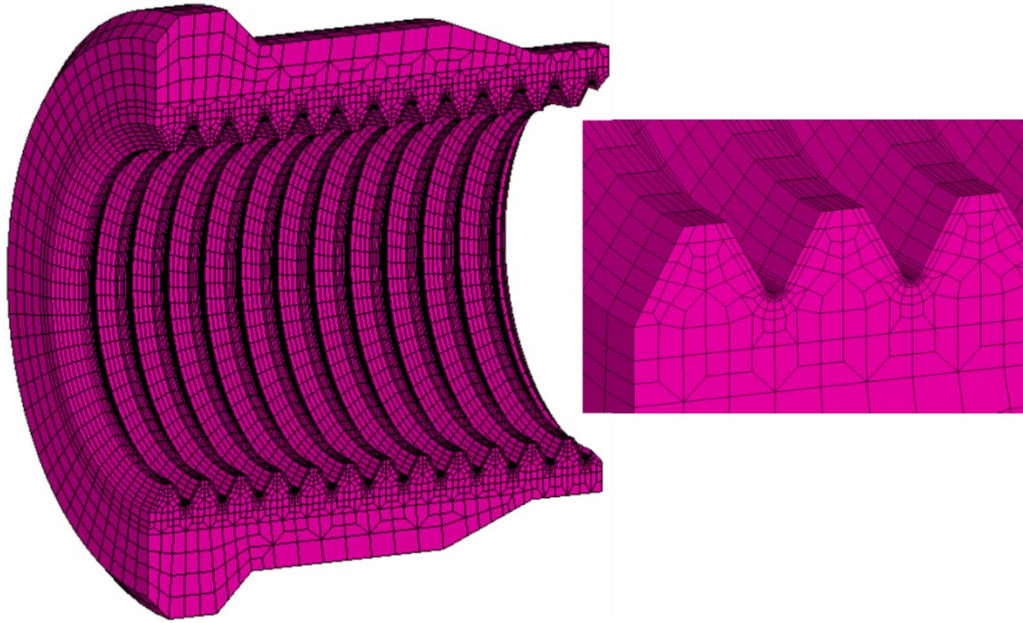
Figure 13: Fine Nut Thread Mesh
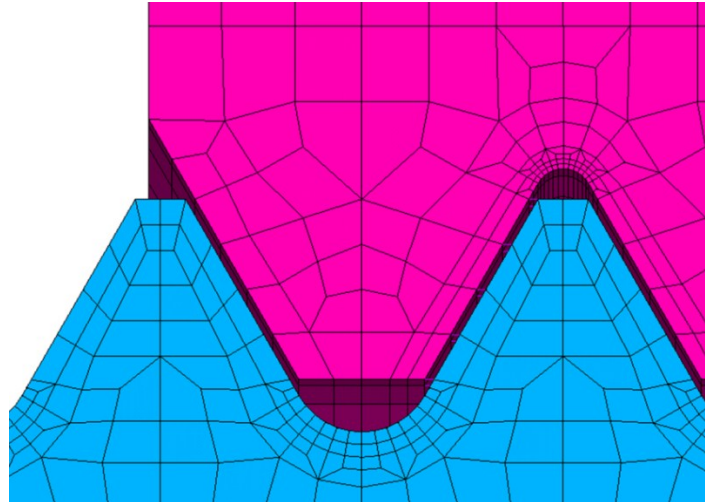
Figure 14: Fine Thread Mesh

The other four mesh configurations are composed of a mesh where threads are not explicitly modeled, a coarse threaded mesh, and a coarse helically shaped thread

mesh. Figure 15 contains pictures of the four configurations of assembled bolt

and nut mesh.
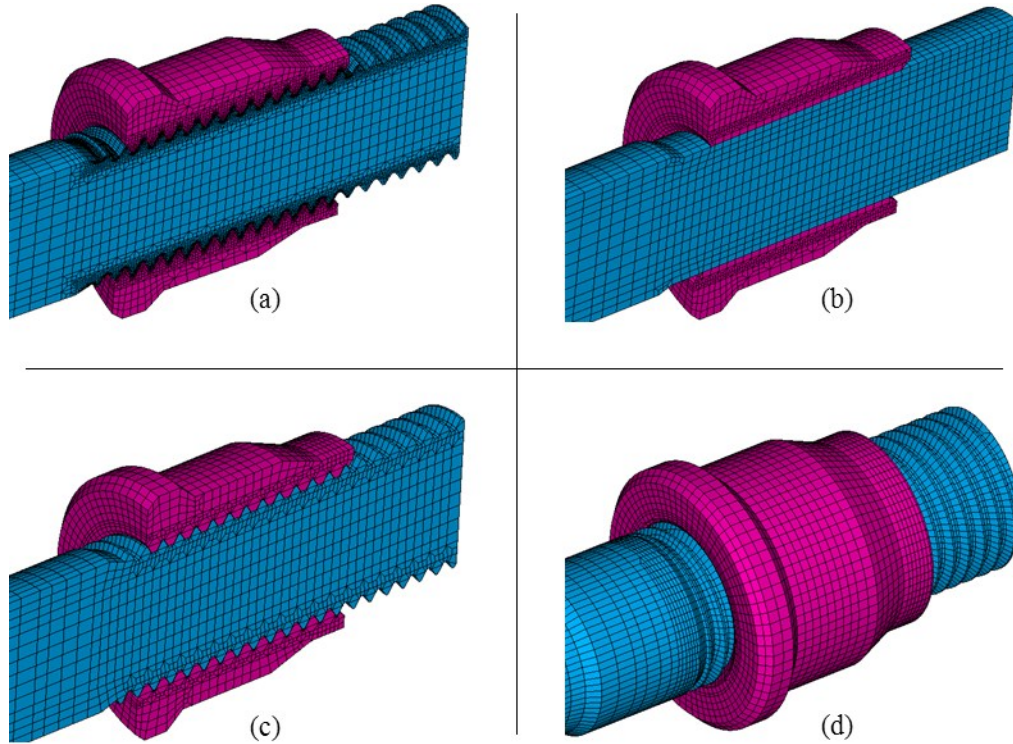
Figure 15: Thread Mesh Configurations – (a) Fine Thread Mesh, (b) Threads Not Explicitly Modeled, (c) Coarse Thread Mesh, (d) Helically Shaped Thread Mesh

All five parts of the joint are modeled with ANSYS SOLID45 3D hexagonal

elements. However, the study cases that include helically shaped threads have a

mixture of SOLID45 3D hexagonal elements, SOLID92 3D high-order tetrahedral

elements, and SOLID95 3D five-sided transitional pyramid elements in the bolt

and nut. The complex helical shape makes it extremely difficult and impractical

to create a purely SOLID45 hexagonal mesh. Figure 16 shows a cut-away of the

helically threaded mesh, exposing the internal tetrahedral and pyramid elements.
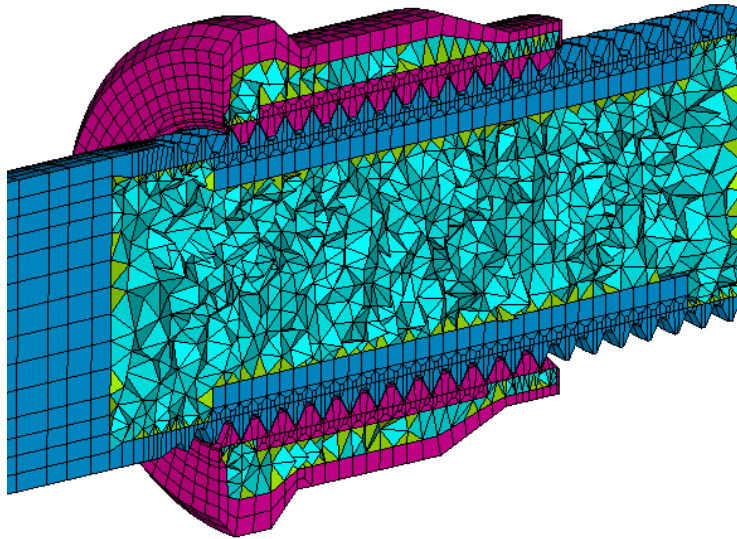
**Figure 16: Cut-away of helical thread mesh, exposing internal
tetrahedral and pyramid elements**

CONTAC173 and TARGET170 surface-to-surface gap elements are used at all
interfaces except at the thread interface. Surface-to-surface gap elements are
chosen because of two specific advantages. First, they do not require node
alignment which eases the meshing process. This helps to reduce the meshing
time and the element count, which also reduces the computational time. Second,
as interfaces slide, surface-to-surface contact appropriately adjusts to account for
the updated relative positions of the two parts. For point-to-point contact, this is
not the case. Each node feels contact with its initially aligned paired node
regardless of the alignment after the parts have moved relative to each other.
However, point-to-point CONTAC52 elements were chosen for the thread
interface for the cases that use contact in this region. In highly-curved surfaces,
like the highly-curved circumferential direction around the bolt, surface-to-

20

surface gap elements produce a faceted-like contact pattern. To limit the faceted effect, the mesh in the circumferential direction in the thread contact area would need to be extremely fine. This is not practical due to the high element count it would produce.

Representative pictures of the assembled mesh for one of the 3.75 degree configuration models and for the helically threaded 7.5 degree model is shown in Figures 17 and 18.
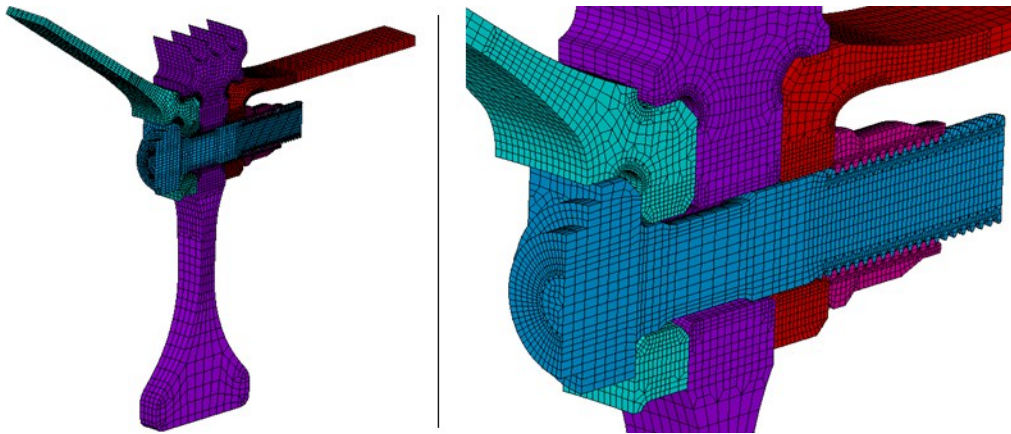
Figure 17: 3.75 Degree Model
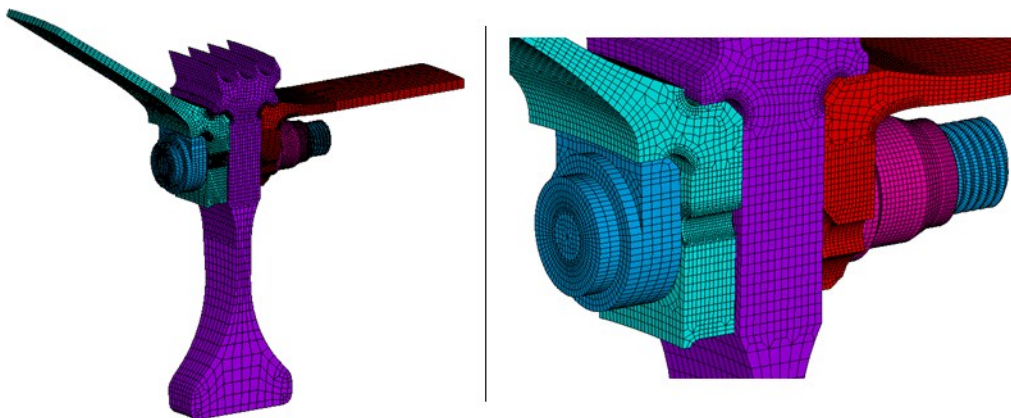
Figure 18: 7.5 Degree Model, Used for Helical Cases

2.4 Analysis Assumptions

Reflective symmetry is applied on the two sector surfaces of the 3.75 degree model. This is achieved by rotating the nodes at these faces to a cylindrical system and applying zero circumferential displacements on each node.

For the helical thread cases where a full bolt is modeled, repeatable symmetry is applied instead. Reflective symmetry would likely produce similar results, however, the reflective assumption would suggest that the nuts on the 360 degree bolted joint would alternate between tightening in clock-wise and in a counter-clock-wise direction. To achieve repeatable symmetry, the nodes at the model sector planes are rotated into a cylindrical system. Next, each sector plane node is coupled to the corresponding node on the opposing sector plane in the radial, hoop, and axial directions.

The 3.75 degree model contains one half of a bolt hole and one half of a scallop. The 7.5 degree model contains a full bolt hole and two halved scallops.

During typical engine operation, stress in the bolted joint is caused by four types of loadings. The first and most significant load is the rotational speed. For this study, a typical take-off speed for this application of 14,775 RPM is used. The second load is the temperature, which causes thermal stress and decreases the material stiffness. The analysis cases performed in this study do not include the effects of temperature. A uniform 70° F temperature is used for all analysis cases. The assumption is that the relative comparison from one analysis case to the next

without temperature would hold true even if temperature is applied. A follow-on study verifying the appropriateness of this assumption is included in this thesis. The follow-on study also quantifies the magnitude of the thermal stress relative to the speed stress. The third type of loading is from the pressure delta between pressure cavities. Finally the fourth type of loading is the axial tension in the joint due to the turbine pull. As the turbine is spun by high energy air leaving the combustor, the turbine is also loaded in the aft direction, creating the turbine pull. The load from pressure and the turbine pull are ignored in this study. The stress created by these loads is small when compared to the speed-induced stress.

A single node in the bore is set to have a zero axial displacement and zero circumferential displacement, preventing rigid body motion in the model. Radial rigid body motion is not an issue as the part is naturally constrained in the radial direction by the symmetry constraints on the two sector surfaces.

A small pressure value of 1E-9 psi is applied to all exterior surfaces. ANSYS requires a pressure load on surfaces to extract surface stress. The intent of applying a very small pressure is to allow surface stress extraction while not impacting the results.

The clamp load in the half-bolt is set to 4,600 lbs. This is done by setting an interference in the contact elements between the nut face and the HPT front shaft flange. The inputted interference value varies from case to case to match the desired 4,600 lbs load because the bolt and nut stiffness is dependent upon the thread modeling assumptions. For all the analysis cases, the interference range is

between 0.0050 and 0.0058 inch. For the helically threaded cases which use a full

bolt, the clamp load is set to 9,200 lbs.

Friction is included in this study because friction tends to have a significant effect

on calculated stress in features near hardware interfaces. A frictional value of

0.55 is assumed in this study for all Inconel 718$^®$ / Inconel 718$^®$ interfaces. This

accounts for all interfaces except the nut / HPT front shaft and the nut / bolt

interface. These interfaces are Waspaloy$^®$ / Inconel 718$^®$ interfaces and use a

frictional value of 0.45. Thread friction sensitivity is addressed through an

analysis case where a frictional value of 0.25 is assumed in the thread interface.

When friction is included in an analysis, that analysis becomes path-dependent.

The result of a particular load case is dependent upon the starting position of the

hardware from the previous load case. For this study, the models were run to

speed and assembly load cases through two cycles of a simple transient. The first

cycle allows the interfaces to slide and adjust into a cyclically stable position. All

results used in this thesis are from the cyclically-stable second cycle, circled in

orange in Figure 19.
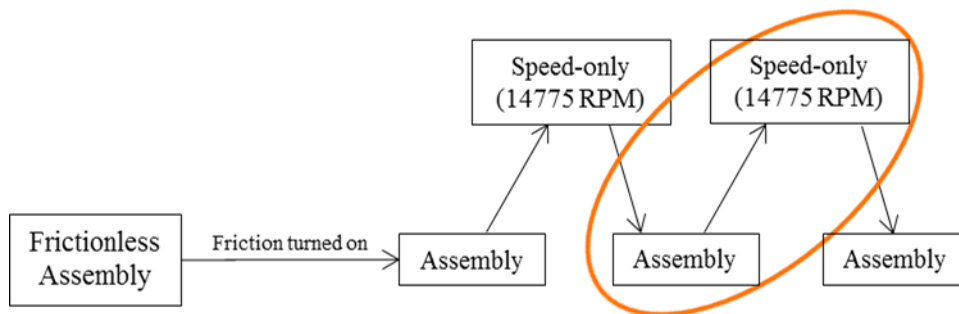
Figure 19: Analysis Path

24

The final assembly time point was run to verify that cycle stability was achieved. In all cases, the results from the final assembly are similar to the results of the assembly that preceded it, indicating that cycle stability has been achieved.

In the initial frictionless assembly case, the bolt is centered in the bolt hole and attached to the top of HPT front shaft hole in the radial direction with a single radial couple, as shown in Figure 20. The couple prevents rigid body motion and also enforces an assumption that the bolt starts in a centered position in the hole. The reflective symmetry plane on the half-bolt prevents rigid body motion in the circumferential direction and rigid body rotation about the centerline of the bolt. Once friction is turned on, the couple is removed. Friction prevents any rigid body motion or rotation.
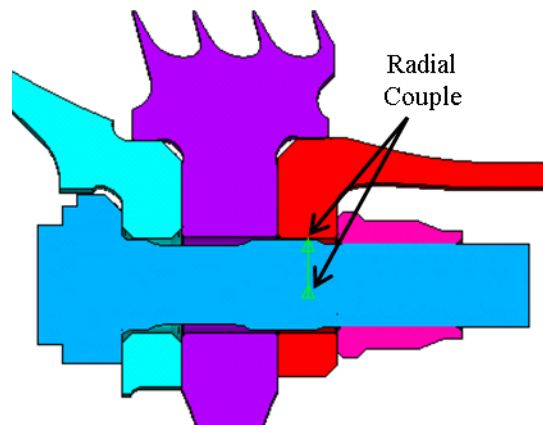
Figure 20: Radial Couple, Centers Bolt and Prevents Rigid Body Motion

For the helically threaded cases where a full bolt is modeled, more constraints are required in the initial frictionless assembly. In addition to the radial couple, a single couple in the circumferential direction between the bolt and the HPT front

25

shaft bolt hole is applied. These two couples prevent bolt rigid body motion in the radial and circumferential direction. Two more sets of couples are required to prevent the bolt from rotating about the centerline of the hole and the nut from unwinding off the bolt. The bolt has a circumferential couple between two nodes near the top and bottom of the bolt. The nut has a circumferential couple between two nodes near the top and the bottom of the nut. Just as was done for half bolt configuration, these couples are removed once friction is turned on.
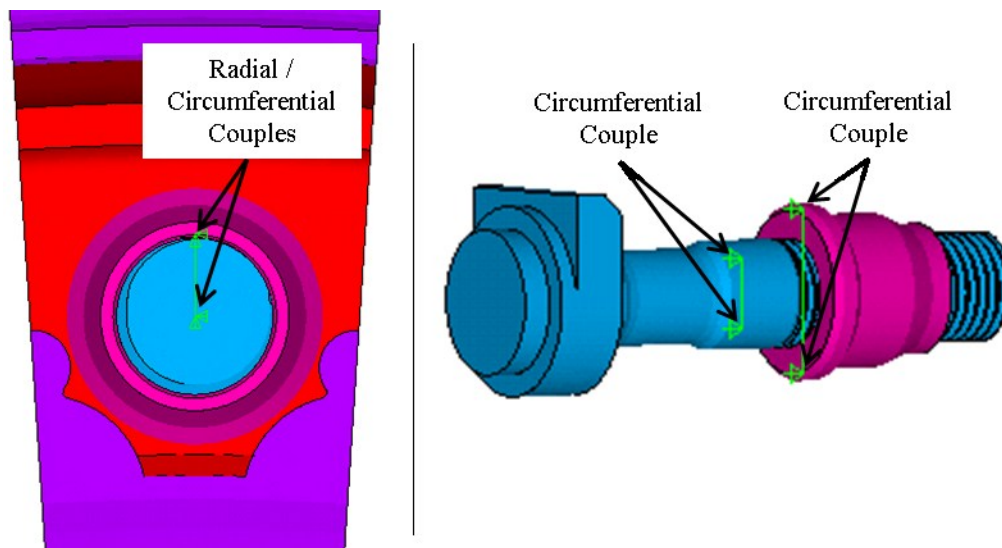
Figure 21: Additional Couples Preventing Rigid Body Motion

2.5 Analysis Cases

A series of analysis cases are presented in this study. These cases have been selected to address a range of assumptions one could make while deciding how to model a bolt/nut interface. This study addresses the following modeling choices:

1) Explicit inclusion of threads – Should the threads be explicitly modeled, or can one model the bolt and nut to the pitch diameter and simply join the two parts?

2) Couples vs contact elements – If the threads are modeled explicitly, should contact elements be included at the interface or are couples sufficient? If couples are sufficient, how do the coupling methods affect the results?

3) Mesh quality – Is a coarse thread mesh adequate or does it need to be fine?

4) Elastic vs elastic/plastic material properties in the threads – Are elastic material properties in the thread adequate or should elastic/plastic material properties be included?

5) Helical thread shape – Is it necessary to model the helical shape or can the helix be simplified into circular rings? If the helix is included, does the angular orientation of the helix have an impact on the results?

6) Starting thread thickness – If a circular thread is modeled, does it matter if the first circular thread is modeled as a full or partial thread?

7) Thread friction coefficient – What is the sensitivity of the friction coefficient used at the thread interface?

To address these modeling choices, eleven analysis cases have been selected. The eleven cases are as follows:

1) Threads excluded from the model, bolt/nut modeled to pitch diameter, node pairs coupled at pitch diameter, elastic material properties.
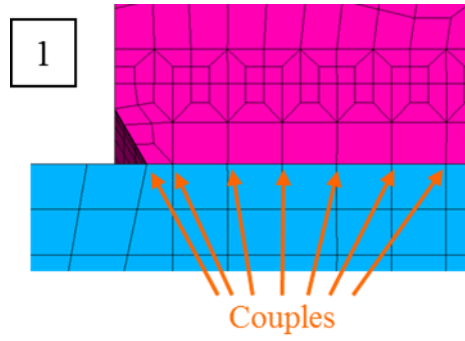
Figure 22: Analysis Case 1

2) Coarsely meshed circular threads, elastic material properties, couples along the thread contact faces on both sides of the thread.
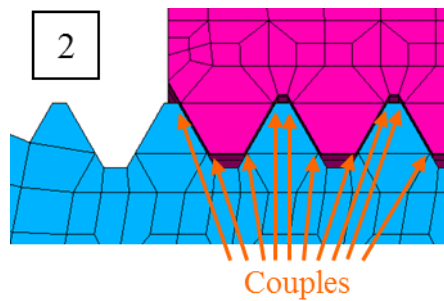
Figure 23: Analysis Case 2

3) Coarsely meshed circular threads, elastic material properties, couples only along the loaded thread contact faces.
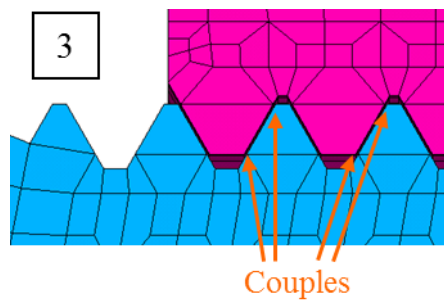
Figure 24: Analysis Case 3

28

4) Threads excluded from the model, bolt/nut modeled to pitch diameter, node pairs coupled at pitch diameter, elastic material properties. First thread couple aligned with the location of the first loaded thread surface.
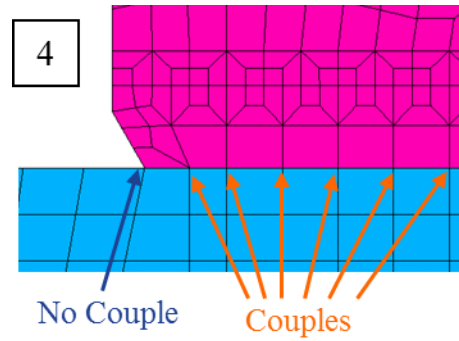
Figure 25: Analysis Case 4

5) Coarsely meshed circular threads, elastic material properties, contact elements with mu=0.45 friction at the contact interfaces.
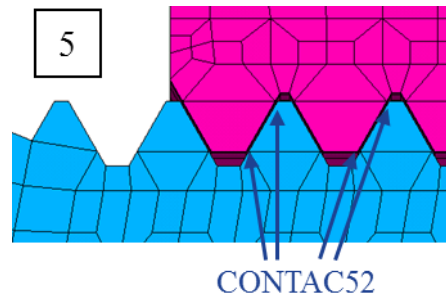
Figure 26: Analysis Case 5

6) Finely meshed circular threads, elastic material properties, contact elements with mu=0.45 friction at the contact interfaces.
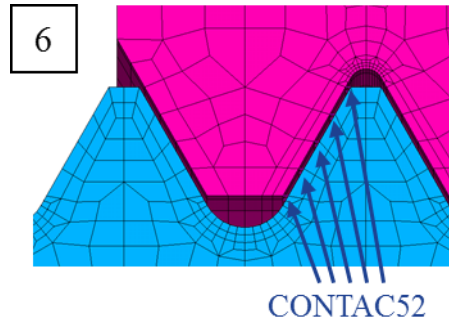
Figure 27; Analysis Case 6

7) Finely meshed circular threads, elastic/plastic material properties, contact elements with mu=0.45 friction at the contact interfaces.
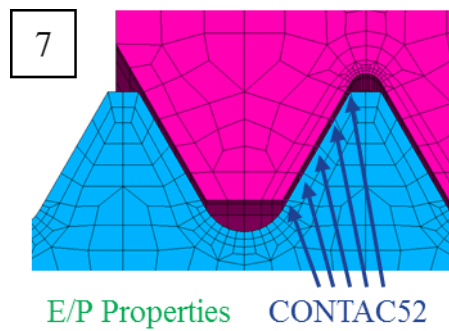
Figure 28: Analysis Case 7

8) Coarsely meshed helical threads, elastic material properties, contact elements with mu=0.45 friction at the contact interfaces.

Figure 29: Analysis Case 8

9) Coarsely meshed helical threads rotated 180 degrees about the centerline of the bolt, making the thread contact begin at the bottom of the bolt. Elastic material properties, contact elements with mu=0.45 friction at the contact interfaces.
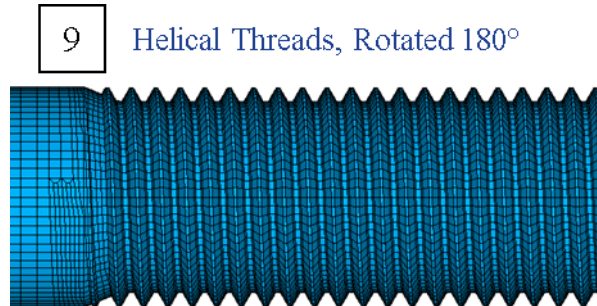
Figure 30: Analysis Case 9

10) Coarsely meshed circular threads with a partial first thread, elastic material properties, contact elements with mu=0.45 friction at the contact interfaces.
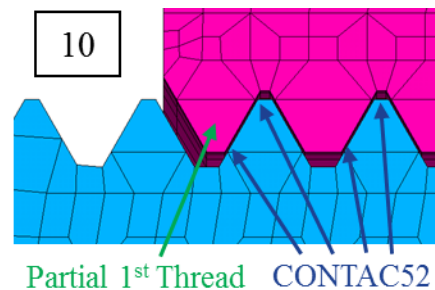
Figure 31: Analysis Case 10

11) Coarsely meshed circular threads, elastic material properties, contact elements with reduced mu=0.25 friction at the contact interfaces.
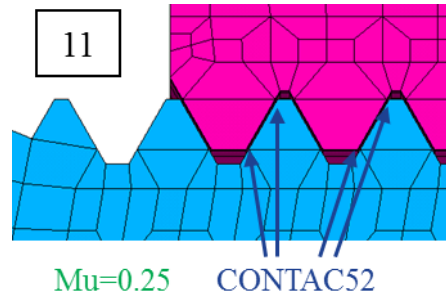
Figure 32: Analysis Case 11

Chapter 3: Governing Equations

Von-Mises effective stress is the fatigue failure theory used in this study [16]. The general Von-Mises effective stress equation is defined as follows

$$\sigma_{eff} = \frac{1}{\sqrt{2}}\sqrt{(\sigma_x - \sigma_y)^2 + (\sigma_y - \sigma_z)^2 + (\sigma_z - \sigma_x)^2 + 6(\tau_{xy} + \tau_{yz} + \tau_{zx})^2}$$

All the locations of interest in this study are located on the surface of the hardware. Conveniently, stress on the surface can be simplified into three in-plane components - σ_x, σ_y, τ_{xy}. This simplifies the Von-Mises effective stress equation

$$\sigma_{eff} = \sqrt{\sigma_x^2 - \sigma_x\sigma_y + \sigma_y^2 + 3\tau_{xy}^2}$$

The equation above appropriately captures the effective stress range when the minimum stress is zero. Often this is not the case. When the minimum stress is not zero, the effective stress range can be calculated as follows:

$$\Delta\sigma_{eff} = \sqrt{\Delta\sigma_x^2 - \Delta\sigma_x\Delta\sigma_y + \Delta\sigma_y^2 + 3\Delta\tau_{xy}^2}$$

where

$$\Delta\sigma_x = \sigma_{x1} - \sigma_{x2}, \quad \Delta\sigma_y = \sigma_{y1} - \sigma_{y2}, \quad \Delta\tau_{xy} = \tau_{xy1} - \tau_{xy2}$$

33

The effective stress range is an important component in fatigue life calculation, however it is not the only stress to consider. The mean stress is also relevant. For example, test bar A is cyclically loaded in uniaxial tension between 0 and 100 ksi. Test bar B is cyclically loaded in uniaxial tension between 50 and 150 ksi. Test bar A and B both are loaded with effective stress ranges of 100 ksi. However, test bar B would fail in fatigue first due to the higher mean stress.

The mean stress can be calculated as follows:

$$\sigma_{mean} = \frac{s}{2}\sqrt{\Sigma\sigma_x{}^2 - \Sigma\sigma_x\Sigma\sigma_y + \Sigma\sigma_y{}^2 + 3\Sigma\tau_{xy}{}^2}$$

where

$$\Sigma\sigma_x = \sigma_{x1} + \sigma_{x2}, \quad \Sigma\sigma_y = \sigma_{y1} + \sigma_{y2}, \quad \Sigma\tau_{xy} = \tau_{xy1} + \tau_{xy2}$$

$$s = sign(\Sigma\sigma_x + \Sigma\sigma_y) \qquad (positive\ or\ negative)$$

Figure 33 diagrams $\Delta\sigma_{eff}$, and σ_{mean} in cyclic loading. The figure also introduces σ_{alt}, σ_{max}, and σ_{min}
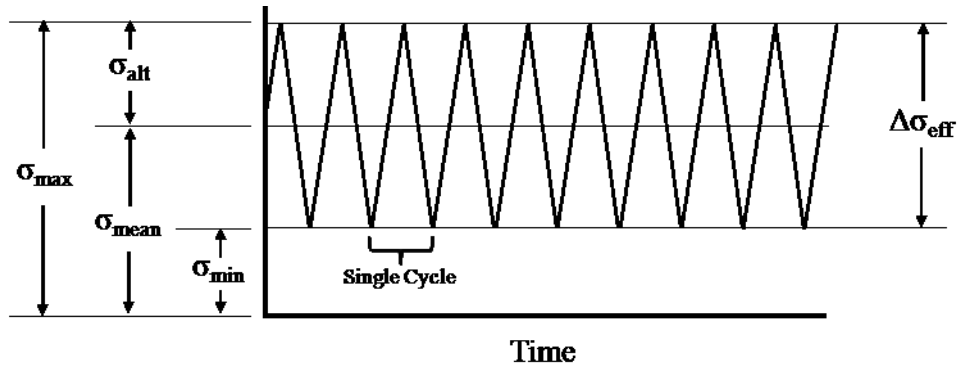
Figure 33: Cyclic Loading

σ_{alt}, σ_{max}, and σ_{min} are defined as follows.

$$\sigma_{alt} = \frac{\Delta\sigma_{eff}}{2}$$

$$\sigma_{max} = \sigma_{mean} + \frac{\Delta\sigma_{eff}}{2}$$

$$\sigma_{min} = \sigma_{mean} - \frac{\Delta\sigma_{eff}}{2}$$

From these three terms, the "A" ratio and the "R" ratio are established

$$A = \frac{\sigma_{alt}}{\sigma_{mean}} \qquad\qquad R = \frac{\sigma_{min}}{\sigma_{max}}$$

Fatigue testing is sometimes performed in conditions where the "A" ratio is 1.
The test specimen is cycled from a fully loaded condition to a fully unloaded
condition. The minimum stress is zero, which makes σ_{alt} and σ_{mean} equal to each
other. When the "A" ratio equals 1, the "R" ratio equals 0. Figure 34 diagrams
the case where the "A" ratio equals 1.

35
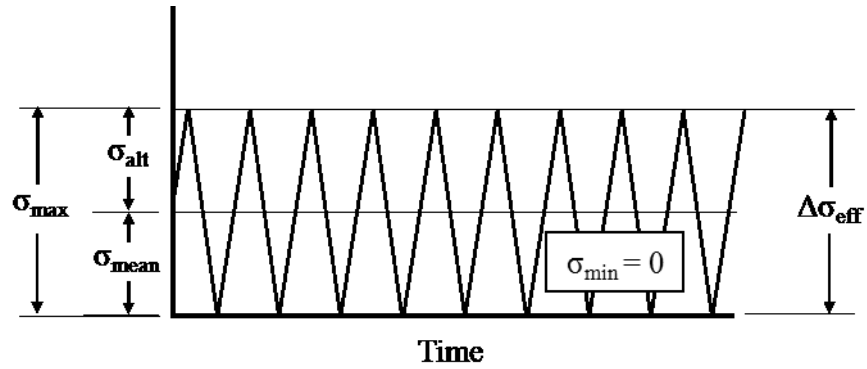
Figure 34: Cyclic Loading, "A" Ratio Equals 1

In many real applications, the min stress is not zero. The Walker Power-Law relationship allows the conversion into an equivalent stress in which the "A" ratio equals 1.

$$\sigma_{0,max} = \sigma_{R,max}(1-R)^m$$

where

$$\sigma_{0,max} = maximum\ stress\ when\ R\ equals\ zero$$

$$\sigma_{R,max} = maximum\ stress\ at\ some\ other\ "R"\ ratio$$

$$m = emperical\ constant, calculated\ from\ fatigue\ test\ data\ over\ a\ range\ of\ "A"\ ratios$$

Finally, the Walker-adjusted alternating stress, $\sigma_{0,alt}$, can be introduced.

$$\sigma_{0,alt} = \frac{\sigma_{0,max}}{2}$$

Figure 35 shows a stress distribution converted to an "A" ratio of 1 using the

Walker Power-Law relationship
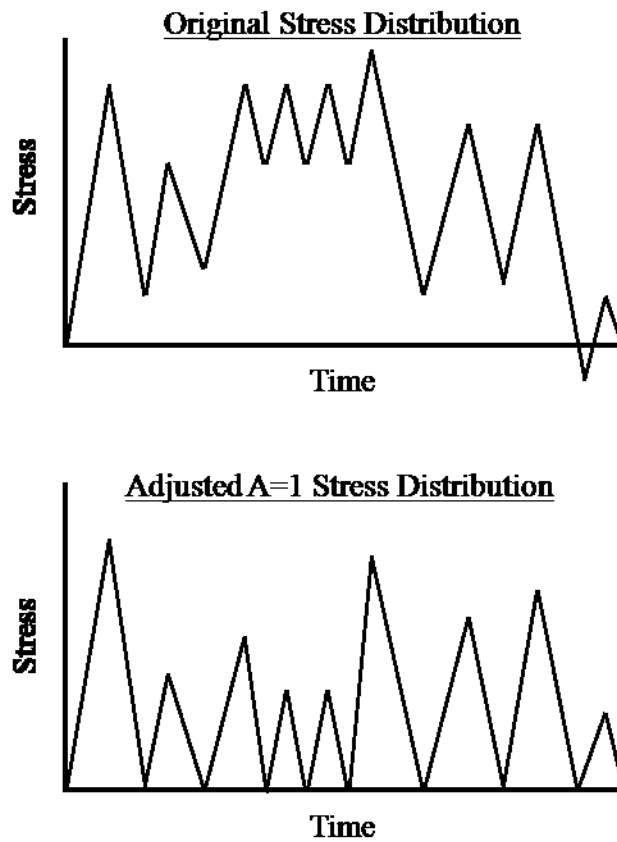
Figure 35: Conversion of Stress Profile to "A" Ratio Equals 1

This study focuses on the how analysis methods can impact calculated LCF life.

Calculated LCF life is a function of $\sigma_{0,alt}$, material, and temperature. Since

material and temperature are not varied in the analysis cases, $\sigma_{0,alt}$ is an

appropriate measurement tool to determine how calculated LCF life is impacted.

Chapter 4: Sample Set of Results

Sample plots showing stress results from the speed run for the spool, CDP seal, and HPT front shaft from analysis case 1 are shown in Figures 36-38.
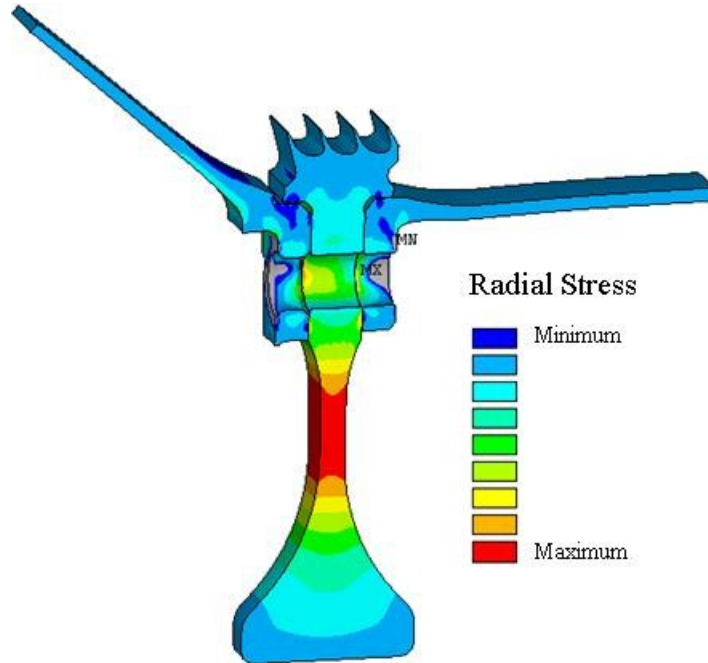
Figure 36: Radial Stress - Analysis Case 1, Speed Condition
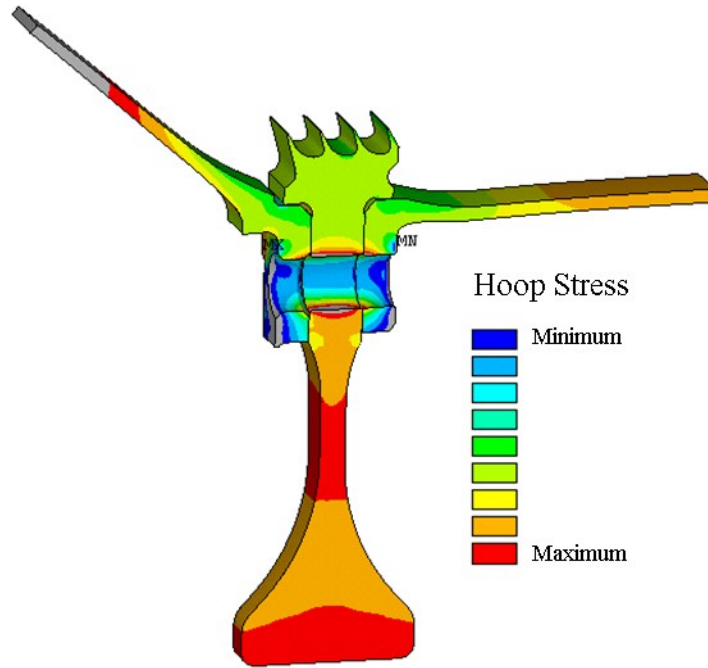
Figure 37: Hoop Stress - Analysis Case 1, Speed Condition
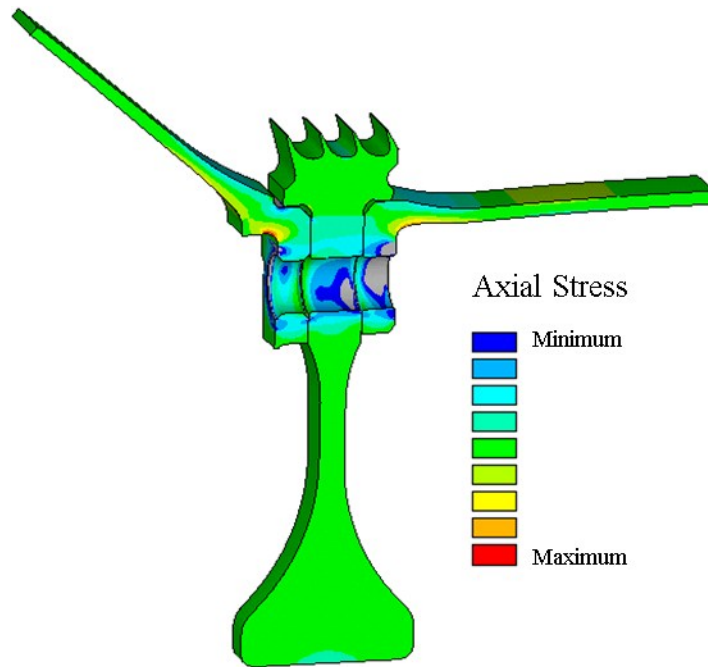
Figure 38: Axial Stress - Analysis Case 1, Speed Condition

A simple hand calculation is used to help validate the accuracy of the results. The

hoop stress in a rotating cylinder with a central hole (bore) can be calculated with

the following equation [17]:

$$\sigma_\theta = \frac{3+\upsilon}{8}\left(r_i^2 + r_o^2 + \frac{r_i^2 r_o^2}{r^2} - \frac{1+3\upsilon}{3+\upsilon}r^2\right)$$

In this equation υ is the Poisson ratio, r_i is the inner radius, and r_o is the outer

radius. This equation can calculate hoop stress, σ_θ, for any radial position, r. The

analysis produces CDP seal bore hoop stress that is 12% higher than the hand

calculation. The higher analytical result is not surprising. The CDP seal has

additional loading from the bolt and nut centrifugal loads. Also the bolt hole in

the CDP seal and the scallops on the spool flange and HPT front shaft flange

reduce the hoop carrying capacity of these regions. These factors cause the hoop

stress in the CDP seal bore to be greater than the hand calculation.

Later in the thesis, stress comparisons from case to case will direct the focus to

the HPT front shaft scallop and bolt hole. The stress results will show the largest

difference in these two features. At this point, it is helpful to take a closer look at

the component stresses to give the reader a better understanding of the stress field

in these features. Plots of the radial, hoop, and axial stress are shown for the

speed time point for analysis case 1.

In the HPT front shaft bolt hole, the top of the hole is the low life area. The stress

at the bottom of the hole is low because the scallop provides shielding from hoop

stress. The side of the hole also has relatively low stress and high life. The focus therefore is on the top of the hole.

As one would expect, a plot of the radial stress (Figure 39) reveals no radial stress at the top of the hole. The top of the hole is a free surface, and therefore has no stress in the direction normal to its surface. If the bolt and nut centrifugal load was greater than the frictional carrying capacity of the bolt head and nut on their respective flanges due to insufficient clamp load, the bolt and nut would slide radially outward at speed and apply radial load at the top of the hole. In this bolted joint, however, no radial stress is induced, as the clamp load is sufficient to prevent the bolt and nut from sliding.
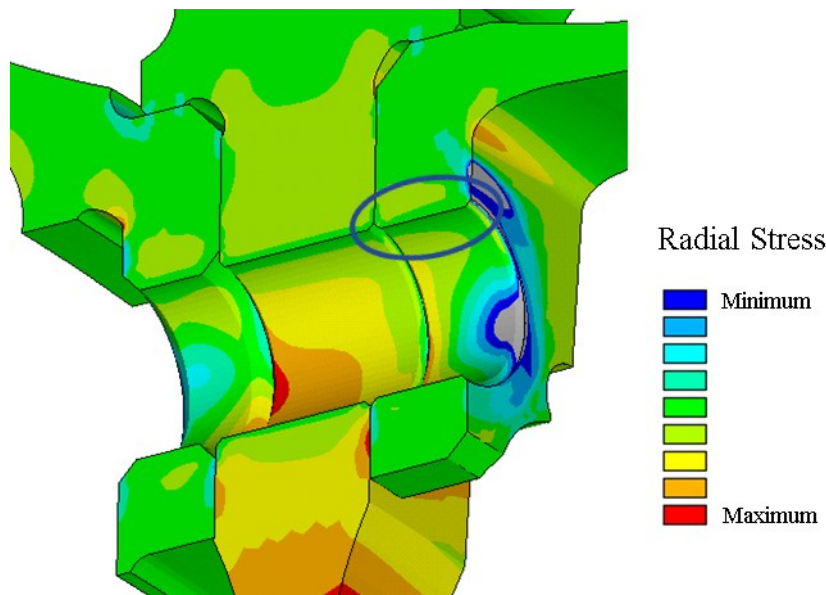
Figure 39: Radial Stress - Analysis Case 1, Speed Condition, Bolt Hole Sector Face View

The hoop stress is easily the dominant stress for this feature. As Figure 40 shows, the hoop stress in the HPT front shaft bolt hole peaks at the forward edge of the

hole. In fact, $\sigma_{0,alt}$ for the forward edge of the hole is nearly twice that of the aft

edge of the hole. However, as stress delta plots later in the thesis will reveal,

none of the stress components at the forward edge of the hole are significantly

impacted by the thread modeling assumptions. Therefore, the focus is directed to

the aft edge of the hole where stress differences exist from case to case. The hoop

stress at the aft edge of the hole is in tension at speed and in compression at

assembly.
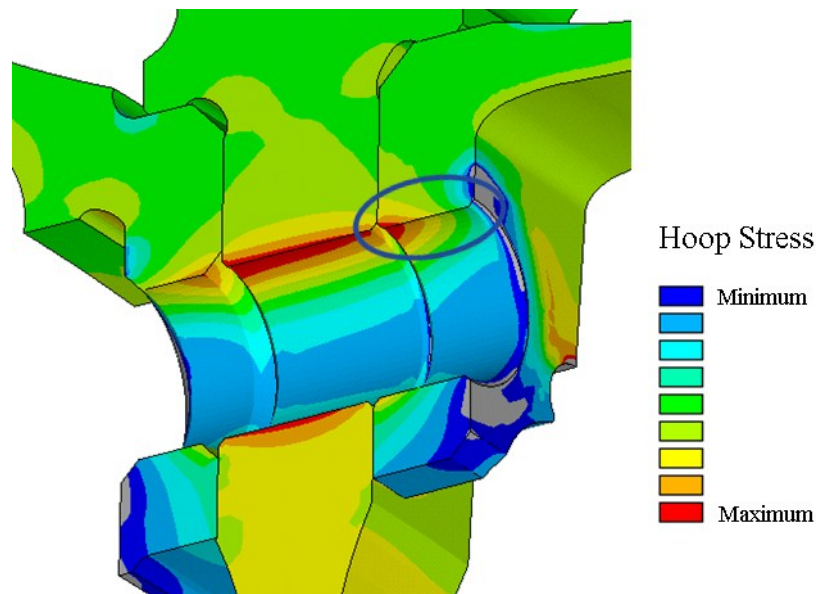
**Figure 40: Hoop Stress - Analysis Case 1, Speed Condition, Bolt
Hole Sector Face View**

The magnitude of the axial stress in the HPT front shaft bolt hole is less than the

hoop stress, but it is still a significant component. At the top of the bolt hole, the

stress is compressive due to the clamp load from the bolt and nut. Both the speed

case (Figure 41) and the assembly case (not shown) have compressive axial stress,

however the axial stress at speed is less compressive than at assembly. The

rotational speed radially stretches the CDP seal, thinning it axially in the bolt hole

area, which lowers the bolt clamp load and reduces the axial stress.
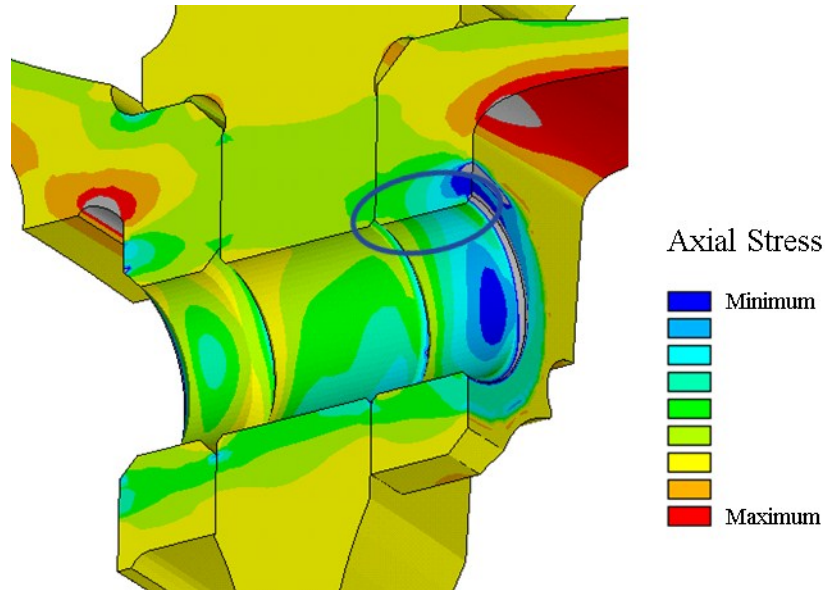
**Figure 41: Axial Stress - Analysis Case 1, Speed Condition, Bolt
Hole Sector Face View**

Similar to the bolt hole top, the HPT front shaft scallop is a free surface, so the

top of the scallop has no radial stress (Figure 42).
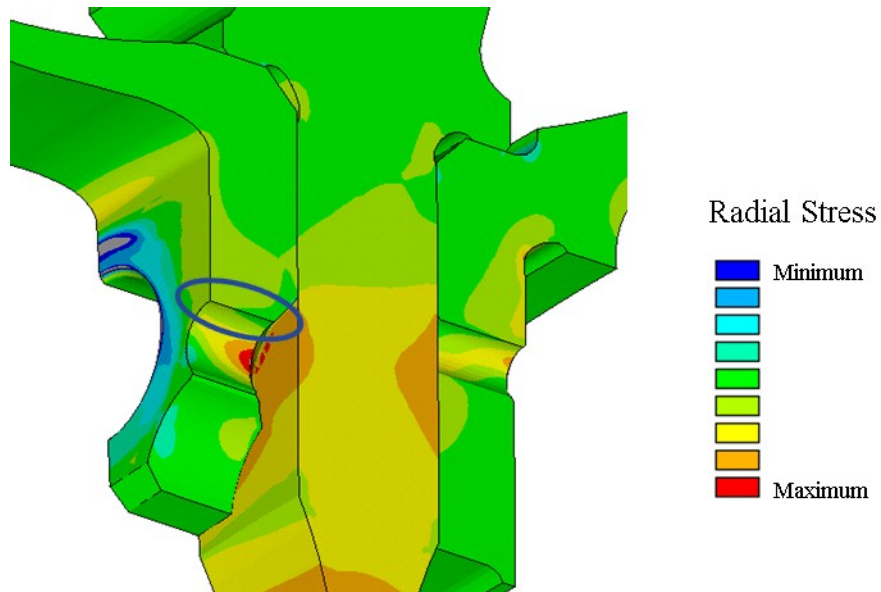
**Figure 42: Radial Stress - Analysis Case 1, Speed Condition,
Scallop Sector Face View**

The hoop stress is once again the dominant stress. However, for this feature the stress peaks at the aft edge of the scallop. $\sigma_{0,alt}$ is more than three times higher at the aft edge than the forward edge. At speed, as shown in Figure 43, the location is in hoop tension. At assembly (not shown), the scallop aft edge hoop stress is close to zero. Some of the eleven analysis cases at assembly show light hoop tension, some show light hoop compression.
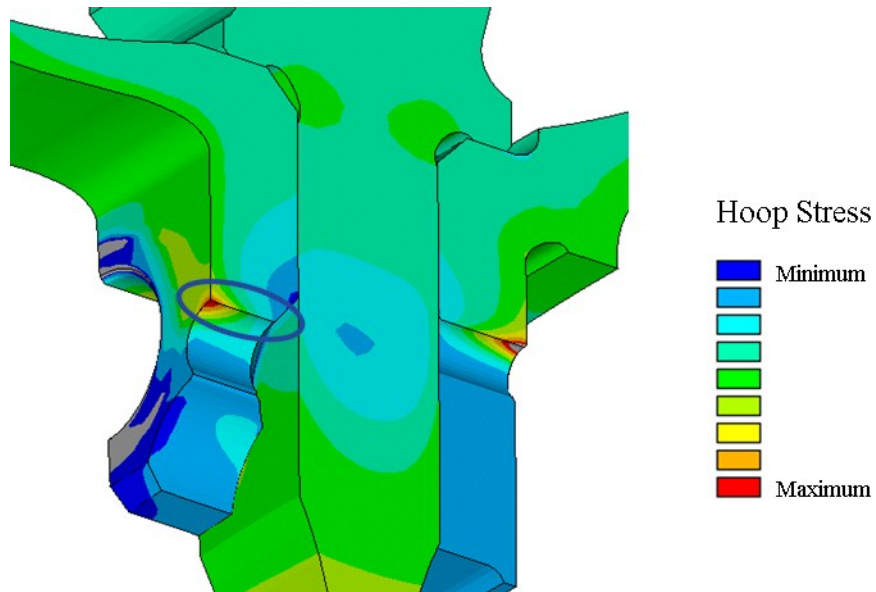
**Figure 43: Hoop Stress - Analysis Case 1, Speed Condition,
Scallop Sector Face View**

The aft edge of the scallop is also a free surface in the axial direction. The blue

and grey ring on the flange around the bolt hole in the axial stress plot, Figure 44,

signifies the compressive area where the nut makes contact with the flange. As

the reader can see, the scallop is close to the ring, but just outside of its diameter.

The scallop aft edge has a free surface in the axial direction. As such, the axial

stress at the aft edge of the scallop is zero.
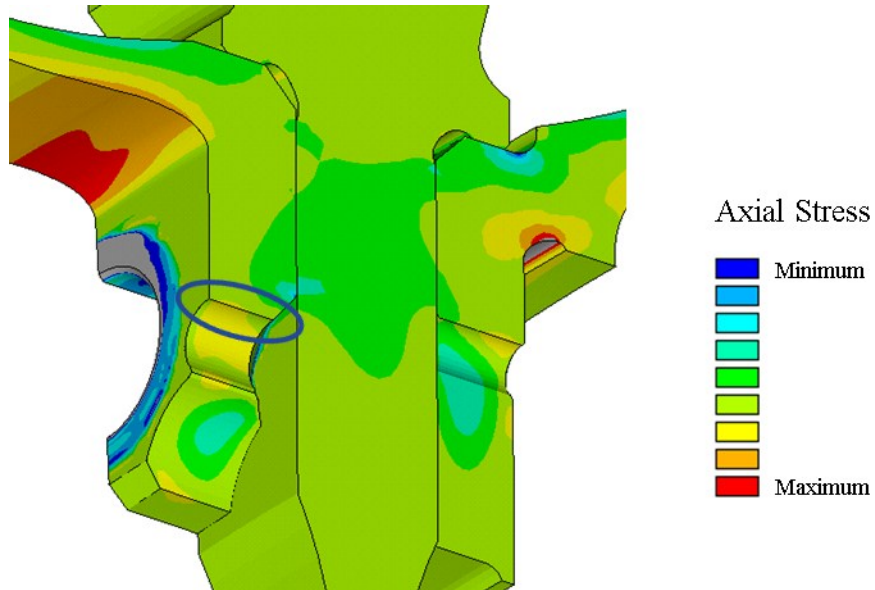
**Figure 44: Axial Stress - Analysis Case 1, Speed Condition,
Scallop Sector Face View**

Since there is no radial and axial stress at this location, the aft edge of the scallop

is in a simple uniaxial hoop stress field.

The $\sigma_{0,alt}$ for the aft edge HPT front shaft scallop is more than twice that of the aft

edge of the top of the bolt hole.

Chapter 5: Results Comparison & Discussion

5.1 Explicit Inclusion of Threads

One of the first decisions an analyst makes when considering how to model the bolt and nut in a bolted joint is whether or not to explicitly include the threads. Creating the CAD model and then later the mesh is significantly more challenging and time-consuming when the analyst creates the actual thread geometry. Also including the threads creates a higher element count, which adds computational time to the analysis and creates larger files. If the threads do not significantly impact the results, including them is a waste of computational time and effort.

Analysis cases 1 and 2 are compared to assess the impact of the explicit inclusion of threads.
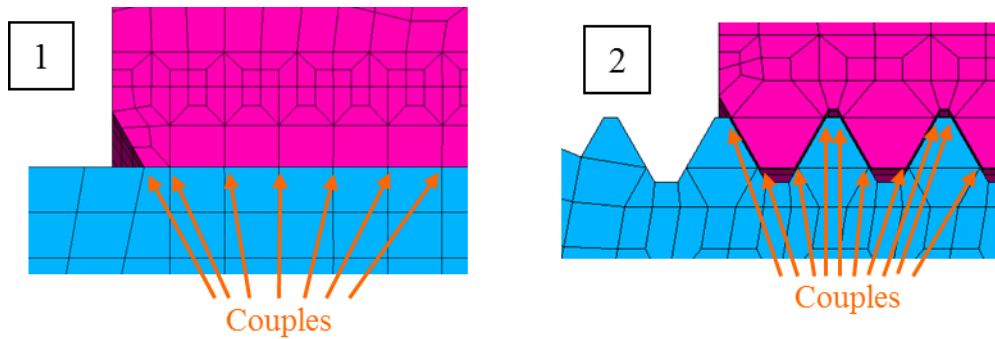
Figure 45: Comparison of Analysis Case 1 and 2

In case 1, the threads are not modeled. The outer diameter of the bolt and the inner diameter of the nut at the interface are set to the nominal thread pitch

diameter. The nodes at the interface are aligned. Each node pair is coupled in all three Cartesian directions, creating a fully bonded connection. Elastic material properties are used.

In case 2, the threads are modeled explicitly. The nominal thread cross-sectional geometry is modeled precisely to the thread specification. The helical shape is not included; the threads are modeled as circular rings. A coarse mesh is used. Couples join the bolt and nut at the threads. The material properties included in this case are elastic.

Delta stress plots compare the speed results from analysis cases 1 and 2. Figure 46 shows the equivalent stress difference of case 1 subtracted from case 2 with a view of the zero-degree sector plane of the model. It is important to recognize that ANSYS's method of calculating delta equivalent stress is to calculate an equivalent stress from the difference of the component stresses. ANSYS does not calculate equivalent stress from case 1 and subtract it from the equivalent stress from case 2. The plots are helpful for showing the locations where stress is different between the two cases. They do not show which results case has the greater stress. Upcoming plots of the individual component delta stresses will be more helpful in that regard.
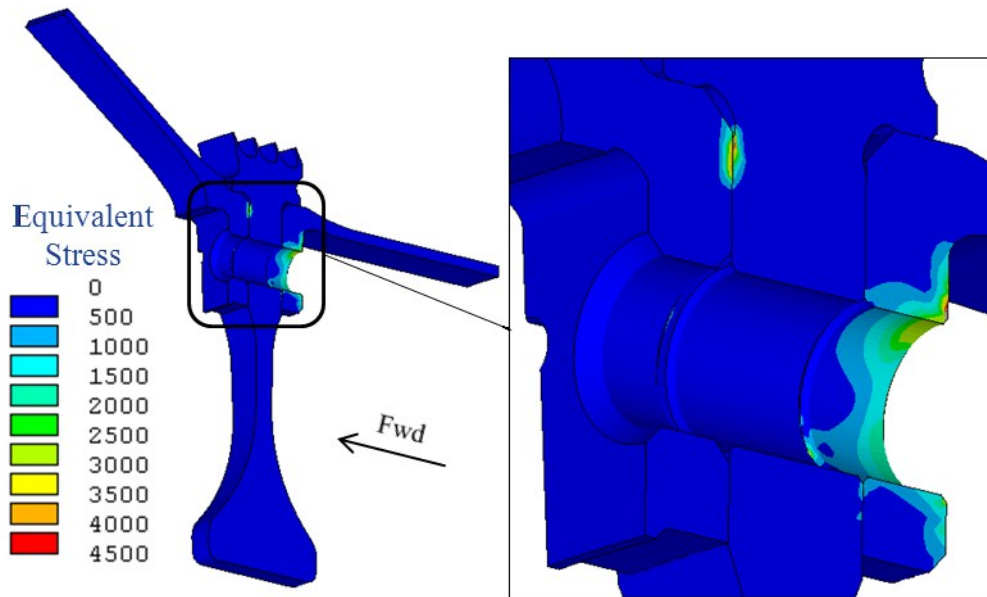
**Figure 46: Equivalent Stress Difference Plot (psi), Bolt Hole
Sector Face View**

Interestingly, these two cases produce similar stress in the vast majority of the

areas of the spool, CDP seal, and HPT front shaft. From what can be seen in this

view, the stress differences are limited to two areas. The most significant stress

differences occur at the HPT front shaft bole hole. The aft edge of the hole sees

the largest impact, which is logical since it is closest to threads. The stress

difference fades away; by the forward edge of the hole the difference is nearly

gone. The second area of stress difference can be seen is a local contact area at

the flange face between the spool arm and the CDP seal. This difference is

caused by a slightly different contact load pattern between these two models,

likely due to very small differences in displacement causing the displaced contact

elements to align slightly differently. The difference is a local contact

phenomenon and does not affect the stress in any critical regions in the hardware.

Figure 47 shows the stress differences from the 3.75 degree sector plane view.
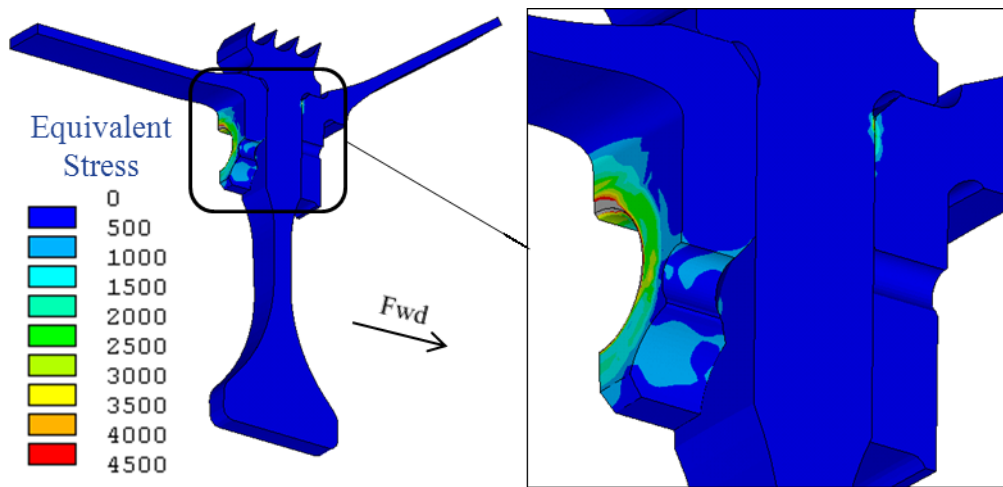
Figure 47: Equivalent Stress Difference Plot (psi), Scallop View

Once again, the stress differences seen in this view are limited to only a few local areas. The largest differences can be seen on the HPT front shaft flange face at the ring of contact with the nut. Not surprisingly, the difference in the thread modeling assumptions affects how the nut deforms and applies load to the flange face. A smaller stress difference can be seen at the HPT front shaft scallop. When comparing case 1 to case 2, the stress difference appears relatively small at the scallop. However, as will be seen later, the scallop is worthy of attention. Finally, the reader will also notice the same local contact stress difference at the flange contact area between the spool and CDP seal that was seen on the zero-degree plane. As mentioned earlier, this stress difference is a local contact difference that does not affect any critical LCF locations. Going forward it will be ignored.

Delta equivalent stress plots of all the cases that are discussed in this thesis produce a similar pattern as the comparison between case 1 and case 2. A few comparisons exhibit local contact hot spots, like what is seen on the flange face between the spool and CDP seal. Most cases show stress differences on the HPT front shaft at the nut contact ring, due to the variation in how the nut loads the flange. In all cases, the only two critical features that are significantly affected are the HPT front shaft bolt hole and scallop. Also, in all cases the stress difference is largest at the aft edge. Therefore, the focus of this thesis moving forward will be on stress impact on the aft edges of the HPT front shaft bolt hole and scallop.

Figure 48 shows delta component stress plots of the results of cases 1 and 2. These plots focus on the HPT front shaft bolt hole. Assembly and speed results are shown. Both time points are relevant because they both factor into the $\sigma_{0,alt}$ calculation. The plots show case 2 minus case 1.
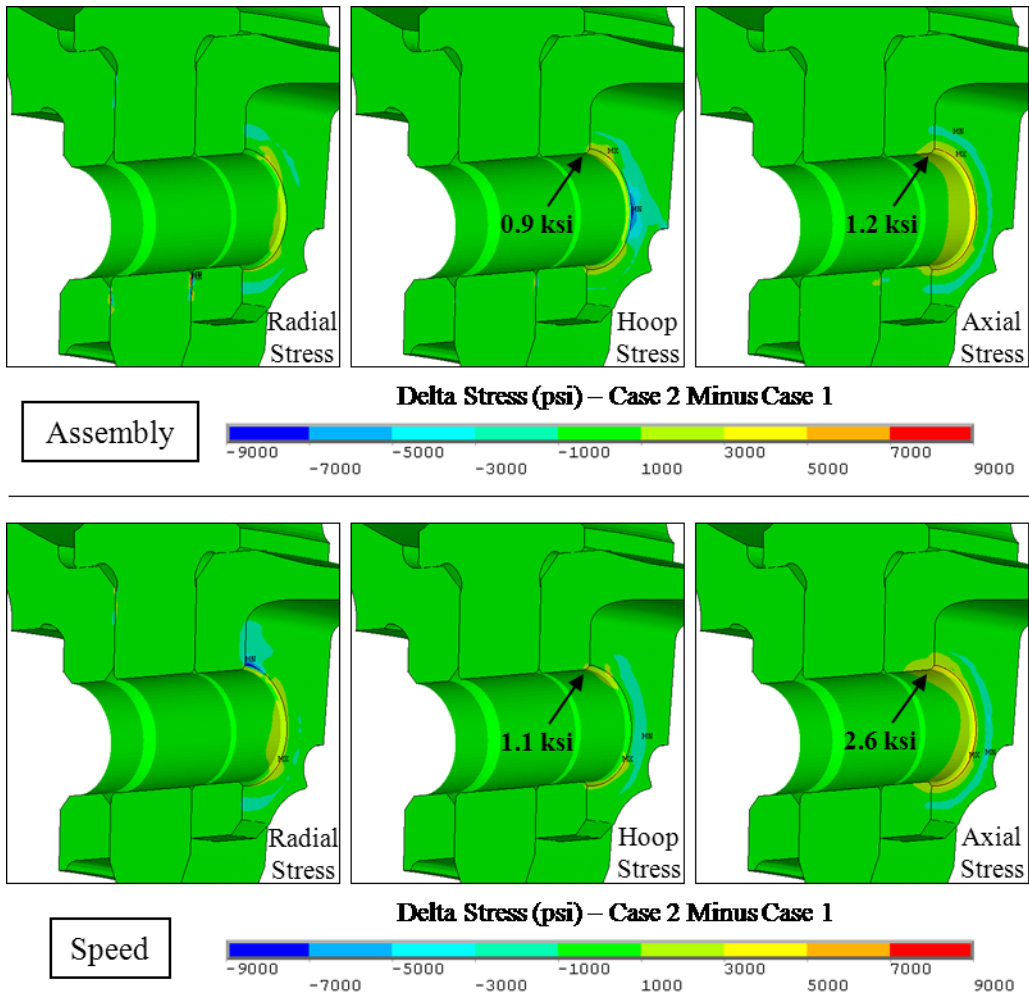
**Figure 48: Delta Stress (psi), Case 2 Minus Case 1, Bolt Hole
Sector Face View**

The inclusion of the threads has increased hoop stress in the aft side of the top of the bolt hole of the HPT front shaft by 0.9 ksi at assembly and 1.1 ksi at speed. The axial stress has also increased 1.2 ksi at assembly and 2.6 ksi at speed. Counter-intuitively, the increase in component stresses decreases the $\sigma_{0,alt}$ by 0.5 ksi, which is 1.5%. This location is in axial compression, so the increase in the axial stress actually reduces the effective stress range and effective mean stress.

Delta plots of the 3.75 degree sector plane provide a good view of the HPT front shaft scallop. Once again, the plots show case 2 minus case 1.
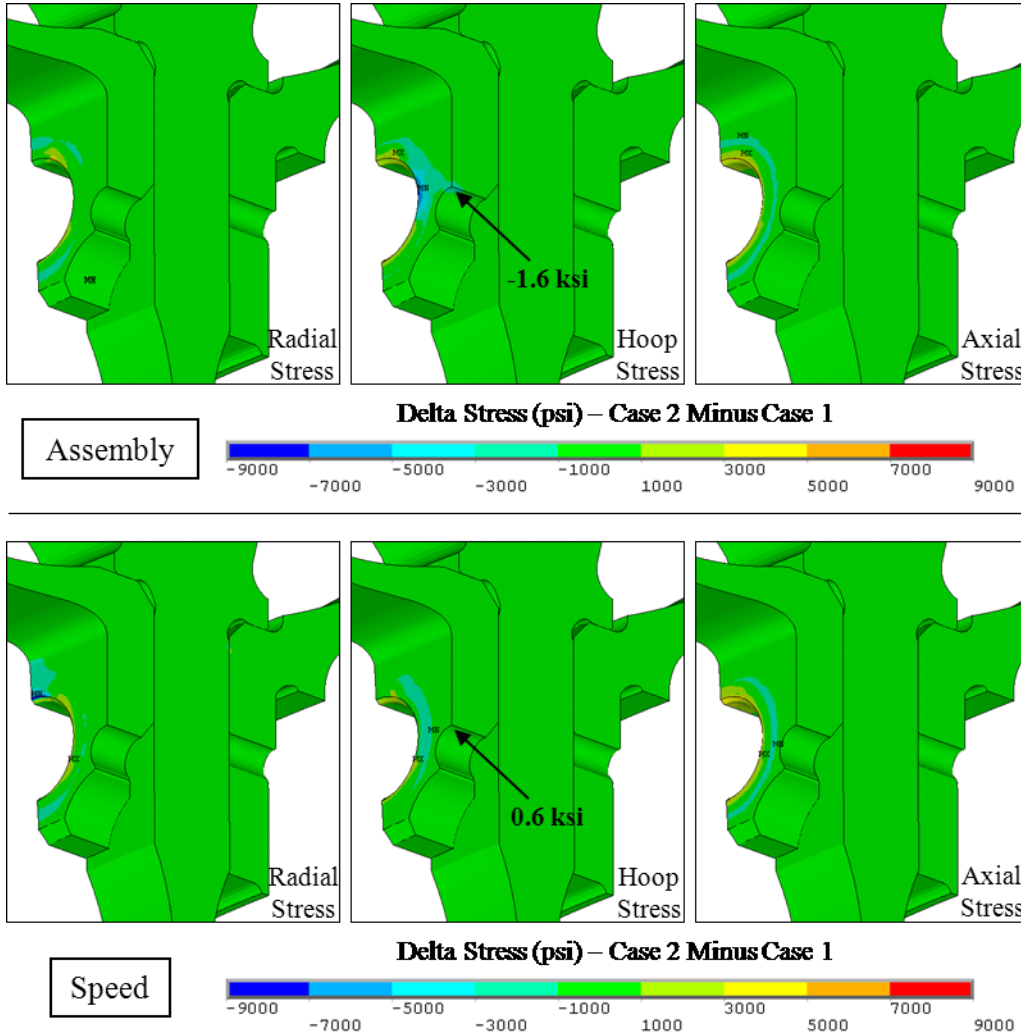
Figure 49: Delta Stress (psi), Case 2 Minus Case 1, Scallop Sector Face View

The inclusion of threads increases the hoop stress in the HPT front shaft scallop by 0.6 ksi at speed and decreases the hoop stress by 1.6 ksi at assembly. Due to the increase in hoop stress range, $\sigma_{0,alt}$ increases by 0.6 ksi, which is 0.8%.

The inclusion of the threads has an impact on both the scallop and the bolt hole, but the effect is relatively small. In both locations $\sigma_{0,alt}$ changed by less than 1.0 ksi. The bolt hole $\sigma_{0,alt}$ decreased and the scallop $\sigma_{0,alt}$ increased.

As discussed earlier, the bolt clamp load for these two analysis cases, and all other analysis cases to be discussed, is initially set to 4,600 lbs per half bolt for the initial assembly time point. After cycle stability is achieved, the assembly clamp load becomes 4,688.6 lbs for case 1 and 4,686.2 lbs for case 2. In the speed results the clamp load is 4,233.8 lbs for case 1 and 4,235.1 lbs for case 2. In the comparison of these two analysis cases, the inclusion of threads has essentially no effect on the analytical clamp load.

Upon closer inspection, it is not hard to imagine why case 2 and case 1 are producing similar clamp loads and stress results. Case 1 has couples along the entire pitch diameter, creating a fully joined and rigid connection between the nut and bolt. In case 2 the connection is also very rigid; all nodes except for the root fillet nodes are joined with couples. In both cases, the bolt and nut are forced to behave like a single part.

In actual bolts and nuts, only one side of the thread is loaded. Case 3 adds a small amount of complexity by simulating this condition. In case 3, couples are only used on the loaded faces of the threads. Otherwise, case 3 is modeled identically to case 2. Figure 50 compares the case 3 threads to the case 2 threads.

54
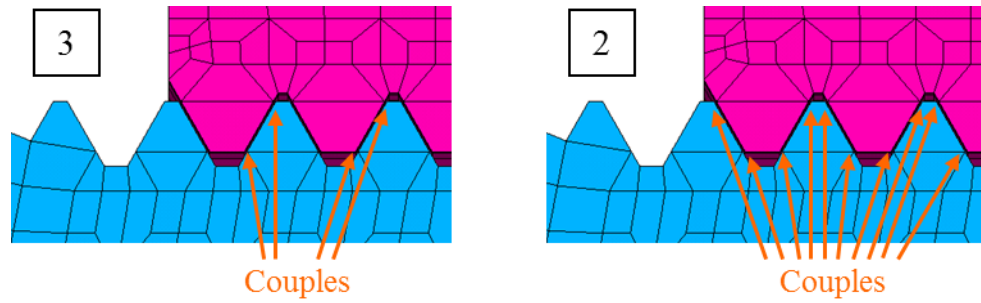
Figure 50: Comparison of Analysis Case 3 and Case 2

Removing the couple on the unloaded thread face causes a more substantial difference in stress. Delta stress plots of the assembly and speed results show the difference between analysis case 3 and case 2. In these plots, the case 2 results are subtracted from the case 3 results. The first two sets of plots show the zero degree sector plane of the model providing a view of the HPT front shaft bolt hole.
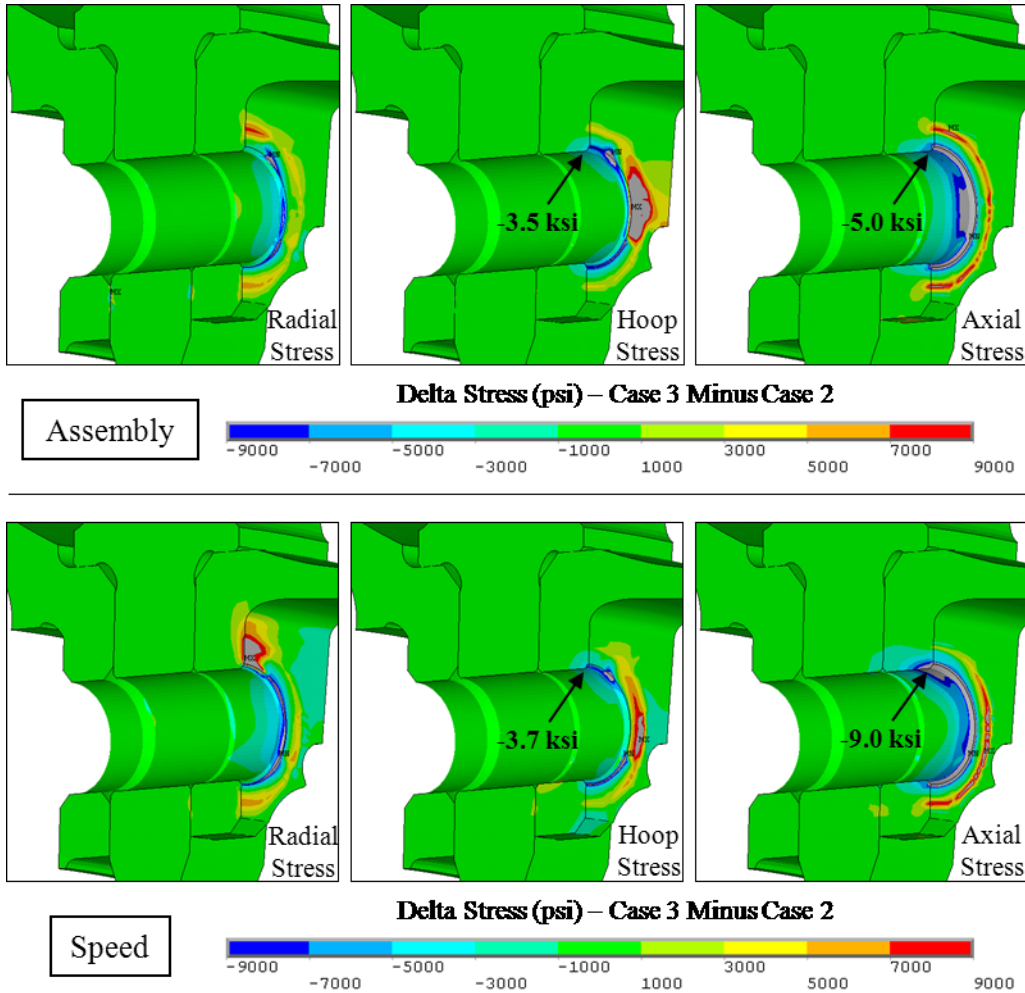
Figure 51: Delta Stress (psi), Case 3 Minus Case 2, Bolt Hole Sector Face View

The removal of the couples on the unloaded thread face cause the bolt hole hoop stress to decrease 3.5 ksi at assembly and 3.7 ksi at speed. The axial stress decreases 5.0 ksi at assembly and 9.0 ksi at speed. These changes in component stress caused $\sigma_{0,alt}$ to increase 2.1 ksi, or 6.2%. The additional axial compression in case 3 is the main driver of $\sigma_{0,alt}$ increase.

Upon a close look at the axial stress delta plots in Figure 51, a compressive blue ring is observed at the aft edge of the HPT front shaft bolt hole. Just outside of

56

the blue ring is a tensile red ring on the HPT front shaft flange surface. The blue
and the red rings represent the inner and outer contact surfaces between the nut
and the flange face. These rings suggest that the nut in case 3 applies more clamp
load at the inner edge of the contact area and less clamp load at the outer edge of
the contact area.

Figure 52 diagrams the clamp load transferred from the nut to the flange for each
ring of nodes on the nut surface. As can be seen in the diagram, more force is
transferred in the inner portion of the node ring in case 3 than in case 2.
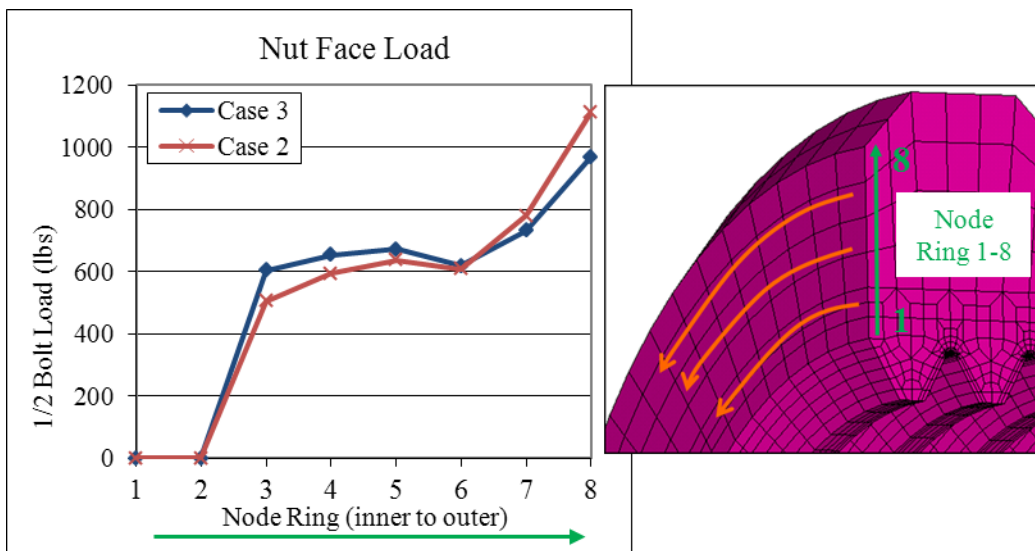
**Figure 52: Distribution of clamp load from inner node ring to
outer node ring on nut face**

The difference in the loading pattern changes the way the bolted joint deforms.
Figure 53 shows a 1000X delta displacement plot of case 3 minus case 2. From
the difference plots it can be observed that the inner edge of the hole deforms
axially further forward in case 3.
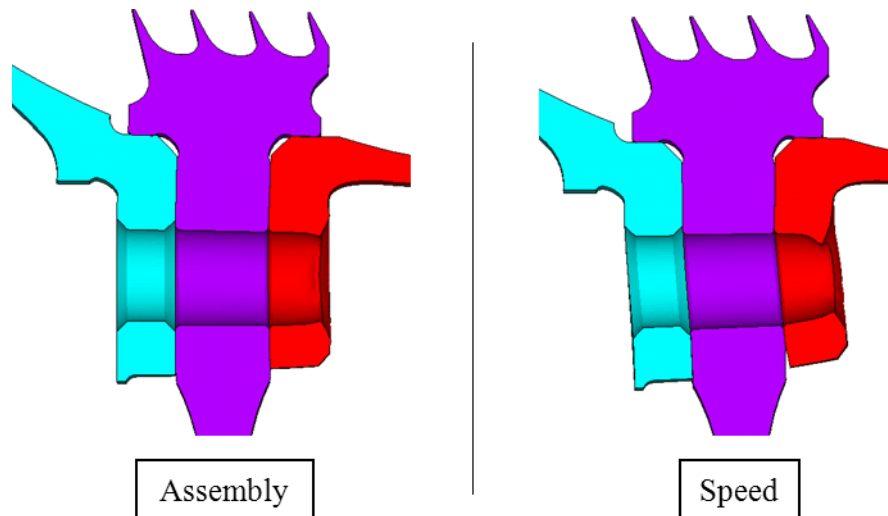
**Figure 53: Delta displaced shape plot for case 3 minus case 2,
1000X Magnification**

At the stabilized assembly, the clamp load for the two cases is nearly identical.

The case 3 clamp load is 4,687.0 lbs and the case 2 clamp load is 4,686.2 lbs.

However, at speed the clamp loads diverge. The case 3 clamp load is 4,247.3 lbs

and the case 2 clamp load is 4,235.1 lbs. Why does this happen? The bolt and

nut pair in case 3 is more flexible, causing the bolt to have a larger effective

length. Case 3's bolt and nut behave like a softer spring. As the spool, seal, and

shaft are loaded in speed they are stretched radially. The Poisson effect decreases

the axial length of these three bolted parts. Both cases 3 and 2 undergo similar

losses in stretch length, however case 3 loses less clamp force. The difference in

effective length can also be noted in the initial assembly analysis point. To match

the desired 4,600 lbs of load, case 3 needs 0.00538" of interference while case 2

needs 0.00504" of interference.

Delta stress plots of the speed and assembly case of the 3.75 degree sector plane

provide a view of the stress in the scallop.

58
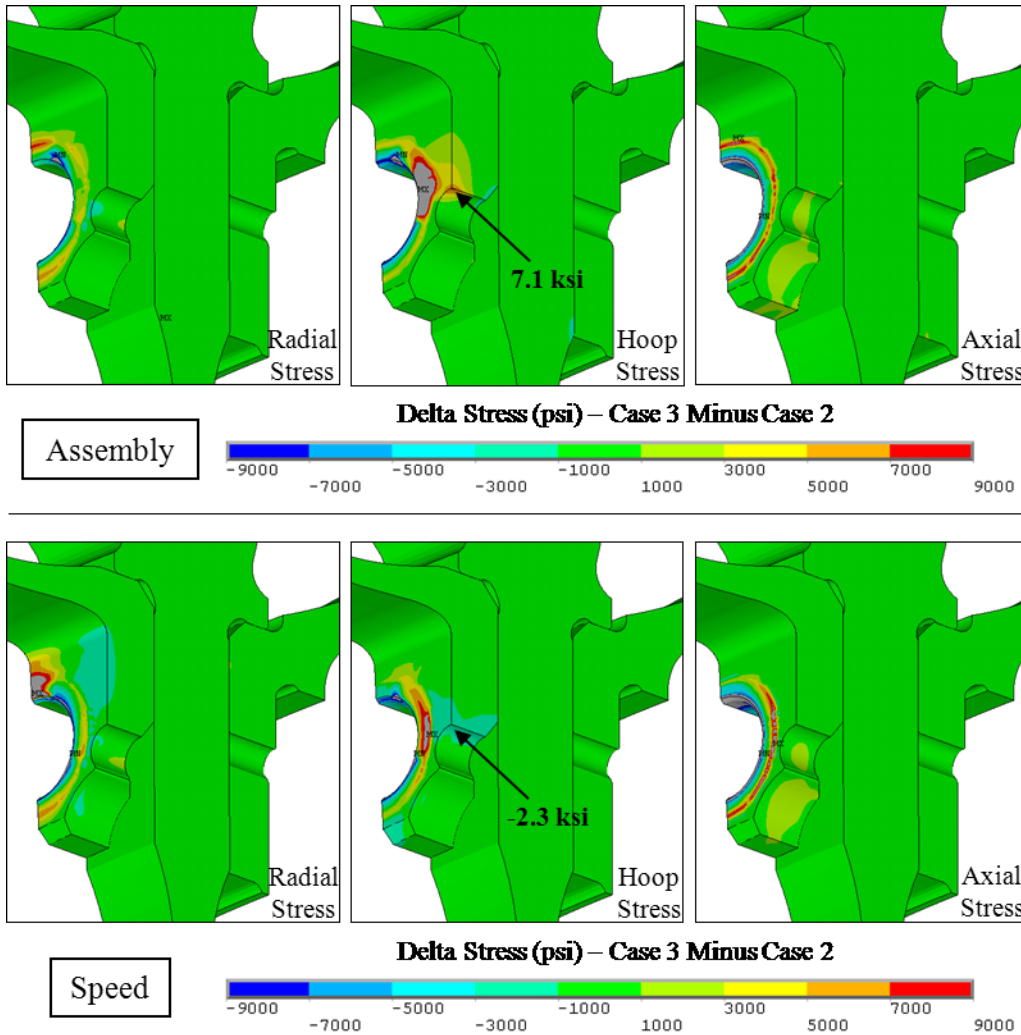
Figure 54: Delta Stress (psi), Case 3 Minus Case 2, Scallop Sector
Face View

The aft edge of the HPT front shaft scallop sees a substantial change in stress. At assembly, the hoop stress in case 3 is 7.1 ksi higher. At speed, the hoop stress is 2.3 ksi lower. The $\sigma_{0,alt}$ at this location decreases 2.6 ksi, or 3.4%.

The magnitude of $\sigma_{0,alt}$ change at the aft edge of the bolt hole is similar to that of the aft edge of the scallop. However, the bolt hole stress increases in case 3 and the scallop stress decreases.

It has been demonstrated thus far from the comparison of cases 1 and 2, that the inclusion of threads alone, if those threads are fully coupled, has a relatively small effect on the calculated stress. However, when couples are applied only to the loaded thread surfaces, as was done in case 3, the impact on stress is much more significant.

Upon closer inspection of the case 3 and 2 models, it can be seen that the couples begin further aft in the case 3 model. The first aligned thread surface in the case 3 model is a non-loaded surface, and therefore not coupled. What causes the difference in stress between case 3 and 2? Is it due to the extra flexibility in all the threads because only the loaded sides are coupled in case 3? Or is it due to the position of the first couple? If the difference is due to the position of the first couple, perhaps an analyst could choose to not explicitly model the threads, and instead place the first couple at the location of the of the first loaded thread interface. Case 4 is analyzed to address this issue.

In the case 4 model the threads are not modeled explicitly. The model is identical to the case 1 model except for the starting position of the first bolt/nut couple. The first couple is in the same axial position as the case 3 model. Figure 55 compares the coupling pattern between the case 4 and case 3 models.
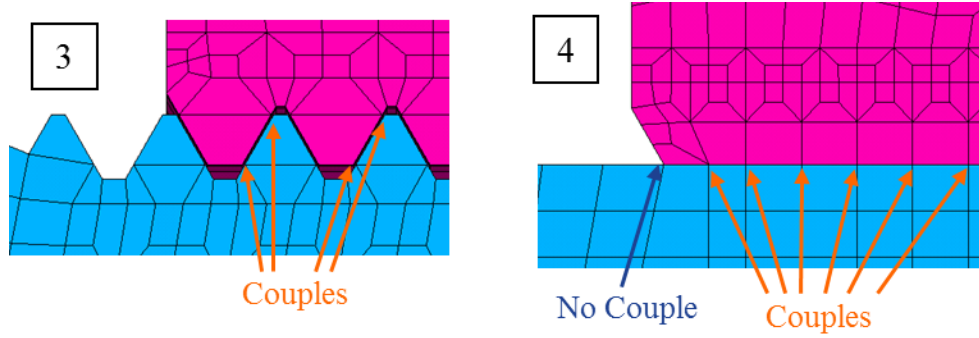
Figure 55: Comparison of Analysis Case 3 and Case 4

Delta stress plots comparing the HPT front shaft bolt hole for case 4 to case 3 are shown in Figure 56. In these plots, case 4 is subtracted from case 3. The plots include the assembly and speed time points.
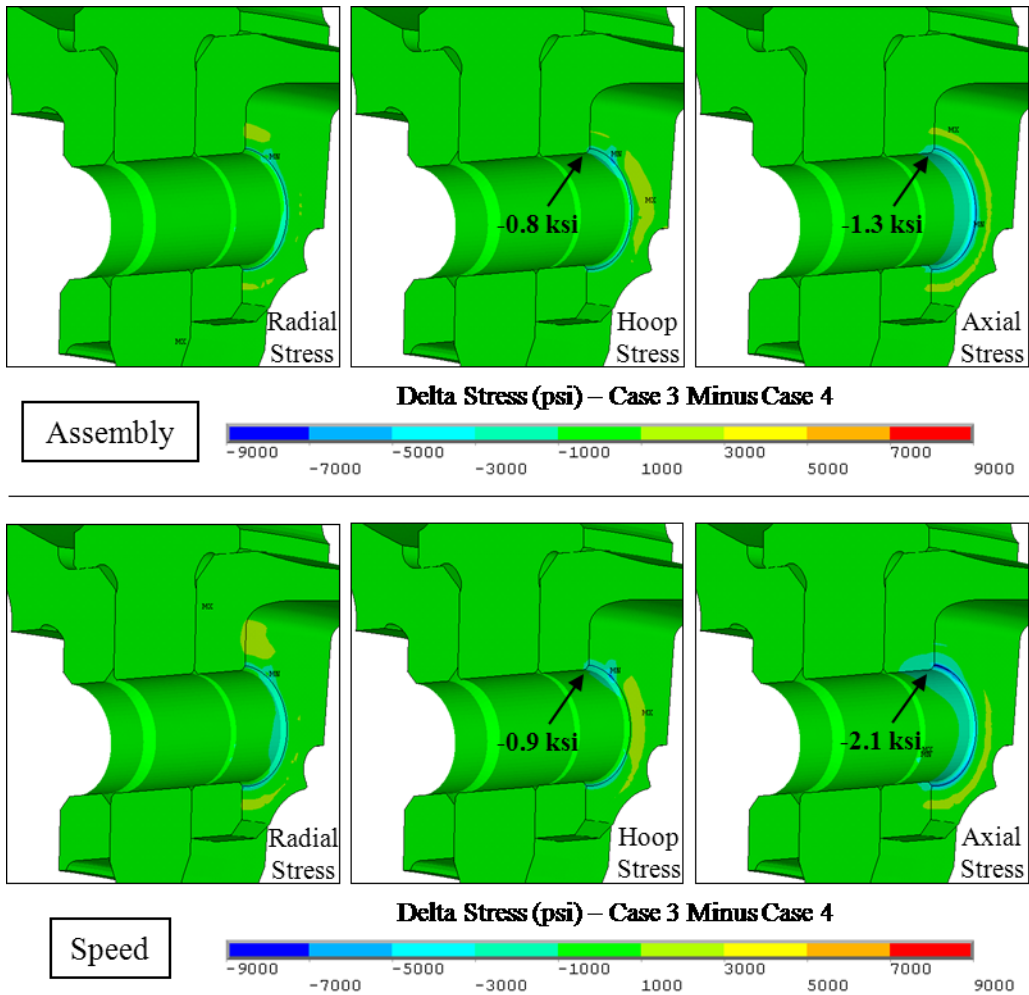
**Figure 56: Delta Stress (psi), Case 3 Minus Case 4, Bolt Hole
Sector Face View**

The axial stress in aft edge of the HPT front shaft bolt hole decreases 1.3 ksi at assembly and 2.1 ksi at speed. The hoop stress decreases 0.8 ksi at assembly and 0.9 ksi at speed. The $\sigma_{0,alt}$ increases by only 0.5 ksi.

Delta stress plots comparing the HPT front shaft scallop stress results are shown in Figure 57. The plots show case 3 minus case 4.
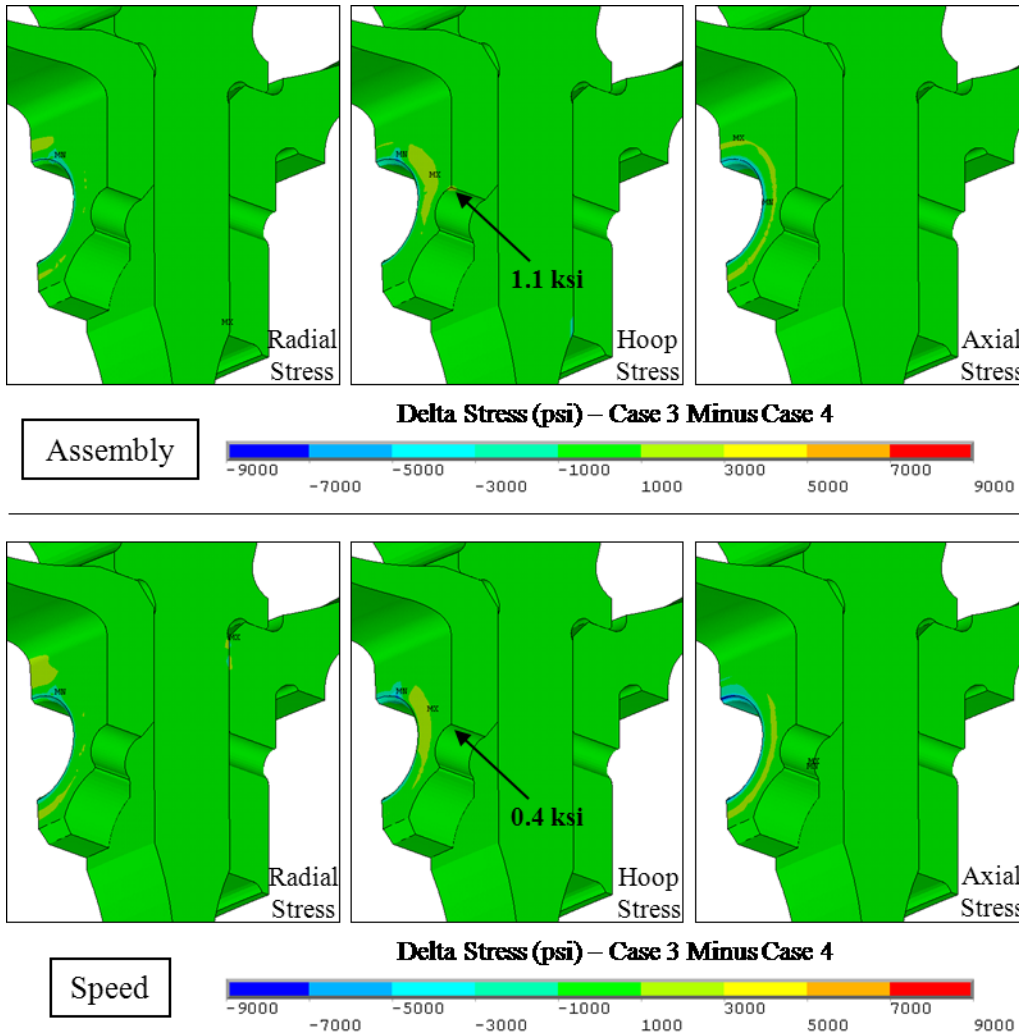
**Figure 57: Delta Stress (psi), Case 3 Minus Case 4, Scallop Sector
Face View**

The hoop stress in the aft edge of the HPT front shaft increases 1.1 ksi at

assembly and decreases 0.4 ksi at speed. $\sigma_{0,alt}$ decreases 0.5 ksi.

Case 4 and case 3 produce relatively similar results. These results suggest that

when couples are used to join the bolt and nut, choosing an appropriate location

for the first couple is significantly more important than explicitly modeling

threads. This is good news for the analyst, as correctly placing a first couple

requires much less effort than explicitly modeling threads.

5.1.1 Summary – Explicit Inclusion of Threads

Table 1 summarizes the four analysis cases addressing the explicit inclusion of threads. The results are listed as relative to case 3, which is the most complex case of the four analyzed. The table contains life results normalized to case 3 in addition to the $\sigma_{0,alt}$ results.

<div align="center">Table 1: Results Comparison - Case 1 through Case 4</div>

Case	$\sigma_{0,alt}$ (ksi), Delta to Case 3		Life, Normalized to Case 3	
	Bolt Hole Aft Edge	Scallop Aft Edge	Bolt Hole Aft Edge	Scallop Aft Edge
1 - No Threads	-1.6	2.0	3.116	0.932
2 - Fully Coupled Threads	-2.1	2.6	4.493	0.912
3 - Threads Coupled on Loaded Face Only	-	-	-	-
4 - No Threads, 1st Couple Aligns w/ 1st Loaded Thread	-0.5	0.5	1.419	0.984

As the reader can observe, both the bolt hole and scallop aft edge stresses vary in the four analysis cases. Modeling changes that increase scallop stress decrease bolt hole stress. Also the reader will notice the large normalized life values for the bolt hole aft edge. These values can be deceiving. The absolute life in this critical feature is very high. In the high life area of the life curve, a small change in stress creates a large change in life. These high normalized values will be seen throughout all the results comparisons at the bolt hole aft edge.

Two observations are made from these four sets of results. First, the location of the first couple has a large effect on $\sigma_{0,alt}$. The cases where the first couple is closer to the flange surface (cases 1 and 2) increase the scallop stress and decrease the bolt hole stress compared to cases where the couple placement is consistent

with the first loaded thread surface (cases 3 and 4). Second, when couples are used to join the bolt and nut, the inclusion of threads has only a minor effect on the results. Cases 1 and 2 produce relatively similar results, as do cases 3 and 4.

5.2 Contact Elements

Couples have been used to attach the bolt and nut in the four cases presented thus far. An alternate and more complex method to attach the two is to use contact elements. Contact elements provide a less rigid connection. The contacting interfaces have the ability to slide relative to each other if the surface shear load reaches the frictional threshold. In the four analysis cases already presented, the more flexible cases produced lower stress in the scallop aft edge and higher stress in the bolt hole. Analysis case 5 will determine if the trend continues.

Analysis case 5 uses the identical mesh as case 3. The couples on the loaded thread face have been changed to CONTAC52 point-to-point contact elements with the friction coefficient set to mu=0.45. In all other ways the two models are identical. Both models contain elastic material properties, nominal thread geometry, coarse thread mesh, and threads modeled as circular rings. Figure 58 shows the modeled threads and the thread connections used in these two analysis cases.
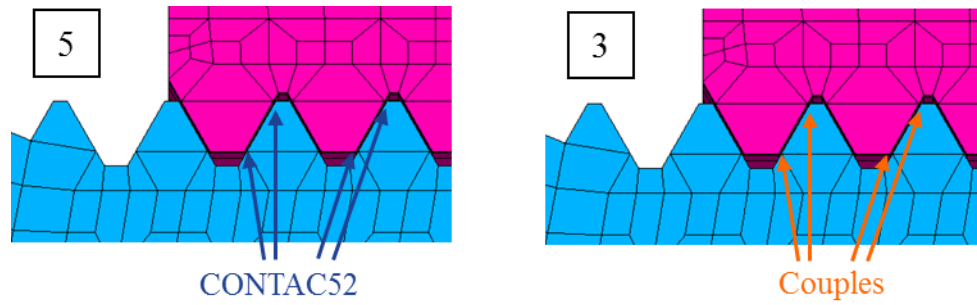
Figure 58: Comparison of Analysis Case 5 and Case 3

Delta stress plots capture the stress differences at the assembly and speed time points. The plots show the case 5 results minus the case 3 results. Figure 59 shows the HPT front shaft bolt hole location.
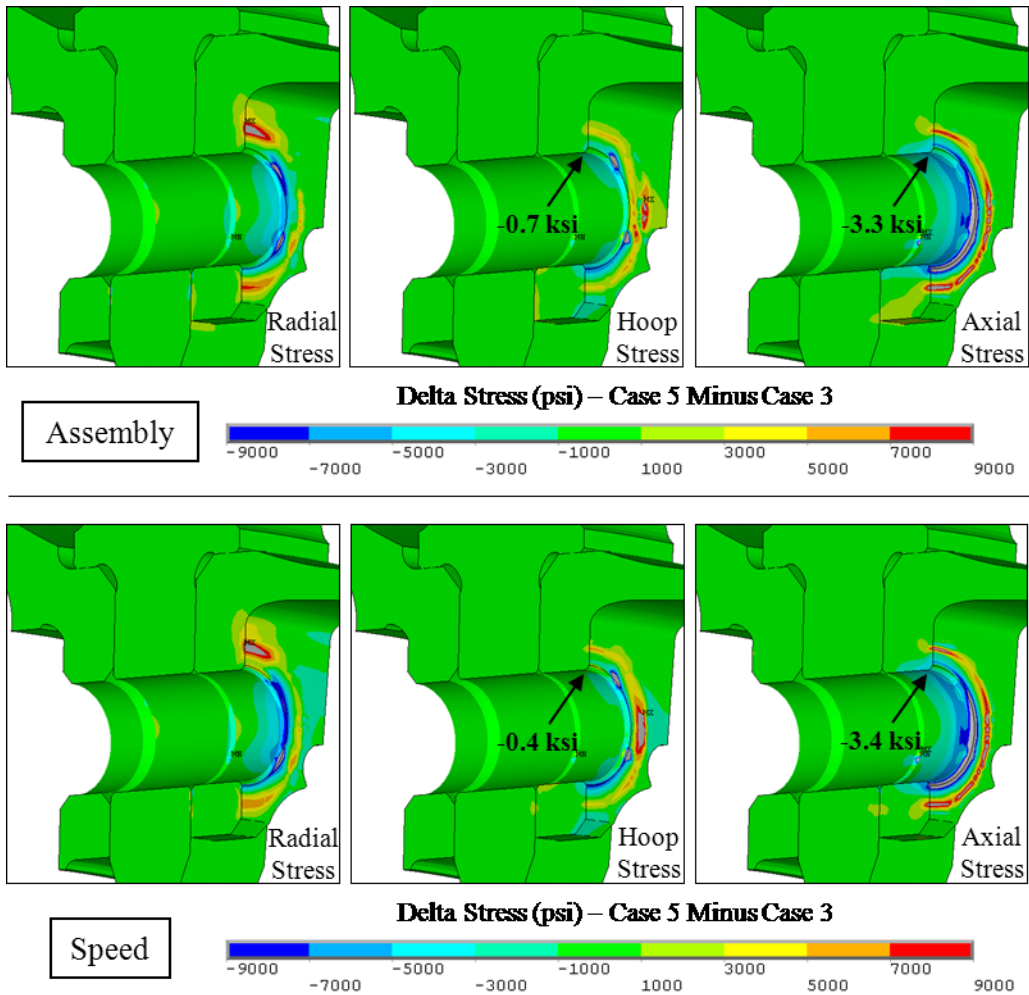
Figure 59: Delta Stress Comparison (psi), Case 5 Minus Case 3,
Bolt Hole Sector Face View

At the aft shaft bolt hole aft edge, analysis case 5 has 0.7 ksi less hoop stress at

assembly and 0.4 ksi less hoop stress at speed. The axial stress is 3.3 ksi lower at

assembly and 3.4 ksi lower at speed. $\sigma_{0,alt}$ increases 1.1 ksi.

A closer inspection of the axial delta stress plots reveals the familiar blue

compressive ring encircled by the red tensile ring on the aft flange of the HPT

front shaft. A similar set of rings was seen in the earlier comparison of cases 3

and 2. On a relative basis, the more flexible bolt/nut joining method loads the

67

interior portion of nut face more and the exterior portion of the nut face less.

Figure 60 diagrams the nut face load comparison for the speed time point.
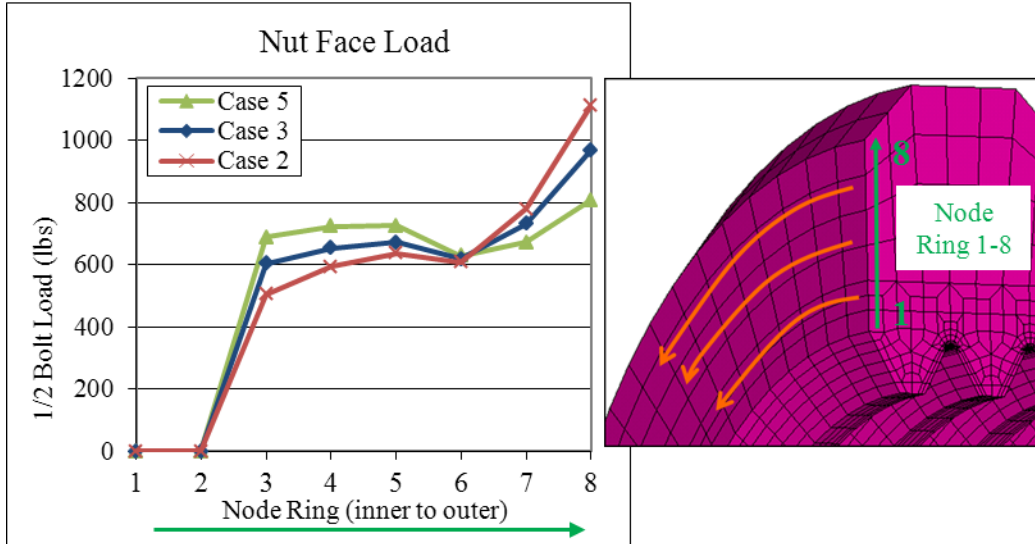
**Figure 60: Distribution of clamp load from inner node ring to
outer node ring on nut face, case 5 results included**

The displaced shape delta plots also help to illustrate the difference in the nut load

pattern. Figure 61 shows 1000X delta displaced shape difference plots of case 5

minus case 3. The reader will notice how the difference in the nut face loading

pattern causes the difference in the axial displacement on the HPT front shaft at

the nut contact area. In these delta plots, the inner portion of the contact area

displaces more axially forward while the exterior portion displaces more axially

aft.
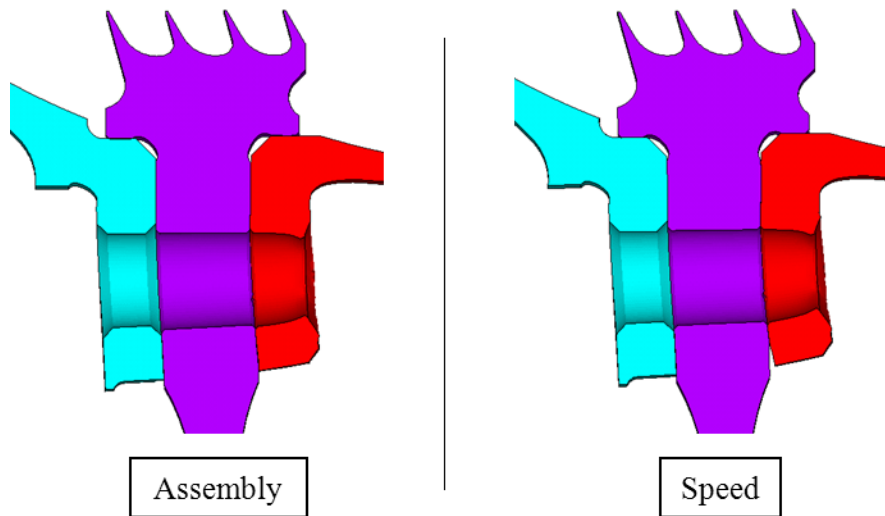
**Figure 61: Delta displaced shape plot for case 5 minus case 3,
1000X Magnification**

The delta plots in Figures 62 capture the stress differences in aft shaft scallop

location. The plots show the case 5 results minus the case 3 results.
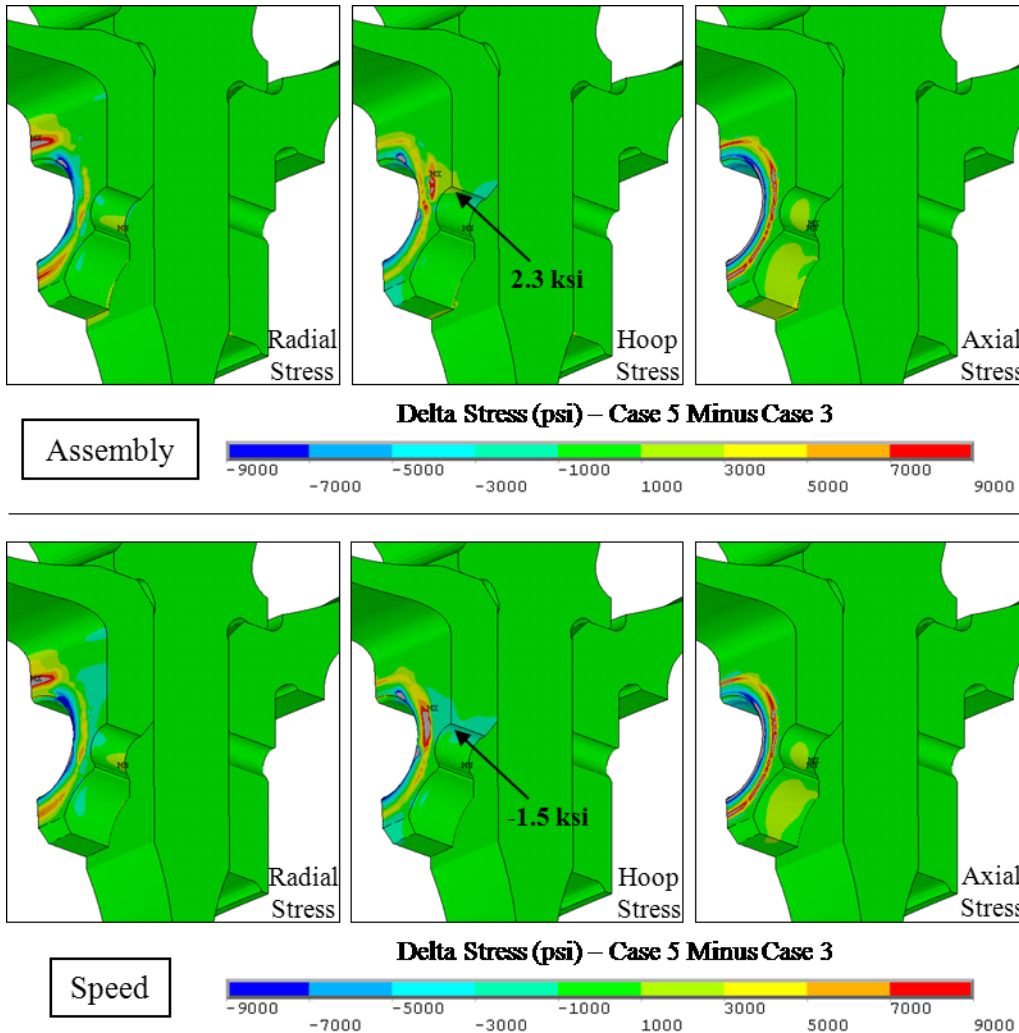
Figure 62: Delta Stress Comparison (psi), Case 5 Minus Case 3, Scallop Sector Face View

For analysis case 5, the HPT front shaft scallop hoop stress is 2.3 ksi higher at assembly and 1.5 ksi lower at speed. The decrease in the hoop stress range causes a decrease in $\sigma_{0,alt}$. The case 5 $\sigma_{0,alt}$ is 1.2 ksi lower than case 3.

Table 2 summarizes the results from all five analysis cases discussed up to this point. The inclusion of thread contact elements (5 vs. 3) has a significant impact on stress for the bolt hole and scallop. Interestingly however, the impact is less

significant than the effect of the appropriate positioning of the first couple (4 vs. 1 or 3 vs. 2) when couples are used instead of contact elements.

Table 2: Results Comparison - Case 1 through Case 5

	$\sigma_{0,alt}$ (ksi), Delta to Case 5		Life, Normalized to Case 5	
Case	Bolt Hole Aft Edge	Scallop Aft Edge	Bolt Hole Aft Edge	Scallop Aft Edge
1 - No Threads	-2.7	3.2	5.850	0.892
2 - Fully Coupled Threads	-3.2	3.8	8.436	0.872
3 - Threads Coupled on Loaded Face Only	-1.1	1.2	1.878	0.957
4 - No Threads, 1st Couple Aligns w/ 1st Loaded Thread	-1.6	1.7	2.663	0.941
5 - Threads with Contact, mu=0.45	-	-	-	-

5.2.1 Additional Discussion

The new results follow a similar trend to the previous section's results. The contact elements created a more flexible bolt/nut interface which increased $\sigma_{0,alt}$ in the bolt hole and decreased $\sigma_{0,alt}$ in the scallop. Why does this trend occur?

In HPT front shaft bolt hole, the stress field is constituted of two significant stress components. The axial stress plays the largest role in the variation of $\sigma_{0,alt}$. The hoop stress plays less of a role, but will still be discussed.

Figure 60 shown earlier demonstrated that the more flexible bolt/nut cases distribute more of the axial clamp load along the inner edge of the bolt hole. The additional load at the edge causes additional axial compression which increases $\sigma_{0,alt}$ for the flexible cases.

One might expect variation in stress shielding to cause the variation in hoop stress from one case to the next. In a rotating bolted joint, centrifugal load causes the joint to grow radially which induces tensile hoop stress and strain in the spool, CDP seal, and HPT front shaft. The bolt and nut, however, are periodic parts. Since they do not form a continuous 360 degree ring about the engine centerline, they are not capable of carrying hoop load on their own. With the help of friction, however, some tensile hoop load is transferred to the bolt head and the nut by its respective mating flange. The bolt holes in those two flanges receive hoop stress relief, commonly called shielding. As one would expect, the shielding effect is greatest close to the bolt head or nut. At assembly, the effect of shielding is reversed. The spool, CDP seal, and HPT front shaft shrink circumferentially. Now friction transfers compressive hoop load to the bolt head and nut. As a result, the spool bolt hole and HPT front shaft bolt hole retain some hoop tension. The total effect of the shielding is a decrease in the hoop stress range between the assembly and speed conditions. One might expect that since the more flexible joint applies more axial load close to the inner edge of the HPT front shaft bolt hole, the shielding effect at the edge of the hole would be magnified for these cases. However, the analysis results do not meet this expectation. Case 5's hoop stress range is only 0.1 ksi different than case 2's. In fact, the hoop stress ranges for all five cases discussed thus far are within 0.3 ksi. While stress shielding does decrease the stress range for the hole, the results suggest that the effect of the shielding on the bolt hole is relatively independent of the nut loading distribution. All cases receive similar stress shielding.

The nut, which provides shielding for the bolt hole, has the opposite effect on the scallop. At speed the nut restricts the circumferential expansion of the bolt hole, forcing the scallop to compensate by expanding more. At assembly, the nut restricts the circumferential contraction of the bolt hole, once again forcing the scallop to compensate by contracting more. The friction on the nut face increases the hoop stress range in the scallop.

Interestingly, the stress results show a significant variation in hoop stress range in the scallop among the analysis cases. Case 5's hoop stress is 9.4 ksi higher at assembly and 3.8 ksi lower at speed than case 2. As a result, case 2's hoop stress range is 13.2 ksi higher than case 5!

Why does the nut shielding produce such similar hoop stress ranges at the bolt hole for all analysis cases, yet at the scallop, the hoop stress range varies so significantly? Pictures showing the frictional loading on the nut help to answer this question.

Figure 63 shows vector plots of the frictional force the nut applies to the flange for the speed condition. The arrows show the direction and the magnitude of the load at each node. The view shows the nut face from a forward-looking-aft direction. These pictures illustrate the nut shielding. The vectors have a significant component pointing to the right, indicating that the nut is providing hoop compression to the flange around the bolt hole. The bolt hole is protected, and the scallop stress is increased.

73
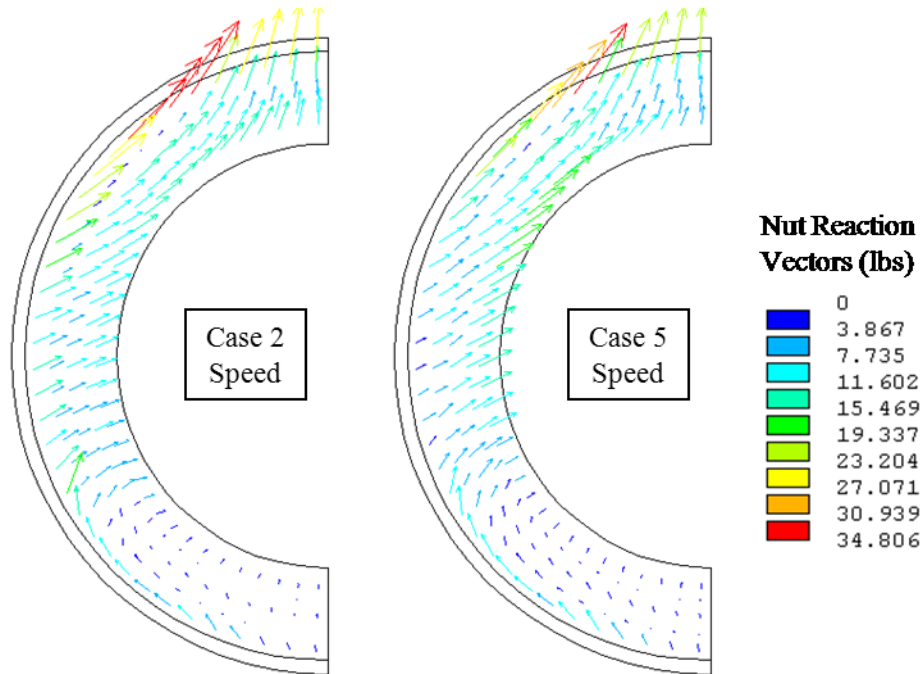
Figure 63: Frictional Force Vector Plot, Speed Condition

Figure 64 shows the frictional force the nut applies to the flange for the assembly condition. The vectors once again have a significant horizontal component, but in these plots they point to the left, indicating the nut applies hoop tension to the flange around the bolt hole. The hoop stress at the hole is increased and at the scallop is decreased.
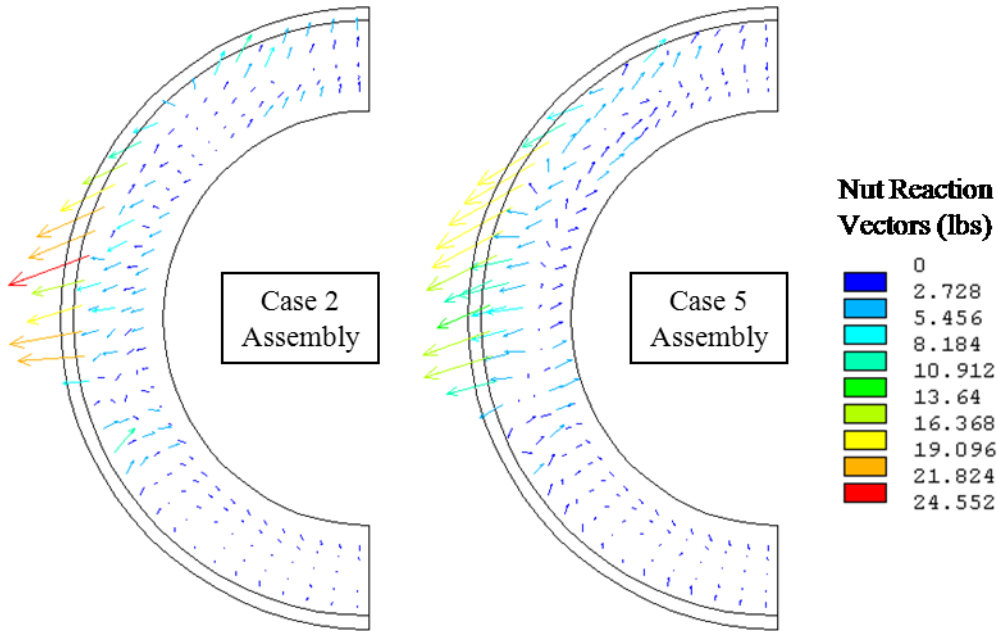
Figure 64: Frictional Force Vector Plot, Assembly Condition

If the reader takes a close look at the vector plots, it is apparent that the vectors at

the 12 o'clock position of the bolt hole point in almost a purely vertical direction

for the speed condition. For the assembly condition, the vectors 12 o'clock are

small. Very little hoop load is transferred from the flange to the nut at the top of

the hole. The nut in case 5 applies more normal load at the inner ring of the nut

face (as shown earlier in Figure 60), however at 12 o'clock it does not take

advantage of its ability to carry more frictional hoop load. Instead, the majority of

the hoop frictional load is transferred to the nut at 9 o'clock position. The reader

will notice that at 9 o'clock the frictional load in case 2 is greater at the outer edge

of the nut and less at the inner edge of the nut than case 5. However, the 9

o'clock position is far enough away from the top of the hole that the difference in

frictional load distribution has little to no effect. Case 5 and case 2 each provide

similar amounts of stress shielding to the top of the hole. As a result, both cases have similar hoop stress ranges.

The scallop, however, is situated close to the 9 o'clock contact area of the nut. Note the close proximity in Figure 65. The scallop is sensitive to the local frictional load distribution. The scallop in case 2 has the higher hoop stress range because the frictional loading from the nut is distributed more towards the outer edge of the nut. What further magnifies this effect is the small amount of circumferential space from the end of one nut to the start of the next. There is little room on the flange between the nuts to absorb the frictional load. Perhaps if the bolted joint was designed with a circumferentially larger scallop or if there was more space between the edge of the nut face and the scallop, the variation in nut shielding from case to case would be less.
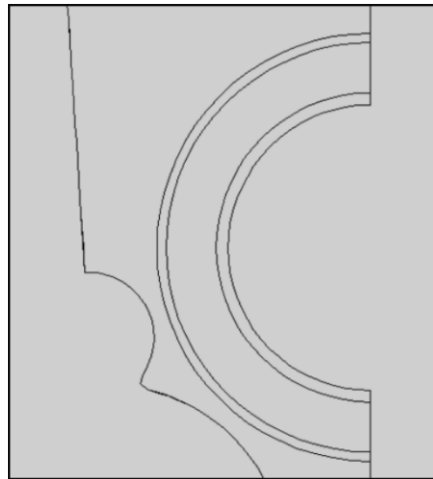
Figure 65: Proximity of Nut Face to Scallop

5.3 Mesh Fineness

Building a high-quality, fine mesh in the threads is a time-consuming task. The fine mesh increases the model size, which increases the file size and the computational time.

Analysis case 6 includes a fine mesh in the threads. Twelve elements are included around each of the small thread fillets. The element count needed to produce a mesh this fine is substantial. Compared to the coarse mesh in case 5, the bolt and nut element count has increased from 24,390 to 136,422. In the entire model, the number of elements has increased from 62,575 to 175,699. Adding the fine thread mesh has increased the model size, and also the computational time, by approximately 3 times! The additional elements in the thread fillets have also allowed the shape of the thread fillets to be more accurately captured.

Figure 66 diagrams the mesh in case 6 compared to case 5. Except for the thread mesh quality and more accurate capture of the thread fillet geometry, the two models are identical. Both models include contact elements in the threads, a thread friction coefficient of 0.45, elastic material properties, nominal thread geometry, and threads modeled as circular rings.
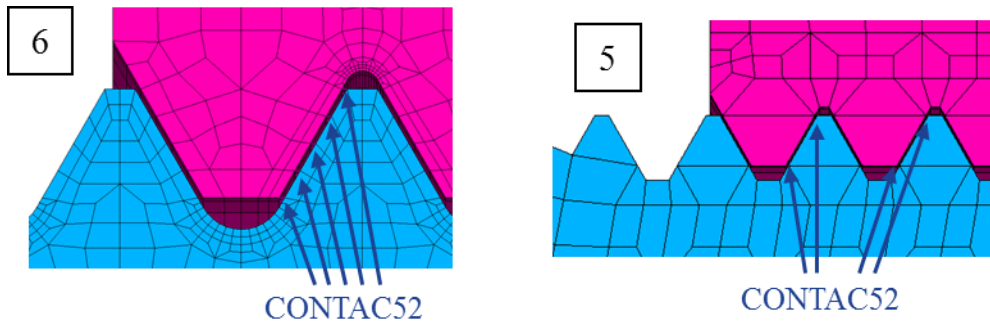
Figure 66: Comparison of Analysis Case 6 and Case 5

Figure 67 contains stress delta plots comparing the two sets of results. The delta plots show the results in the HPT front shaft bolt hole for case 6 minus case 5.

At the bolt hole aft edge, the axial stress for case 6 is 0.6 ksi higher at both the

assembly and speed conditions. The hoop stress is 0.2 and 0.3 ksi higher,

respectively. $\sigma_{0,alt}$ is the same for the two cases.

Figure 68 contains stress delta plots comparing the results in the HPT front shaft

scallop. The plots show case 6 minus case 5.
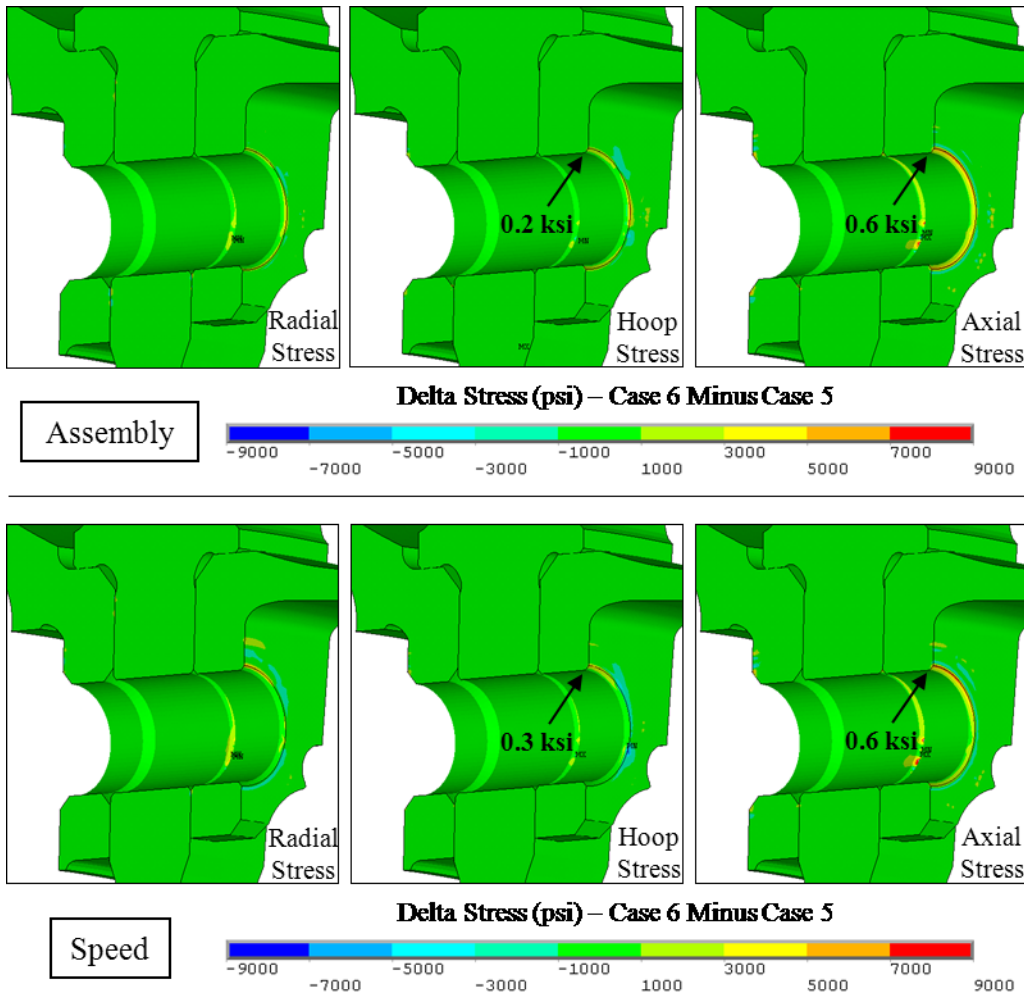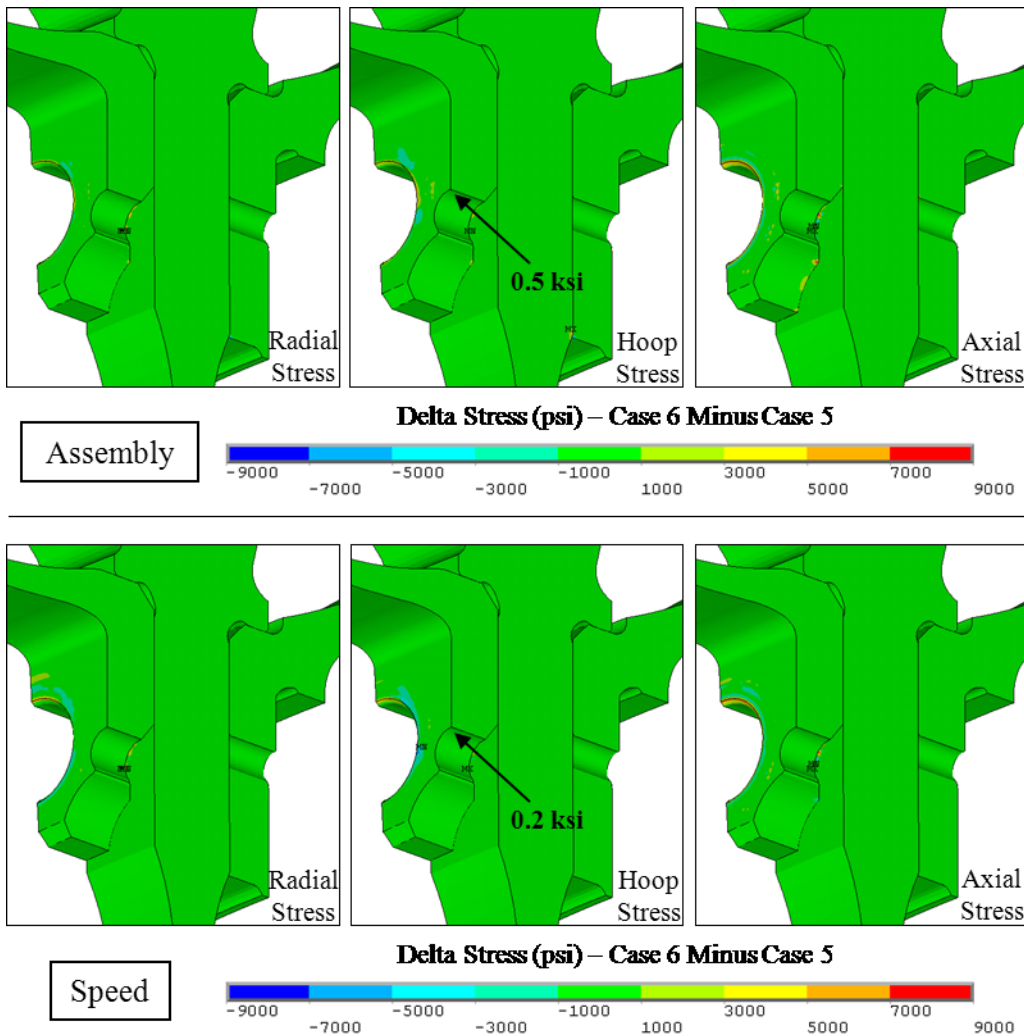
Figure 68: Delta Stress Comparison (psi), Case 6 Minus Case 5,
Scallop Sector Face View

At the aft edge of the scallop, the hoop stress is 0.5 ksi higher at assembly and 0.2

ksi higher at speed. $\sigma_{0,alt}$ at this location is also the same for these two cases.

Figure 69 shows a 1000X delta displaced shape plot of the two sets of results.

The results are shown as case 6 minus case 5. The displacements of the two

analysis cases are nearly identical.
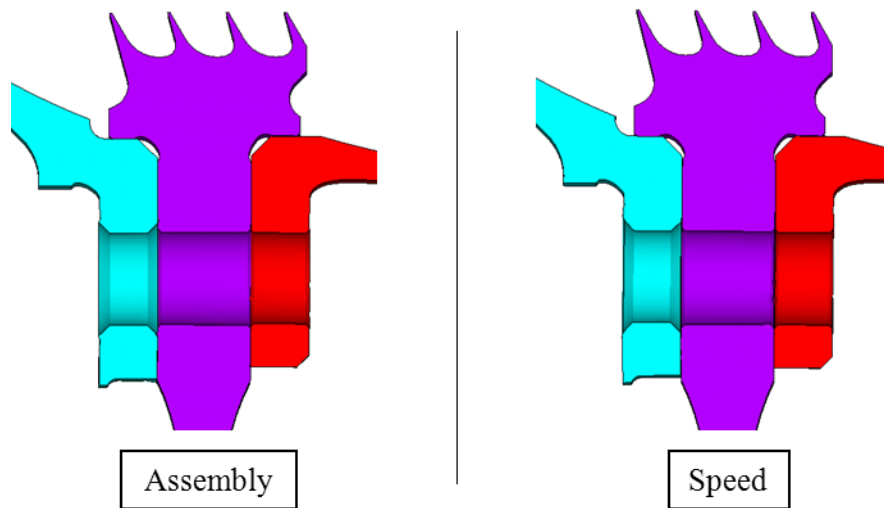
Figure 69: Delta displaced shape plot for case 6 minus case 5,
1000X Magnification

These results suggest that a course mesh is adequate; a fine thread mesh does not

change $\sigma_{0,alt}$.

5.4 Elastic vs Elastic/Plastic Material Properties

All the analysis cases discussed thus far have been performed with elastic material

properties. The bolt and nut have not been allowed to yield. The vast majority of

the volume of the bolt and nut are well below yield strength. However, the

80

geometry of a thread naturally creates a stress concentration in each thread root fillet. In addition, the loading of the thread teeth causes tooth bending, which further magnifies the stress on the thread root fillets. In the previous analysis cases, the local elastic stress in the thread root fillets significantly exceeded the material yield strength of both the nut and the bolt.

Analysis case 7 was analyzed to understand the impact of including elastic-plastic material properties in the threads. The elastic-plastic material properties used in both the bolt and nut represent bar stock properties. In the nut, this is likely a good assumption as the threads are tapped. In the bolt, however, the threads are cold-rolled. The cold-rolled process creates a compressive stress at the surface and strengthens the local thread material, which raises the yield strength at the surface. The bar stock material property assumption in the bolt will cause additional yielding in the analysis, and therefore magnify the analytical effect of the elastic-plastic material property assumption.

Since the stresses in the bolt and nut are significantly concentrated in the thread fillets, a fine thread mesh is necessary to capture the plastic strain for analysis case 7. The case 7 model is identical to the case 6 model with the exception of the added elastic-plastic material properties. Both models have nominal thread geometry, circular threads, and CONTAC52 point-to-point contact elements.
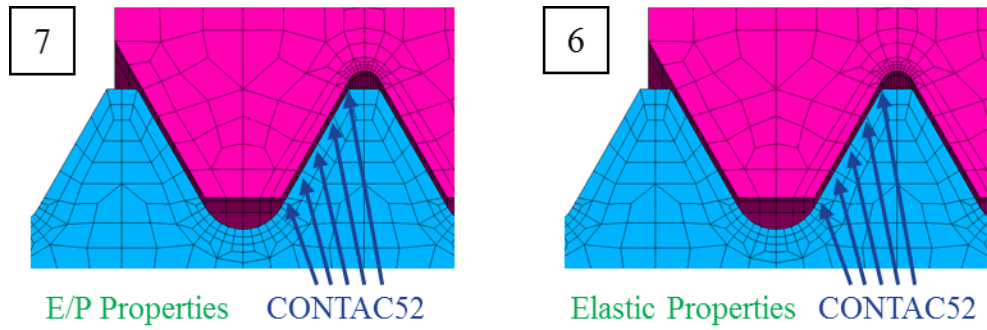
Figure 70: Comparison of Analysis Case 7 and Case 6

Plots of the equivalent plastic strain from the speed results are shown in Figure 71. The equivalent plastic strain at the assembly time point is similar to the speed point, and therefore plots of assembly are not shown. The contours are set so that the colored regions are plastically strained beyond the 0.02% offset yield strength. The grey areas remain below the 0.02% yield strength threshold.
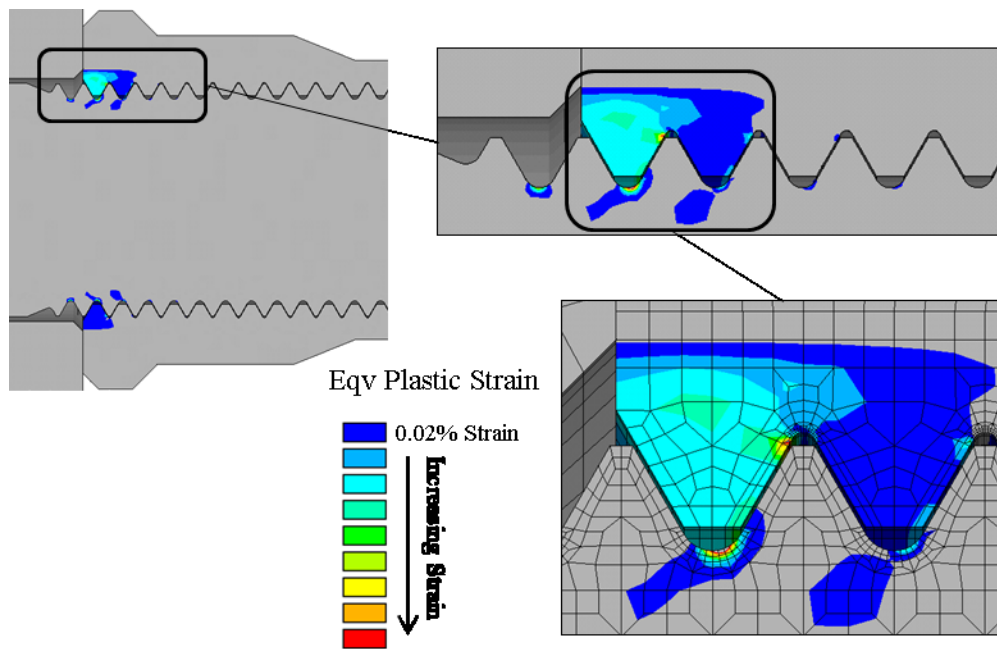
Figure 71: E/P Bolt and Nut Plastic Strain
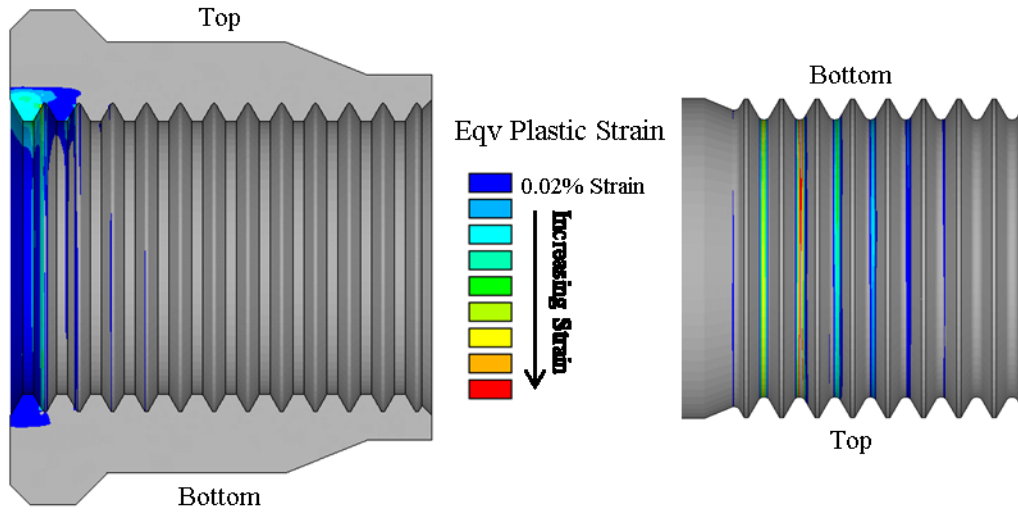
**Figure 72: E/P Bolt and Nut Plastic Strain, Individual Bolt and
Nut Plots**

The first few threads are the most highly loaded so the majority of the plastic

strain occurs in these regions. The later threads have no plastic strain.

The plastic deformation causes the clamp load to be transferred from the nut to

the bolt with a different distribution of thread loading. The load in the first thread

changes significantly. The load on later threads is very similar. Figure 73

compares the thread loading distribution between case 6 and case 7.
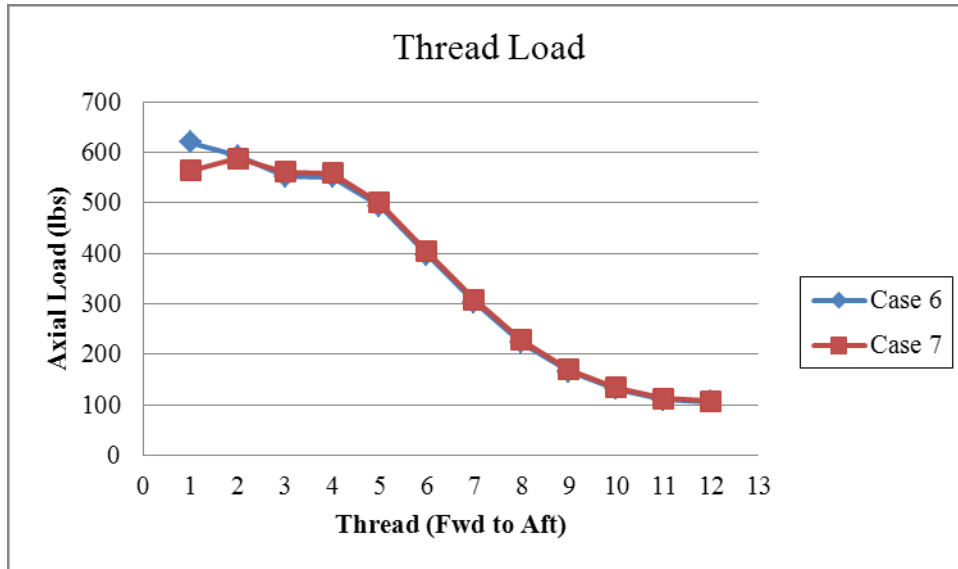
Figure 73: Thread Load Distribution

The total clamp loading on these two models is similar. At the cyclically
converged assembly point, the clamp loads are 4680.3 and 4665.3 lbs for cases 6
and 7. At speed, the loads are 4247.3 and 4271.9 lbs, respectively.

Figure 74 compares the stress results between analysis cases 7 and 6 at the HPT
front shaft bolt hole. The delta stress plots show case 7 minus case 6.
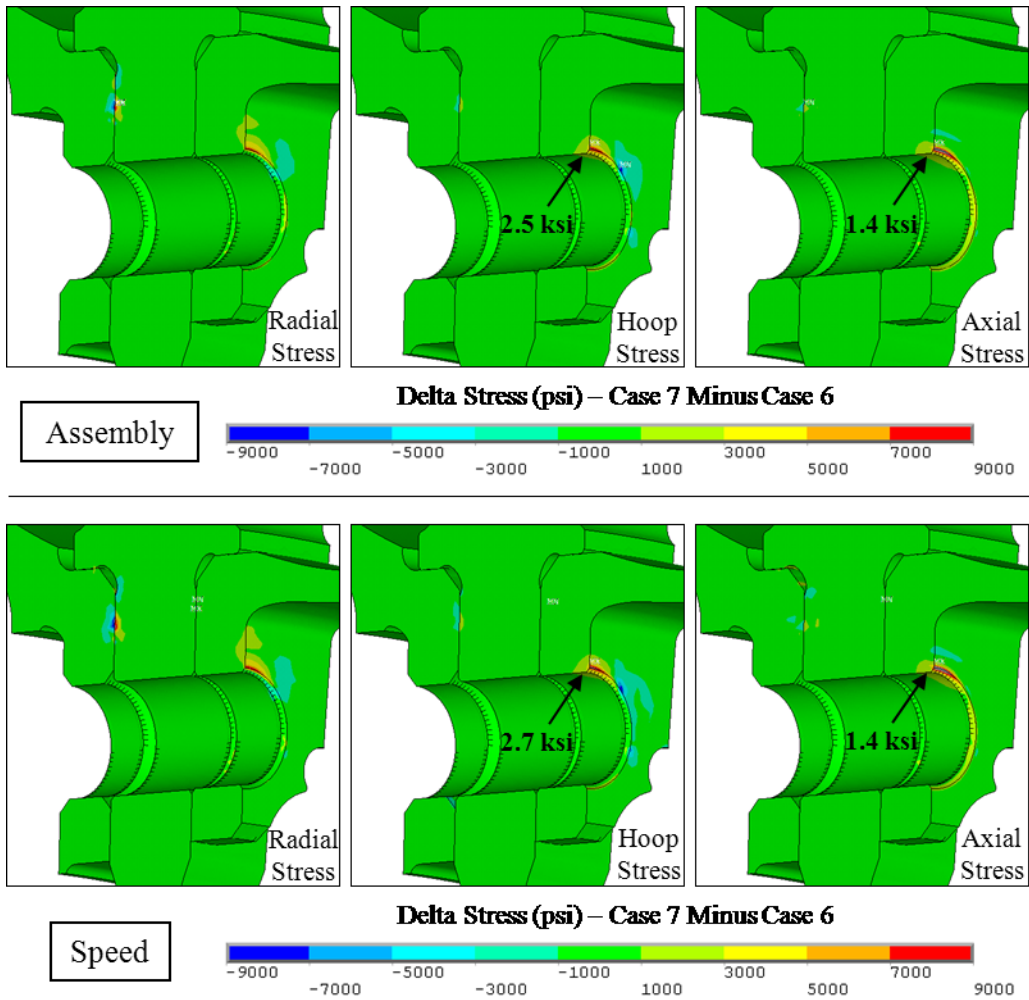
**Figure 74: Delta Stress Comparison (psi), Case 7 Minus Case 6,
Bolt Hole Sector Face View**

At the aft edge of the aft shaft bolt hole, the hoop stress increases 2.5 ksi at assembly and 2.7 ksi at speed. The axial stress increases 1.4 ksi at assembly and at speed. $\sigma_{0,alt}$ decreases 0.1 ksi.

Figure 75 compares the stress results between analysis cases 7 and 6 at the HPT front shaft scallop. The delta stress plots show case 7 minus case 6.
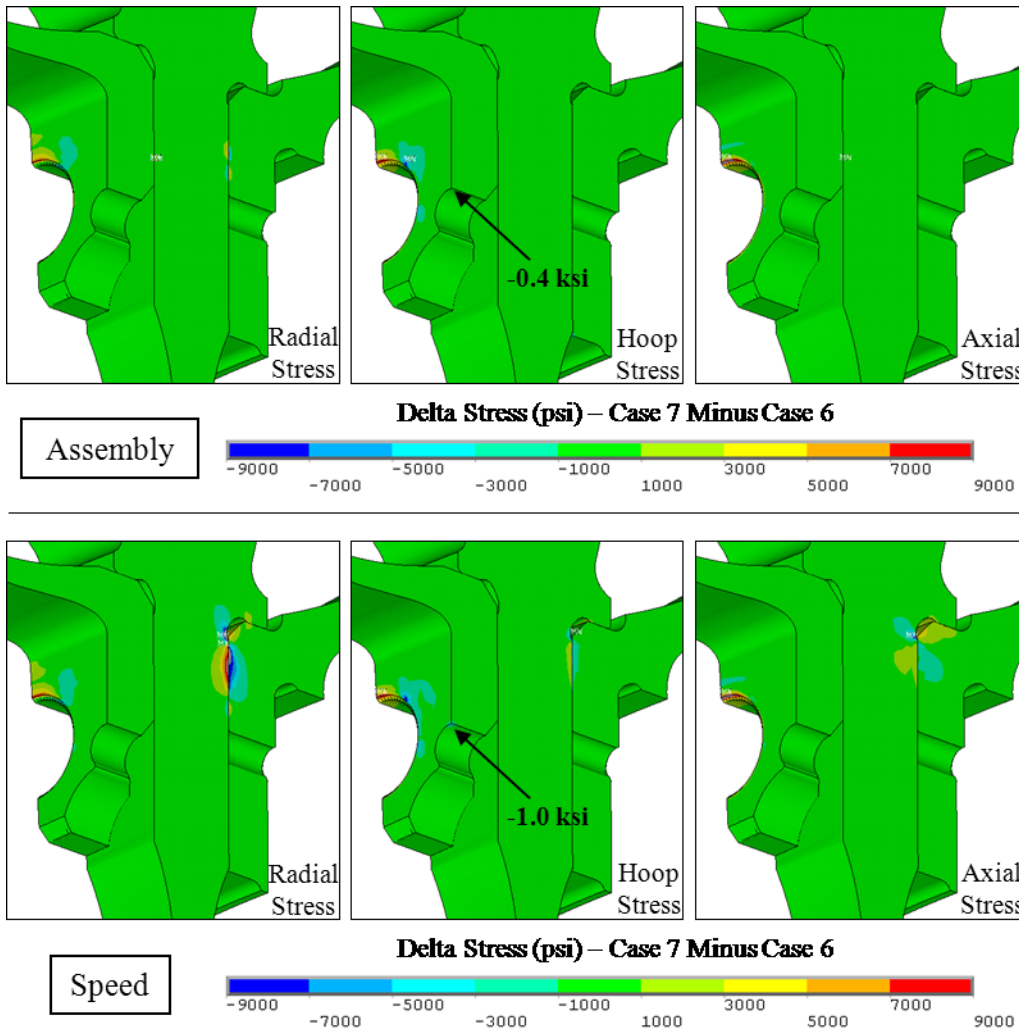
Figure 75: Delta Stress Comparison (psi), Case 7 Minus Case 6, Scallop Sector Face View

At the aft edge of the aft shaft scallop, the hoop stress decreases 0.4 ksi at assembly and 1.0 ksi at speed. $\sigma_{0,alt}$ decreases 0.4 ksi.

The elastic-plastic properties in the thread had a relatively small impact on the stress results in the critical locations. Little value was added for the amount of effort needed to include these properties.

The analysis cases in the previous section addressing mesh fineness demonstrated that a coarse thread mesh produced similar $\sigma_{0,alt}$ in the critical locations as a fine thread mesh. In the current section, the fine mesh was still necessary to be used to ensure the plastic strain in the fillets was appropriately captured. Now that mesh fineness and elastic-plastic material properties have been demonstrated to have little impact on the results, all remaining analysis cases have been analyzed with a coarse thread mesh and elastic material properties.

5.5 Helical Threads

For the stress analyst, building the helical shape of threads requires substantially more effort than simplifying the threads into circular rings. Due to the complexity, many choose to ignore the helical shape [8] [9].

First, the helical shape itself creates meshing challenges. If an analyst meshes the threads of a bolt with circular rings, the analyst can simply create a 2D planar mesh of the thread region and revolve it to create the 3D elements. Next a 2D planar mesh can be swept axially to create the elements to fill in the bolt core. For helical threads the process is more complex. The 2D planar thread mesh must be translated axially as it is revolved to create the wound shape. Filling in the bolt core with an axially swept mesh is not an option due to the wound shape. Chen [18] opted to leave a small hollow core to avoid the meshing challenge. For this study, the core was filled with a hybrid mesh that consisted of tetrahedral

elements and five-sided pyramid elements to transition between the hexagonal and tetrahedral elements.

Second, the helical shape requires the analyst to mesh the transition area at the beginning and end of the thread on both the nut and bolt. In circular threads, these transition areas are axisymmetric and are therefore much simpler to build.

Third, the setup of the contact elements is more complex. With circular threads, only the flank angle needs to be considered when setting the appropriate contact element direction. For a helical thread, the additional angle due to the thread travel must also be considered.

Fourth, the sector size of the model must be doubled. A circular thread has reflective symmetry. A helical thread does not. While a half-bolt may be appropriate for a circular threaded model, a full bolt must be used for helical threads.

Fifth, a helically threaded model is not reflective symmetric about its sector planes. Cyclic symmetry must be modeled, which requires the mesh on the two sector planes to be identical to allow the coupling of each node pair.

Analysis case 8 includes helically shaped threads. This full bolt model contains elastic properties, nominal thread geometry, a coarse thread mesh, and contact elements in the threads with a friction value of 0.45. The case 8 results are

compared to the case 5 results. The case 5 model is similar to the case 8 model

except it contains a half-bolt and the threads are modeled as circular rings.
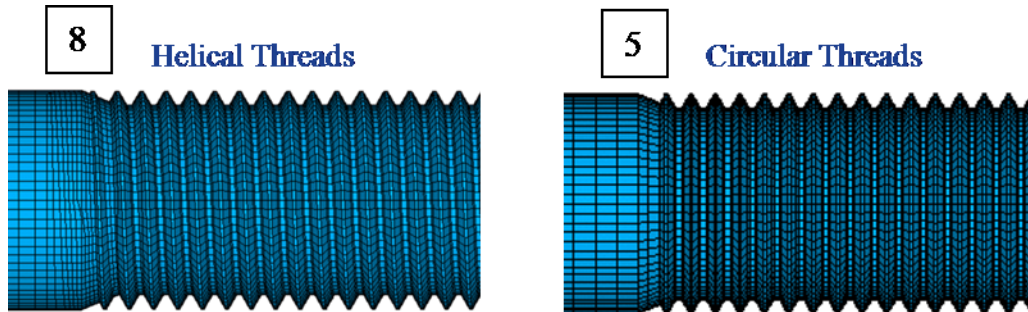
Figure 76: Comparison of Analysis Case 8 and Case 5

Delta stress plots capture the stress differences at the assembly and max speed

time points. The plots show the case 8 results minus the case 5 results. Figure 77

shows the HPT front shaft bolt hole location.

**Figure 77: Delta Stress Comparison (psi), Case 8 Minus Case 5,
Bolt Hole Sector Face View**

At the bolt hole aft edge, the axial stress decreases 3.1 ksi at assembly and 1.8 ksi at speed. The hoop stress decreases 1.4 ksi at assembly and 0.5 ksi at speed. $\sigma_{0,alt}$ increases 0.9 ksi.

Figure 78 shows the scallop location.
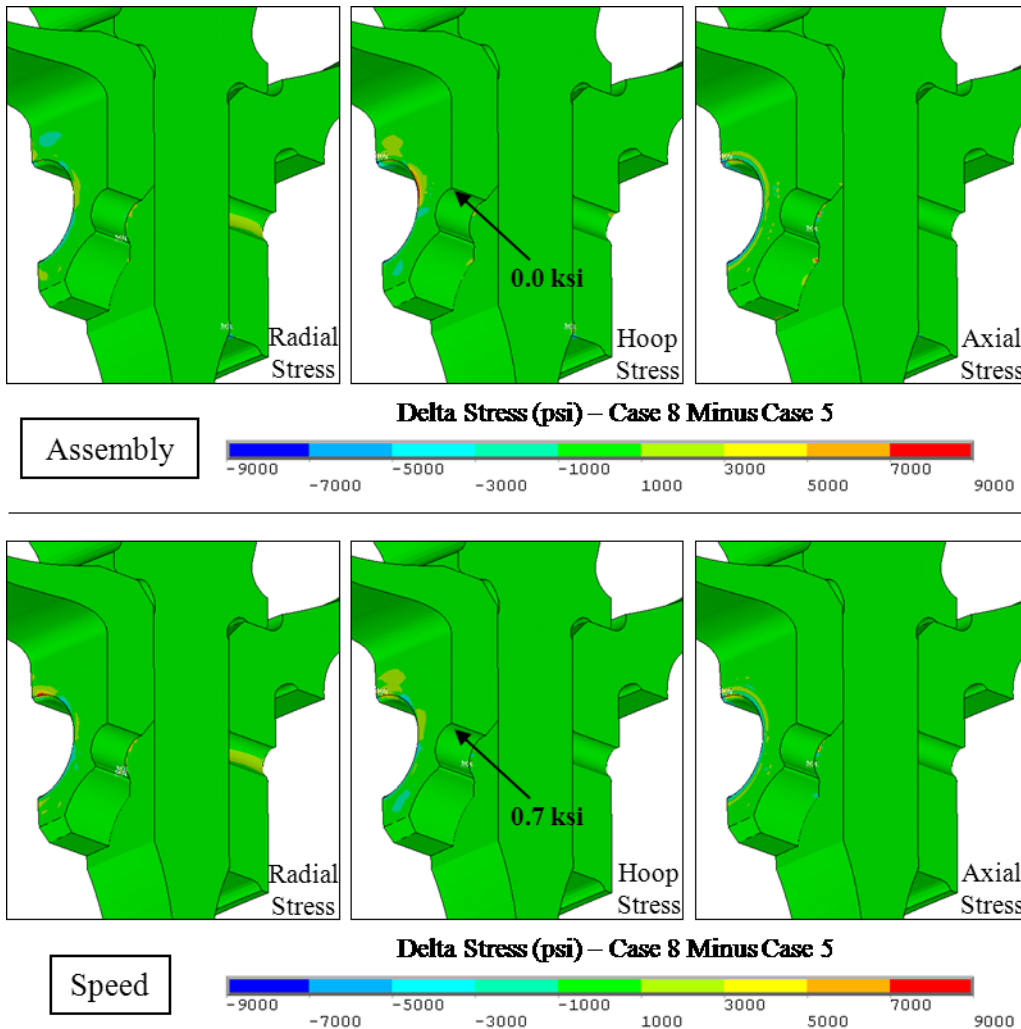
Figure 78: Delta Stress Comparison (psi), Case 8 Minus Case 5,
Scallop Sector Face View

The hoop stress is unchanged at assembly and increases 0.7 ksi at speed. $\sigma_{0,\text{alt}}$

increases 0.4 ksi.

Compared to the bolt/nut modeling assumptions discussed up to this point, the

impact of the helical thread is moderate. The fineness of the mesh and the

inclusion of elastic-plastic material properties had less of an effect. When couples

are used to join the bolt and nut, the appropriate axial position of the first couple

is more significant. Also including contact elements with friction instead of couples has a larger effect.

What makes the helical thread unique is that its inclusion increased $\sigma_{0,alt}$ for both the bolt hole and scallop. For all other case comparisons, modeling assumptions that decreased the bolt hole stress increased the scallop stress, and vice versa.

When building a model with helically shaped threads, the analyst must make an assumption about the angular orientation of the threads. For case 8, the threads are oriented so that the contact at the first thread began at the top of the bolt hole. This location is purely arbitrary. Depending on the precise positioning of the threads when the bolt is manufactured, the contact can begin at any angular position.

What effect does the angular orientation of threads have on the results? Case 9 was analyzed to address this question. In case 9, the threads are rotated 180 degrees about the bolt centerline so that the first thread contact begins at the bottom of the bolt hole.
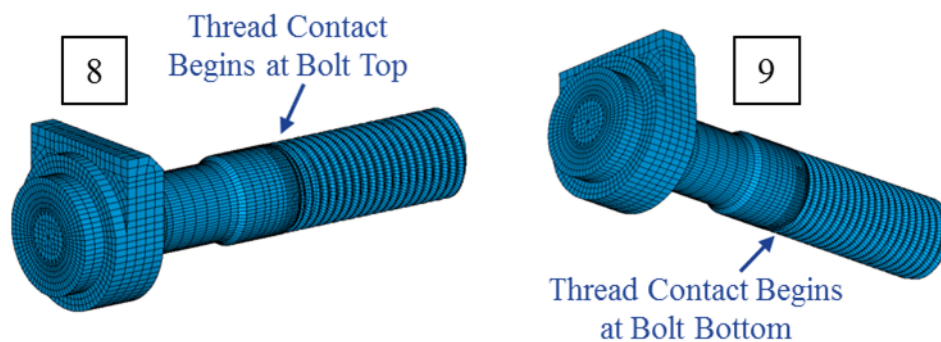
Otherwise, the model is identical to the case 8 model. Both models contain

coarsely-meshed helical threads, contact elements at the thread interface, mu=0.45

in the threads, and elastic material properties in the bolt and nut.

Figure 80 compares the stress results between cases 8 and 9. These delta plots

show case 9 minus case 8.

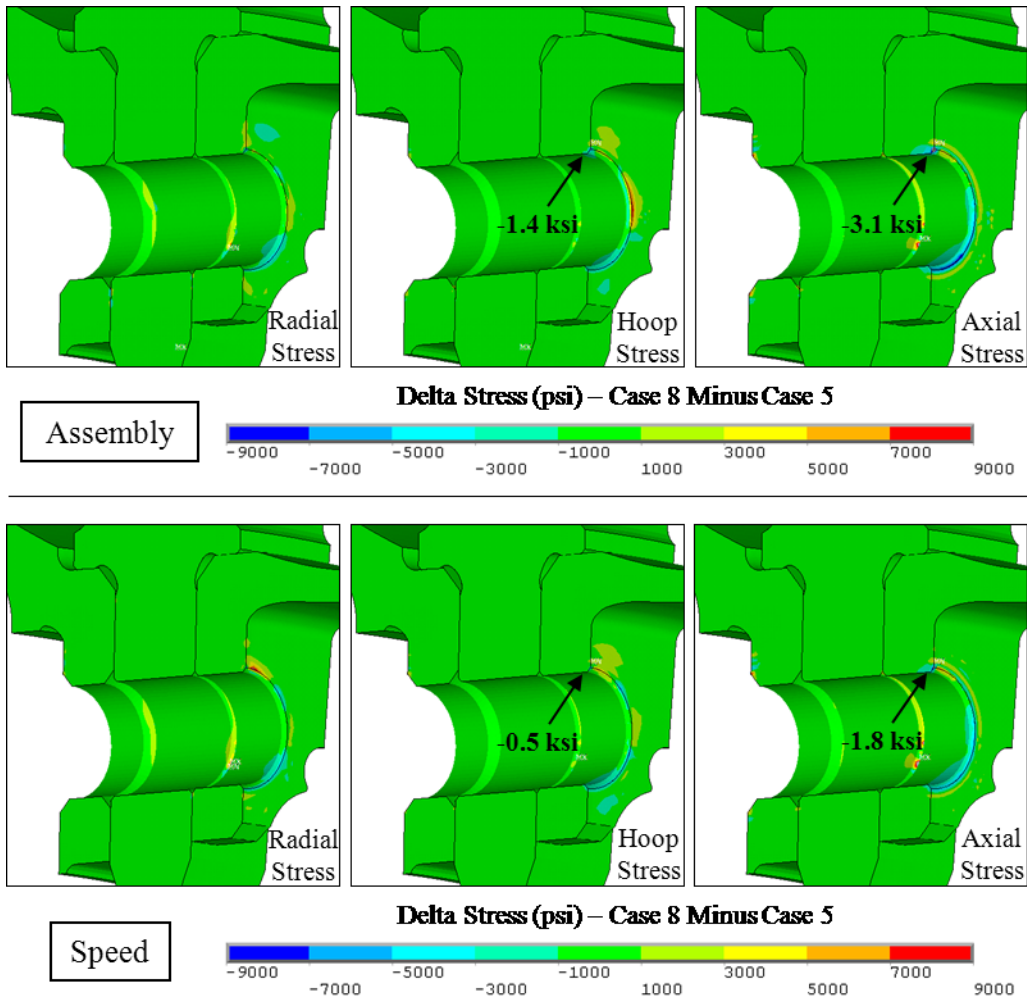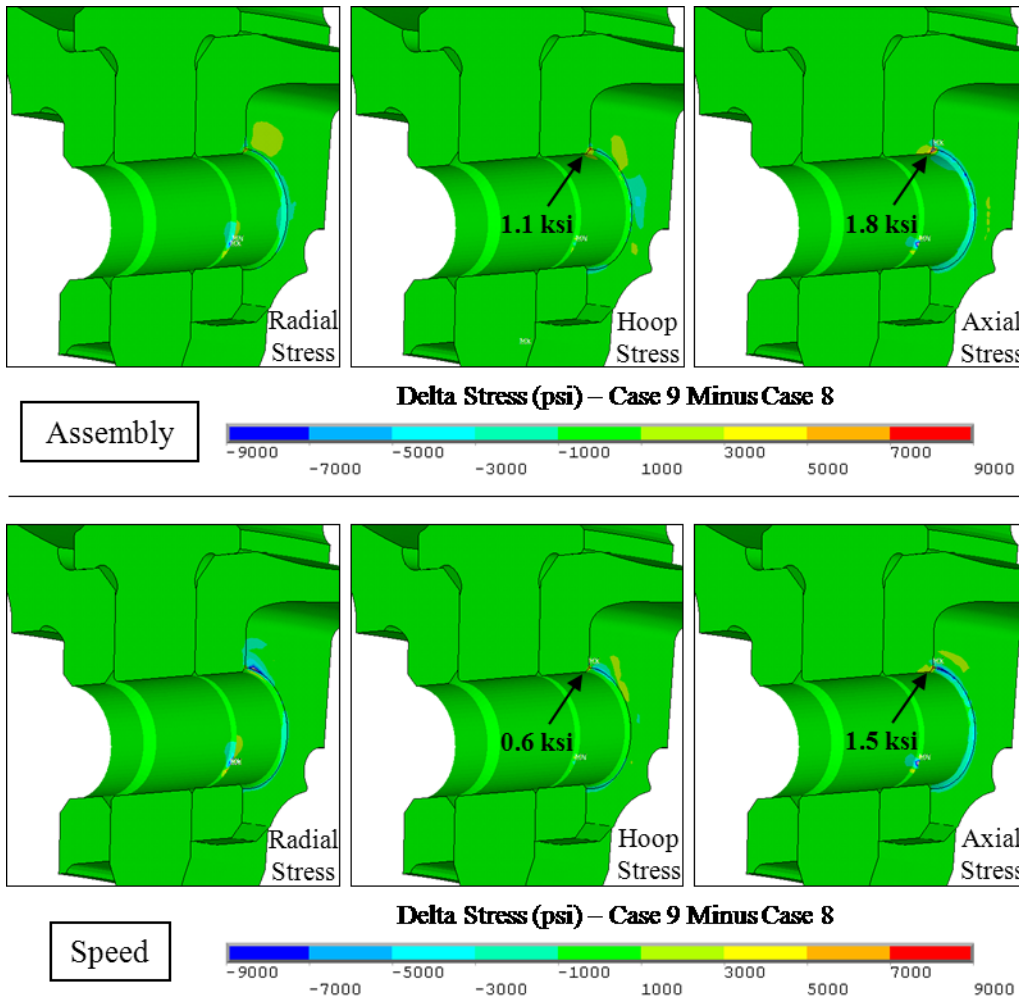**Figure 80: Delta Stress Comparison (psi), Case 9 Minus Case 8,
Bolt Hole Sector Face View**

The bolt hole axial stress increases 1.8 ksi at assembly and 1.5 ksi at speed. The

bolt hole hoop stress increases 1.1 ksi at assembly and 0.6 ksi at speed. These

changes in stress decrease $\sigma_{0,alt}$ by 0.6 ksi.

Figure 81 shows delta stress plots for the scallop.
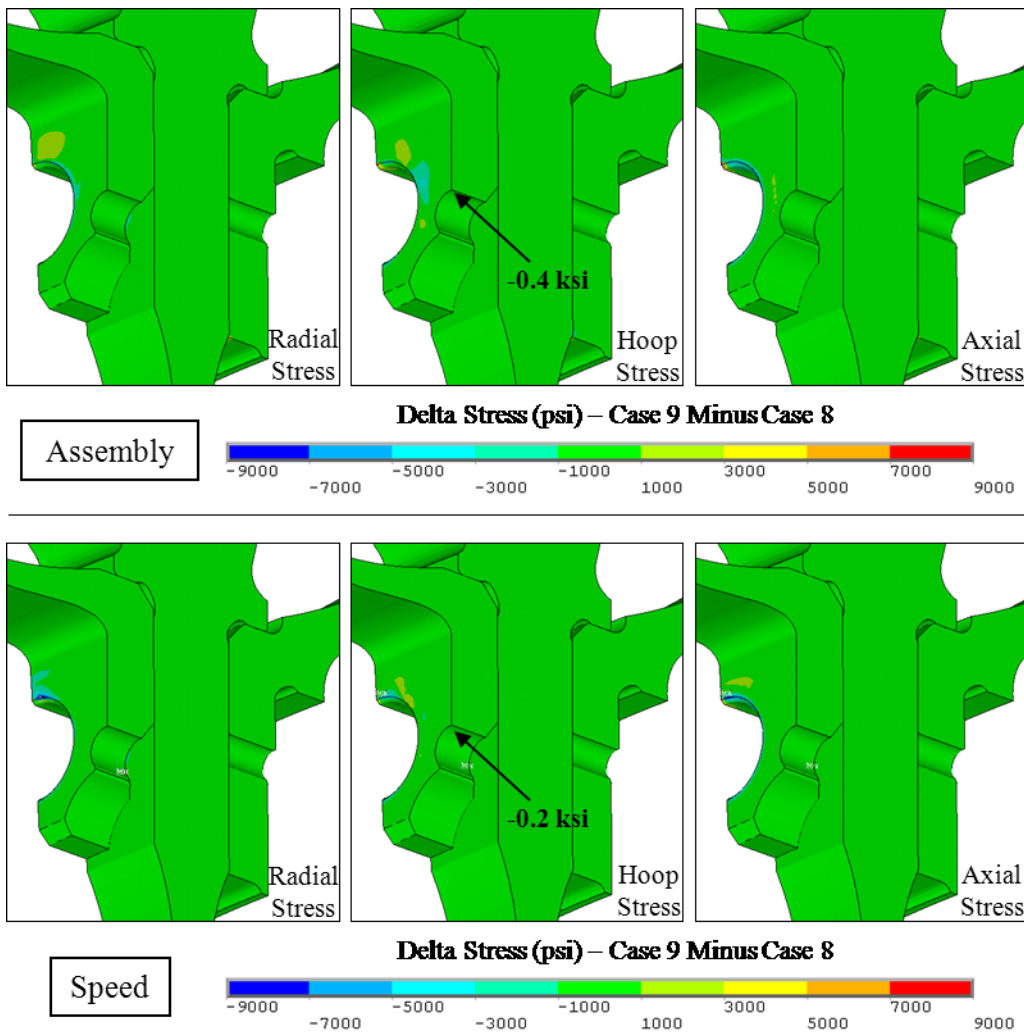
Figure 81: Delta Stress Comparison (psi), Case 9 Minus Case 8,
Scallop Sector Face View

For the scallop, the hoop stress decreases 0.4 ksi at assembly and 0.2 ksi at speed. $\sigma_{0,alt}$ is identical for these two cases.

Table 3 compares the results of the two helically threaded cases to the circular threaded case. Overall, the helical threads have a relatively small impact on the results. At the bolt hole, all three cases are within 1 ksi. Both helically threaded cases produce greater $\sigma_{0,alt}$ than the circular thread.

At the bolt hole, the difference in the results between the two helically threaded cases (0.6 ksi) is larger than the difference between the circular threaded case and the re-oriented helical thread case (0.3 ksi). The simplifying assumption of the circular thread has less of an effect than the assumption of thread orientation, and any thread orientation is possible in the actual hardware.

At the scallop, the range of results is small. The two helically threaded cases produce identical results. The circular thread $\sigma_{0,alt}$ is only 0.4 ksi lower.

Table 3: Results Comparison - Cases 5, 8, 9

Case	$\sigma_{0,alt}$ (ksi), Delta to Case 5		Life, Normalized to Case 5	
	Bolt Hole Aft Edge	Scallop Aft Edge	Bolt Hole Aft Edge	Scallop Aft Edge
5 - Circular Threads	-	-	-	-
8 - Helical Threads	0.9	0.4	0.766	0.987
9 - Helical Threads, 180 Degree Re-oriented	0.3	0.4	0.914	0.988

The inclusion of helical threads and the angular orientation of those helical threads has only a minor effect on the calculated life in the bolted joint.

5.6 Partial First Thread

If one looks at the cross-section of a nut at different positions around the circumference, one observes the differences in the thread profile at each cross-section. In some sections, the first thread is merely a small partial stub. In other sections, the first thread reaches its maximum height, but its thickness is less than full. In one section, the first thread is a fully-formed complete thread. Figure 82 diagrams the cross-section of the thread from Case 8 at the 12 o'clock, 3 o'clock, 6 o'clock, and 9 o'clock positions. The stiffness of the nut thread varies from one cross-section to the next.
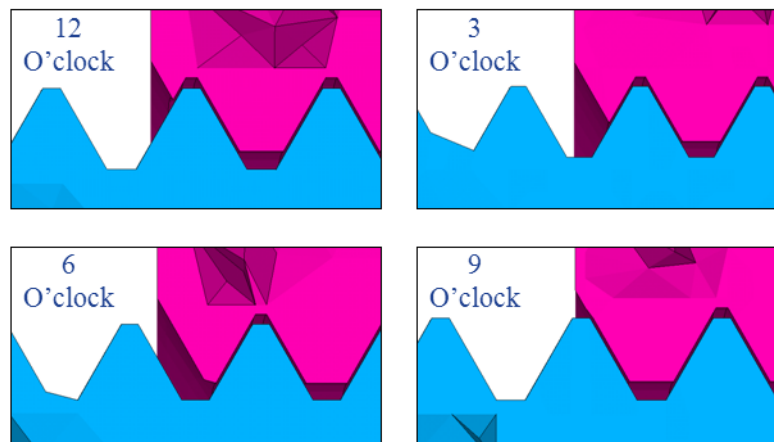
Figure 82: Helical Thread Cross-Sections at 3, 6, 9, and 12 O'clock

When an analyst builds a helically threaded model, all the various thread cross-sections are included. The appropriate total stiffness is captured.

All the circularly threaded analysis cases presented thus far have used the same nut cross-section. The first thread was arbitrarily chosen to be a fully-formed

96

complete thread. Does this thread cross-section appropriately represent an average cross-section? With just a visual inspection, the full first thread appears stiffer than average. However, the first point of bolt-nut contact for this cross-section is the furthest aft of all thread cross-sections.

As discussed earlier, the helically threaded models (case 8 and 9) produced relatively similar results as the circular threaded model (case 5). The scallop in the two helically threaded case produced identical Walker-adjusted alternating stresses. The circular thread case (case 5) produced 0.4 ksi lower stress. If a more representative thread cross-section is chosen, could the small gap in the results be closed?

Analysis case 10 was performed to address this question. Analysis case 10 uses circular threads, however, the first nut thread was thinned by half of the thread thickness at the thread minor diameter. Figure 83 diagrams the geometry difference between the full first thread in case 5 and the partial first thread in case 10.
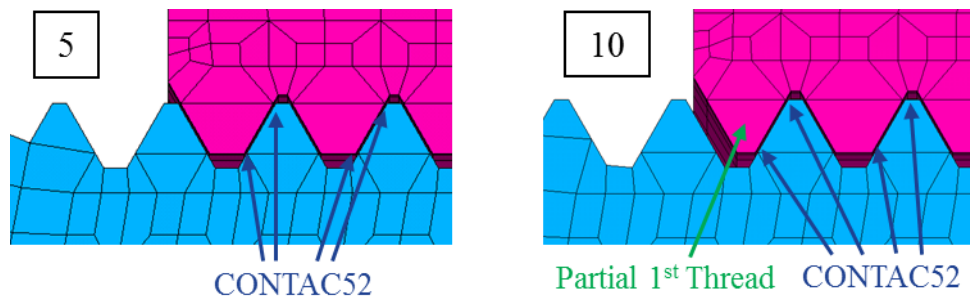
Figure 83: Comparison of Analysis Case 5 and Case 10

Delta stress plots show the impact of the change. The plots show case 10 minus case 5.
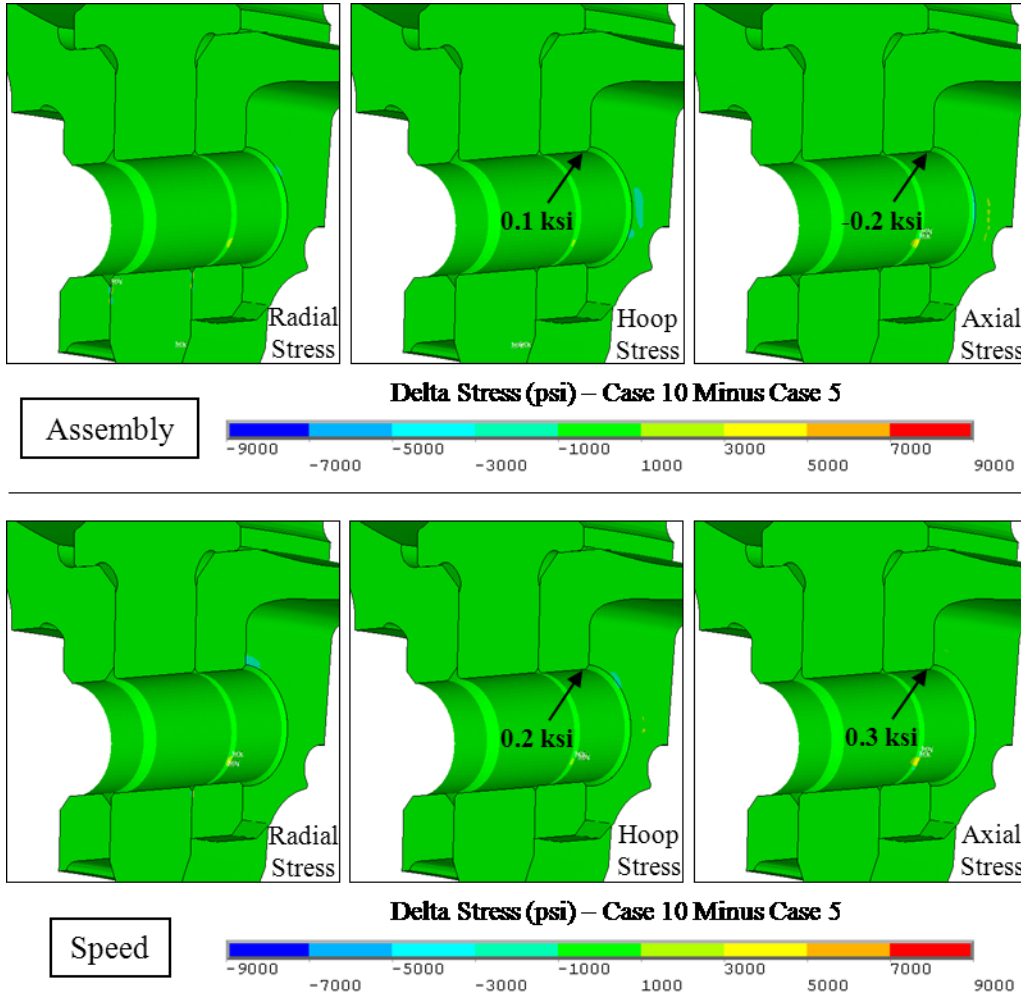
**Figure 84: Delta Stress Comparison (psi), Case 10 Minus Case 5,
Bolt Hole Sector Face View**

At the aft edge of the HPT front shaft bolt hole, the axial stress decreases 0.2 ksi assembly and increases 0.3 ksi at speed. The hoop stress increases 0.1 ksi at assembly and 0.2 ksi at speed. The two cases share the same $\sigma_{0,alt}$.

Figure 85 shows the difference in stress in the HPT front shaft scallop. The plots show case 10 minus case 5.
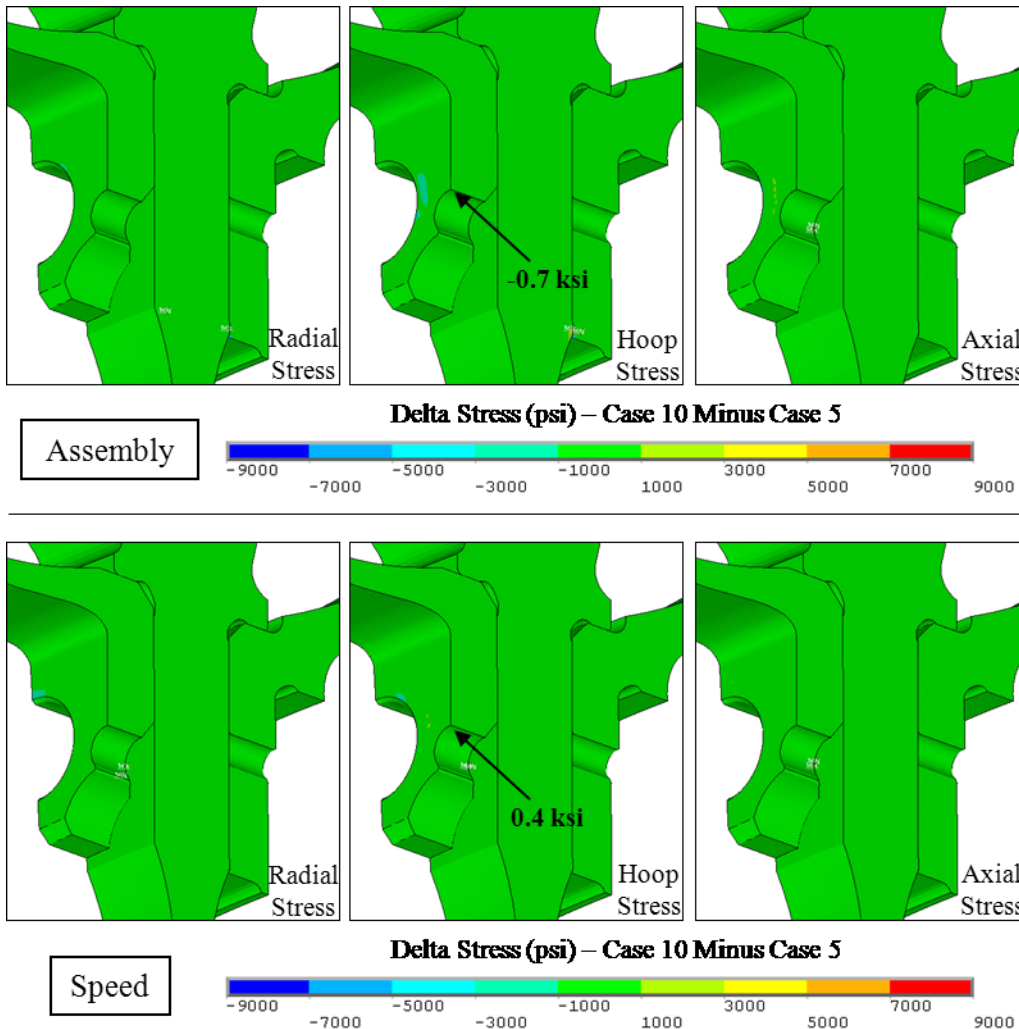
**Figure 85: Delta Stress Comparison (psi), Case 10 Minus Case 5,
Scallop Sector Face View**

The scallop stress decreases 0.7 ksi at assembly and increases 0.4 ksi at speed.
$\sigma_{0,alt}$ increases 0.4 ksi.

Interestingly, thinning the first thread brings the scallop results in-line with the

helically threaded cases. Cases 8, 9, and 10 all have the same $\sigma_{0,alt}$. While

thinning the first thread has only a minor effect on stress, these results suggest

that the thinned first thread better simulates the effect of the helical thread for the

scallop location. The bolt hole results are unchanged.

99

Table 4 summarizes the results for the circular thread and helical thread cases.

Table 4: Results Comparison - Cases 5, 8, 9, 10

Case	$\sigma_{0,alt}$ (ksi), Delta to Case 5		Life, Normalized to Case 5	
	Bolt Hole Aft Edge	Scallop Aft Edge	Bolt Hole Aft Edge	Scallop Aft Edge
5 - Circular Threads	-	-	-	-
8 - Helical Threads	0.9	0.4	0.766	0.987
9 - Helical Threads, 180 Degree Re-oriented	0.3	0.4	0.914	0.988
10 - Circular Threads, Partial First Thread	0.0	0.4	1.000	0.988

5.7 Friction Sensitivity

All the analysis cases discussed up to this point that have used contact elements in the threads have been run with mu=0.45 as the assumed friction coefficient. The actual friction coefficient a thread feels is dependent on the bolt and nut materials, the type of lubrication used if one is used, how that lubrication behaves in the harsh engine conditions, and other factors. It can be difficult to predict the correct coefficient of friction with any accuracy. Therefore, it is worth-while to study how the assumed friction value impacts the calculated stress.

Analysis case 11 was run with mu=0.25 in the threads. The model is identical to the case 5 model, except for the change in thread friction coefficient. The threads are modeled as circular rings, the thread mesh is coarse, and contact elements are used at the interface of the explicitly modeled thread teeth.
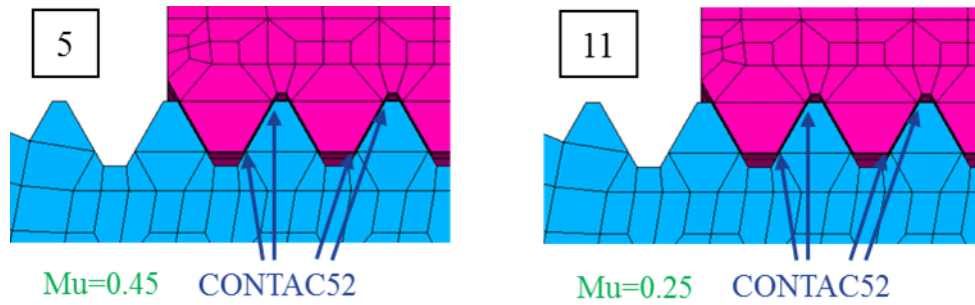
Figure 86: Comparison of Analysis Case 5 and Case 11

Delta stress plots compare the results between these two cases with different thread coefficients of friction. Figure 87 shows case 11 minus case 5.
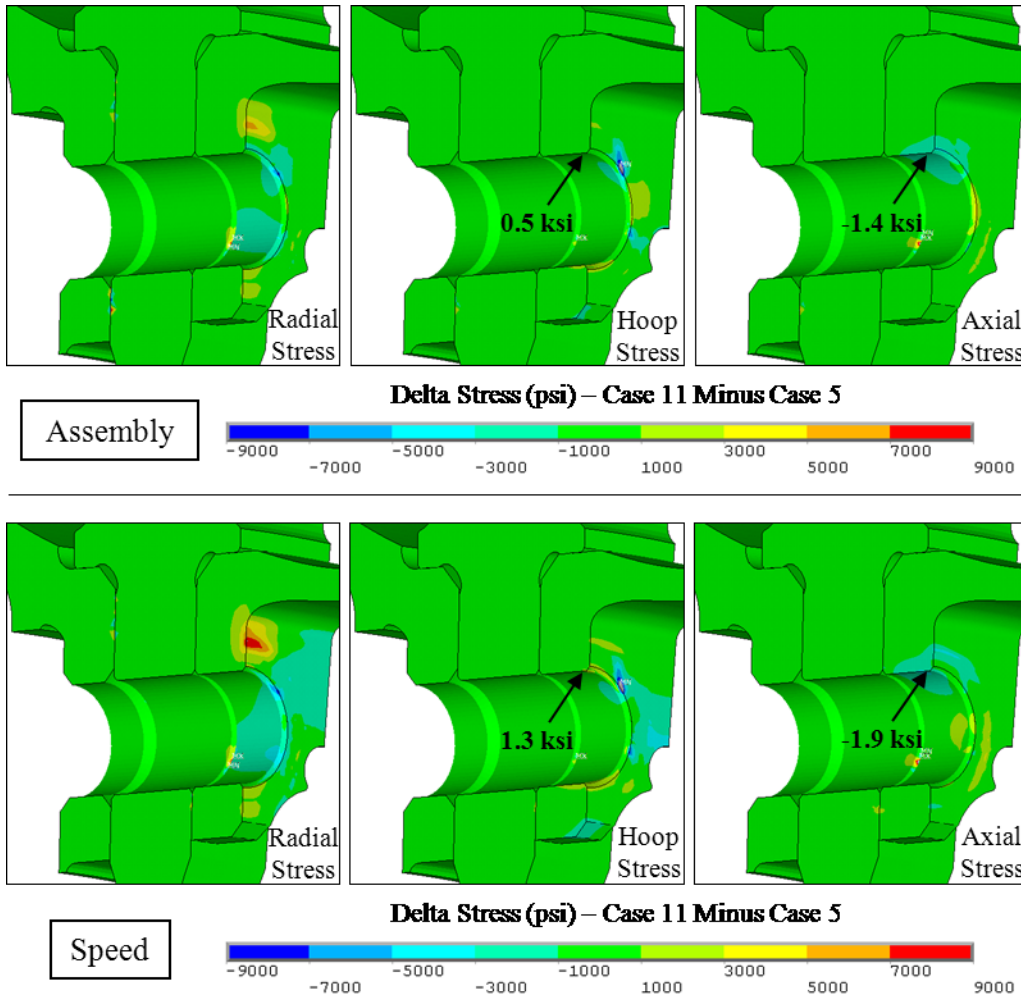
**Figure 87: Delta Stress Comparison (psi), Case 11 Minus Case 5,
Bolt Hole Sector Face View**

101

The hoop stress at the aft edge of the aft shaft bolt hole increases 0.5 ksi at assembly and 1.3 ksi at speed. The axial stress decreases 1.4 ksi at assembly and 1.9 ksi at speed. $\sigma_{0,alt}$ increases 0.9 ksi.

Figures 88 shows delta stress plots of the scallop for case 11 minus case 5.
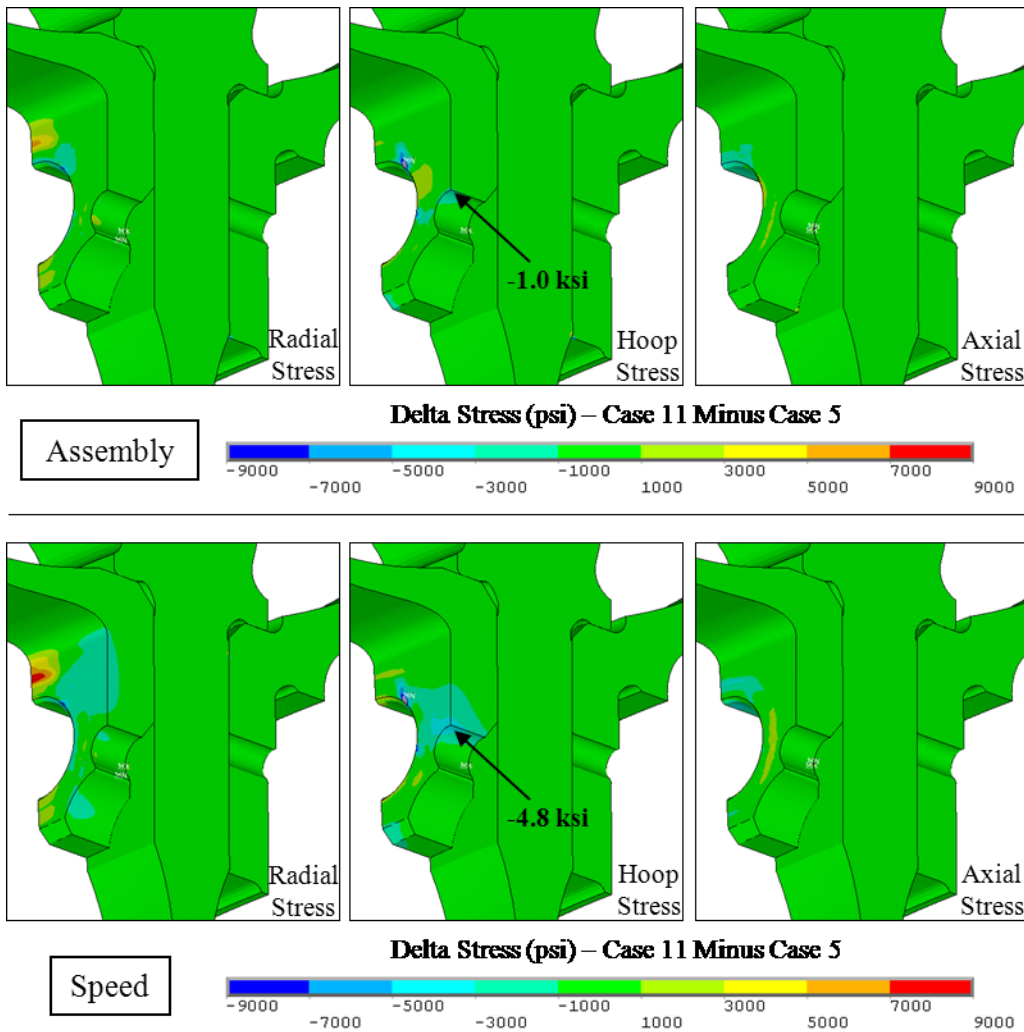
**Figure 88: Delta Stress Comparison (psi), Case 11 Minus Case 5,
Scallop Sector Face View**

The hoop stress at the aft edge of the aft shaft scallop decreases 1.0 ksi at assembly and 4.8 ksi at speed. $\sigma_{0,alt}$ decreases 2.2 ksi.

102

These two sets of results are also appropriate to compare to the results from analysis case 5 which used couples on the loaded thread faces. Couples are in essence sticking friction. Table 5 compares the results from all three cases.

Table 5: Results Comparison - Cases 3, 5, 11

	$\sigma_{0,alt}$ (ksi), Delta to Case 5		Life, Normalized to Case 5	
Case	Bolt Hole Aft Edge	Scallop Aft Edge	Bolt Hole Aft Edge	Scallop Aft Edge
3 - Coupled Threads	-1.1	1.2	1.878	0.957
5 - Mu=0.45 Threads	-	-	-	-
11 - Mu=0.25 Threads	0.9	-2.2	0.766	1.088

The joint shows some sensitivity to the thread coefficient of friction. As before, flexibility in the bolt/nut connection increases $\sigma_{0,alt}$ in the bolt hole and decreases it in the scallop.

Table 6 summarizes the stress results from all analysis cases.

Table 6: Results Summary - All Analysis Cases

Case	Explicit Threads	Interface Method	Elastic vs E/P	Mesh Size	Thread Shape	$\sigma_{0,alt}$ (ksi), Delta to Case 5 Bolt Hole Aft Edge	$\sigma_{0,alt}$ (ksi), Delta to Case 5 Scallop Aft Edge
1	No	Couples	Elastic	N/A	N/A	-2.7	3.2
2	Yes	Couples	Elastic	Coarse	Circular	-3.2	3.8
3	Yes	Couples, Loaded Side Only	Elastic	Coarse	Circular	-1.1	1.2
4	No	Couples, 1st Couple Aligned w/ 1st Loaded Thread	Elastic	N/A	N/A	-1.6	1.7
5	Yes	Mu=0.45	Elastic	Coarse	Circular	-	-
6	Yes	Mu=0.45	Elastic	Fine	Circular	-0.1	0.0
7	Yes	Mu=0.45	E/P	Fine	Circular	-0.2	-0.4
8	Yes	Mu=0.45	Elastic	Coarse	Helical	0.9	0.4
9	Yes	Mu=0.45	Elastic	Coarse	Helical, Re-Oriented 180°	0.3	0.4
10	Yes, Partial 1st Thread	Mu=0.45	Elastic	Coarse	Circular	0.0	0.4
11	Yes	Mu=0.25	Elastic	Coarse	Circular	0.9	-2.2

Chapter 6: Thermal Sensitivity Study

All eleven analysis cases compared in this thesis were analyzed at a uniform temperature of 70 degrees. If one wanted to understand the absolute stress levels in the joint, this assumption makes little sense. Thermal stress due to the gradient of temperature in the hardware is a significant player in the total stress. For the bolt hole aft edge, the application of temperatures decreases $\sigma_{0,alt}$ by approximately 8 ksi, or 27%. For the scallop aft edge, $\sigma_{0,alt}$ increases approximately 8 ksi, or 10%. However, the assumption was made that on a relative basis, the differences in the eleven analysis cases would be similar with or without the application of realistic temperatures. A follow-on study was performed to verify this assumption.

Cases 3, 5, and 8 were chosen for this thermal sensitivity study. The thread modeling assumptions for these three cases were discussed earlier and are summarized below in Table 7.

Table 7: Modeling Assumptions - Thermal Sensitivity Cases

Case	Explicit Threads	Interface Method	Elastic vs E/P	Mesh Size	Thread Shape
3	Yes	Couples, Loaded Side Only	Elastic	Coarse	Circular
5	Yes	Mu=0.45	Elastic	Coarse	Circular
8	Yes	Mu=0.45	Elastic	Coarse	Helical

Temperatures representing a typical take-off condition were mapped onto the model. Figure 89 shows the temperature profile.
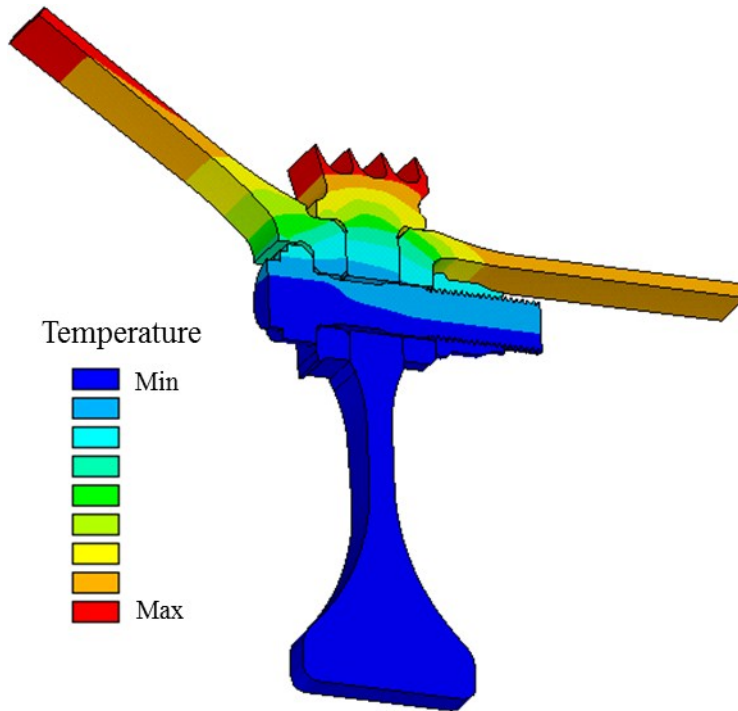
Figure 89: Temperature Profile

The model was run through a similar series of time points as had been done previously, only in this simple transient the temperatures were included. Figure 90 diagrams the transient. The circled results indicate the two time points used to calculate $\sigma_{0,alt}$.
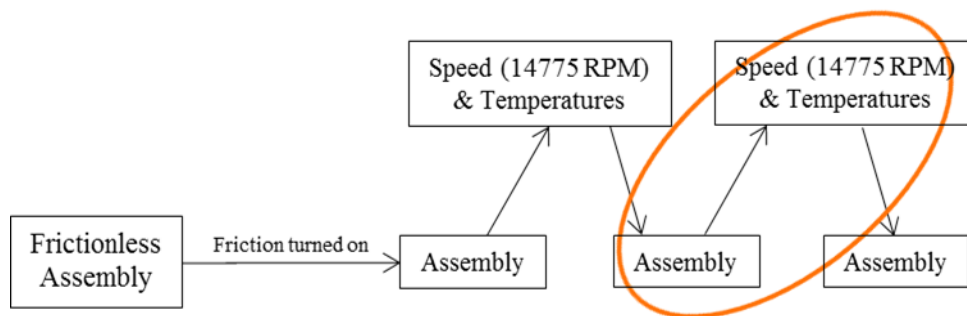

Figure 90: Analysis Path - Thermal Sensitivity Loading

106

Tables 8 and 9 list the stress results of the three analysis cases from the speed-only transient and the speed and temperature. The displayed $\sigma_{0,alt}$ results are listed relative to the analysis case 3 results for the appropriate transient.

Table 8: Results Summary - Speed-only Loading

Speed-only Transient	$\sigma_{0,alt}$ (ksi), Delta to Case 5	
Case	Bolt Hole Aft Edge	Scallop Aft Edge
3 - Coupled (Loaded Side Only) Circular Threads	-1.1	1.2
5 - Mu=0.45 Gapped Circular Threads	-	-
8 - Mu=0.45 Gapped Helical Threads	0.9	0.4

Table 9: Results Summary - Speed and Temperatures Loading

Speed and Temperature Transient	$\sigma_{0,alt}$ (ksi), Delta to Case 5	
Case	Bolt Hole Aft Edge	Scallop Aft Edge
3 - Coupled (Loaded Side Only) Circular Threads	-1.2	1.0
5 - Mu=0.45 Gapped Circular Threads	-	-
8 - Mu=0.45 Gapped Helical Threads	0.9	0.2

Interestingly, the relative difference between the three analysis cases is similar whether or not the temperature is included in the transient. For example, at the aft edge of the bolt hole, case 5 produces 1.1 ksi less stress than case 3 for the speed transient. When temperatures are added, case 5 produces 1.2 ksi less stress than case 3. The largest difference caused by the inclusion of temperatures occurs at the aft edge of the scallop. The inclusion of temperatures decreases the stress difference by 0.2 ksi for both cases 5 and cases 8 relative to case 3.

These results suggest that the original assumption was appropriate. The speed-only transient used for the eleven analysis cases discussed in this thesis is appropriate to capture the relative stress differences between the analysis cases.

Chapter 7: Conclusions

7.1 General Conclusions

The bolt-nut interface modeling assumptions have no significant impact on the calculated stress in any critical locations except for the aft edges of the HPT front shaft bolt hole and scallop. This is good news for the analyst. If the aft edge of either of these features has adequate margin to the LCF life of the part, the assumptions made in bolt-nut interface is not critical to the analysis. Complexity adds little value. A simplified assumption in which the threads are not explicitly modeled, such as those made in case 1 or 4, may be adequate.

The stress differences that are seen in the aft edge of the HPT front shaft bolt hole and scallop are driven by the stiffness of the bolt-thread interface. A less stiff interface allows the nut to further deform, which distributes more clamp load to the inner edge of the bolt hole. In general, an increase in flexibility increases $\sigma_{0,alt}$ in the bolt hole and decreases $\sigma_{0,alt}$ in the scallop.

Some modeling assumptions are demonstrated to have minor or no effect on the calculated stresses in the aft edges of the HPT front shaft bolt hole and scallop. First, a coarse thread mesh and a fine thread mesh produce the same $\sigma_{0,alt}$ results r both the HPT front shaft and scallop. Second, elastic or elastic-plastic bolt and nut material properties produce 0.4 and 0.1 ksi stress difference in the bolt hole and scallop, respectively. Third the impact of simplifying the helical thread into a series of circular rings is small. The change in $\sigma_{0,alt}$ is less than 1.0 ksi at both
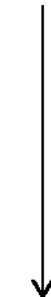
locations. The helical thread shape especially adds significant complexity to the

model, but only has a relatively minor effect on the calculated stress.

Adding contact elements at the thread instead of couples had a moderate impact.

The bolt hole stress increased 1.1 ksi and the scallop hole decreased 1.2 ksi.

When couples are used to join the bolt and nut, the inclusion of explicitly

modeled threads has only a minor effect. The change in the $\sigma_{0,alt}$ at the aft edge of

the HPT front shaft bolt hole and scallop is approximately 0.5 ksi. However, the

analyst should use care in the selection of the location of the first couple. $\sigma_{0,alt}$

differences between 1.1 and 2.6 ksi were observed in the hole and scallop when

the first couple was placed at the start of the interface versus placing it at the

location of the first loaded thread surface.

The impact of the modeling assumptions, ordered from greatest impact to least

impact, is summarized in Table 10.

Table 10: Summary of Impact of Each Modeling Assumption

	Modeling Assumption	σ0,alt (ksi) Impact		Added Complexity to Model Creation	Observed Computational Time Impact
		Bolt Hole Aft Edge	Scallop Aft Edge		
Greater Impact	Couple Axial Placement, When Couples Are Used	1.1 - 2.1	1.5 - 2.6	Low	Negligible
	Incusion of Thread Contact Elements	1.1	1.2	Moderate	Negligible
	Helical Thread Inclusion	0.3 - 0.9	0.4	High	520% Increase
	Explicit Inclusion of Threads	0.5	0.5 - 0.6	Moderate	Negligible
	Inclusion of Elastic/Plastic Material Properties	0.1	0.4	Low	80% Increase
	Partial 1st Thread	0.0	0.4	Low	Negligible
Lesser Impact	Fine Mesh	0.0	0.0	Moderate	300% Increase

The reader should note, however, that each of the modeling assumptions listed in Table 10 cannot necessarily be included independently of each other. For example, to include thread contact elements (second on the list) the threads themselves must be explicitly included (fourth on the list).

The model is sensitive to the friction coefficient chosen for the threads. Comparisons of the analysis cases with friction coefficients of 0.25, and 0.45, and couples (which are essentially infinite friction) show a range of 2.0 ksi of $\sigma_{0,alt}$ in the aft edge of the bolt hole and 3.4 ksi in the aft edge of the scallop. If the friction coefficient in the actual hardware is relatively high, the use of couples to join the bolt and nut might be an appropriate simplification. Also, if the coefficient of friction at the thread interface in the actual hardware is not known, the error introduced by the friction assumption may outweigh the benefits of some of the discussed interface modeling complexities.

Thermal stress has approximately an 8.0 ksi impact on the aft edge of the bolt hole and scallop. Depending on accuracy of the temperatures, the error in thermal stress could be larger than the error introduced by the thread modeling assumptions.

7.2 Suggested Future Work

While this study yielded valuable results, future work on the topic would be beneficial. The scallop differences were magnified by the close proximity of the scallop to the nut. Future work could include a study of the same bolted joint, but with the scallop spaced farther away. A study of this type would help an analyst understand when to consider scallop stress when determining how to model the bolt-nut interface.

This study focused on a single bolted joint. Future work could include a study of additional joints. The work can investigate whether certain joint configurations are more sensitive to bolt-nut modeling assumptions.

Bibliography

[1] Federal Aviation Regulations, "Section 33.70 - Engine Life Limited Parts," Amendment 33-22, 2007.

[2] Federal Aviation Regulations, "Section 33.75 – Safety Analysis," Amendment 33-24, 2007.

[3] "LOT Flight 7," Wikipedia, July 2012. Available: http://en.wikipedia.org/wiki/LOT_Flight_7

[4] National Transportation Safety Board, "Aircraft Accident Report – United Airlines Flight 232, McDonnell Douglas DC-10-10, Sioux Gateway Airport, Sioux City, Iowa, July 19, 1989," Report No. NTSB/AAR-90/06, 1990.

[5] Goodier, J.N. "The distribution of load on the threads of screws," *Journal of Applied Mechanics*, vol. 7, n 1, pp. A10–A16, 1940.

[6] Sopwith, D.G. "Distribution of load in screw threads," *Institution of Mechanical Engineers*, vol. 159, pp. 373-383, 1948.

[7] Pedersen, N.L. "Optimization of bolt thread stress concentrations," Archive of Applied Mechanics, pp. 1-24, 2012.

[8] Honarmandi, P., J.W. Zu, and K. Behdinan. "Elasto-plastic fatigue life improvement of bolted joints and introducing FBI method," *Mechanics Based Design of Structures and Machines*, vol. 33, n 3-4, pp. 311-330, 2005.

[9] Venkatesan, S. and G.L. Kinzel "Reduction of stress concentration in bolt-nut connectors," *Journal of Mechanical Design, Transactions of the ASME*, vol. 128, n 6, pp. 1337-1342, 2006.

[10] Chakherlou, T.N., M. Mirzajanzadeh, J. Vogwell, et al. "Investigation of the fatigue life and crack growth in torque tightened bolted joints," *Aerospace Science and Technology*, vol. 15, n 4, pp. 304-313, 2011.

[11] Chakherlou, T.N., and B. Abazadeh. "Experimental and numerical investigations about the combined effect of interference fit and bolt clamping on the fatigue behavior of Al 2024-T3 double shear lap joints," *Materials and Design*, vol 33, n 1, pp. 425-435, 2012.

[12] Siemens PLM Software, 5800 Granite Parkway, Suite 600, Plano, TX 75024, "Unigrahics NX," ver. 7.5.

[13] CD-adapco, 60 Broadhollow Road, Melville, NY 11747, "Star-CD," ver. 3.26.

[14] Ansys Inc., Southpointe, 275 Technology Drive, Canonsburg, PA 15317, "ANSYS," ver. 11 with Service Pack 1, 2007.

[15] SAE International Group, *Aerospace Standard 887*9, Rev. D, 1996.

[16] Wang, W. Reverse Engineering: Technology of Reinvention. Boca Raton, FL: CRC Press, 2011, pp.101-108.

[17] Hamrock, B.J., B. Jacobsen, and S.R. Schmid. Fundamentals of Machine Elements. New York: McGraw-Hill, 1999, Equation 10.35, p. 401.

[18] Chen, J., and Y. Shih. "A study of the helical effect on the thread connection by three dimensional finite element analysis," *Nuclear Engineering and Design*, Vol. 191, n 2, pp. 109-116, 1999.